UNIVERSITY OF GLASGOW

AIR FLOW AND PARTICLE MOVEMENT INTO

FLANGED CIRCULAR LOCAL EXHAUST HOODS

Thesis submitted for the degree of Master of Science in

the Building Services Research Unit of the Department

of Mechanical Engineering, University of Glasgow.

FAISAL MUSTAFA AHMAD AL-ATWAH

JULY 1993

ProQuest LLC.
789 East Eisenhower Parkway
P.O. Box 1346
Ann Arbor, MI 48106 – 1346

ACKNOWLEDGEMENTS

I would like to thank most sincerely my supervisor Mr Bill Carson and Professor B.F. Scott, the Head of Department for their guidance and supervision throughout this study, in the writing and reviewing this thesis. Without their help, support and encouragement, this work could not have been achieved.

I wish to thank Mr T.J. Graham from the Photography Department and Mr I. Watson for their helpful advice in developing and printing the photographs. I want to thank all the staff in the Workshop Department for helping me in building the experimental rig.

I would also like to thank Mrs Barbara Macleod for her help and advice in typing this thesis. I want also to thank my wife for helping me in typing this thesis.

I want to thank my parents for their love and support and for teaching me that I could do anything if I worked hard and was honest.

Finally I would like to thank the Jordanian Government and the British Council for helping and supporting me in my study.

SUMMARY

Current practice for designing and dimensioning local exhaust hoods is largely based on empirical values and rules of thumb. Efforts to model the contaminant movement process have attracted increasing interest in recent years. This kind of modelling work was previously scarcely feasible because it needs large computational resources. However, rapid improvements in the performance and availability of personal computers have made the modelling of contaminant movement a practical reality.

Local exhaust hoods are used to protect workers from hazardous materials. Increasing emphasis on health and safety means that hood performance is becoming more important. At the same time economic pressures make over design less acceptable. An accurate model to show if particles are captured should result in better protection and more economic local exhaust hood design.

A review of the development of exhaust hood design from the pioneering work of Dalla Valle in (1930) is followed by an examination of the behavior of airborne particles. The objectives of the present study are then defined as the development of computer programs to predict particle trajectories and suitable for use on a personal computer and the validation of these programs by comparison with experimental trajectories.

Six models for air flow fields outside exhaust hoods are presented, discussed and evaluated. They describe flow fields outside circular and rectangular flanged exhaust hoods in ideal stagnant air locations. Two models for flow into circular flanged hoods are selected for further work on the basis of probable validity, ease of computation and scope for experimental validation.

Cross draughts are identified as having a significant effect on the flow fields. These are incorporated into the models by superimposition (vectorial addition). The motion of particles in the resultant flow fields is then calculated taking into account the effects of gravity, buoyancy, drag force and inertia.

The program was written in BASIC and calculates the positions and velocities of a particle at specific time intervals and can be used for testing capture of particles under different conditions. The program is interactive and enables users to define and change conditions. Exhaust hood configuration and flow, particle size, density, initial position and velocity are the variable parameters.

Soap bubbles were used to simulate airborne particles in a wind tunnel fitted with a circular exhaust. A combination of constant and stroboscopic lighting enabled bubble trace photographs with time marks to be obtained. This enabled a quantitive comparison to be made between corresponding calculated and experimental trajectories. Measurements from the photographs also allowed individual bubble diameters and densities to be obtained. These were used when predicting the trajectory of that bubble.

The major difficulty for designers in using the program developed is in estimating appropriate cross draughts. Further work is suggested in this area while the need for in site testing is emphasized.

CONTENTS

APPENDICES

NOMENCLATURE

Symbol	Description	Dimension*
a	Hood radius	L
A_p	Projected particle area	L^2
A_s	Ellipse surface area	L^2
b	Distance	L
b(x,ds)	Distance from the point x to an infinitesimal sink ds	L
c	A constant	
C	Cunningham correction factor	
C_d	Drag force coefficient	
C_r	Radial correction factor	
d	A constant	
D	Hood diameter	L
D_p	Particle diameter	L
$D_{p.e}$	Equivalent volume diameter	L
ds	Infinitesimal area element vector	
e	Base for natural logarithms	
E	Mean error	
E_i	Error at i–th iteration	
F_c	Cohesion force of a particle	F
F_d	Drag force on a particle	F
g	Acceleration of gravity	L/t^2
i	Nodal coordinate	
I	A constant	
j	Nodal coordinate	
K	A constant	

*F – force, L – length, M – mass, t – time,T –Temperature

L	Length of a rectangular exhaust opening	L
m	Particle mass	M
n	Number of iterations	
P	Pressure	F/L^2
Q	Hood flow rate	L^3/t
r	Distance(from an opening centerline)	L
s	Area of an exhaust opening	L^2
S	Standard error of deviation	
t	Time	t
T	Absolute temperature	T
U, U_x, U_y, U_z, U_r	Air velocity and its vector components	L/t
Uo	Hood face velocity	L/t
U'	Non-dimensional air velocity	
U_∞	Fluid velocity far from the particle	L/t
V	Particle velocity	L/t
V_c	Cross wind velocity	L/t
V_{c1}	Centerline velocity	L/t
V_{cf}	Capture velocity at the face of the hood	L/t
V_j	Emission velocity of a particle	L/t
V_r	Relative velocity,(V - U)	L/t
$V_s(t)$	Intantaneous settling velocity	L/t
V_t	Terminal settling velocity	L/t
V_x, V_y	X and Y component of particle velocity	L/t
V_R	Hood radial velocity	L/t
V_T	Hood total velocity	L/t
V_Z	Hood axial velocity	L/t

W	Width of a rectangular exhaust opening	L
x	Distance (from a rectangular opening centerline along the opening width)	L
x_i	Distance at i–th iteration	L
X	Distance from the hood face	L
y	Distance (from a rectangular opening centerline along the opening length)	L
y_i	Distance at i–th iteration	L
Y	Percentage of the hood face velocity	
z	Distance (from an exhaust opening surface, perpendicular to it	L

Greek	Description	Dimension
α	Integration variable (an angle)	
β	Angle	
δt	Increment of time	t
θ	Angle	
ϵ	Ellipse eccentricity, a variable	
γ	Angle	
η	Integration variable (a distance)	L
λ	Carrier gas mean free–path	L
ξ	Integration variable (a distance)	L
π	3.14159...	
ρ	Air density	M/L^3
ρ_p	Particle density	M/L^3
μ	Viscosity	Ft/L^2
τ	Particle relaxation time	t
X	Particle dynamic shape factor	

Φ	Velocity potential	L^2/t

Abbreviations	Description
CFM	Cubic feet per minute
Kn	Knudsen number
Re	Reynolds number
STP	Standard temperature (25°C) and pressure (101 KPa)
.	Dot product
X	Cross product
∇	Gradient of a scalar
$\nabla.$	Divergence of a vector
∇^2	Laplacian
' and *	Denotes non-dimensional quantities

CHAPTER 1 LITERATURE REVIEW

1.1 INTRODUCTION

Ventilation may be defined as control of the environmental contaminants by using air flow. Ventilation is not a new idea in human life. It has been used for centuries and on this subject Goodfellow(1) reported that the Egyptians have used ventilation since immemorial time.

The two main types of industrial ventilation are general ventilation sometimes called dilution ventilation and local exhaust ventilation. General ventilation can be defined as blowing and removing air in the workplace in order to reduce the concentration of contaminants in the whole area of the workplace. Local exhaust ventilation may be defined as a system of removing contaminated air from a specific processing operation. A simple local exhaust consists of a hood connected by ducting to a fan exhausting to outside the building. The hood may be defined as the inlet of a local exhaust system.

Local exhaust hoods have different shapes, such as circular, elliptic, quadratic, rectangular or slot-shaped. The hoods can be divided into three types, enclosures, recieving hoods, and capture hoods as shown on Figure 1.1. Enclosures surround the point of emission or contaminant generation, either completely or partially. Booths and laboratory fume hoods are examples of partial enclosures. Enclosures require the lowest exhaust rate of the three hood types.

Recieving hoods are those hoods which use some characteristic of the process to help air contaminants flow into the hood. Canopies are common types of recieving hoods. Canopy hoods are located directly above hot processes. They recieve contaminated air which rises into the hood due to buoyancy.

Capture hoods differ from enclosures in that they must capture contaminants being generated at a point outside the hood itself and from recieving hoods in that they must capture contaminants without the aid of supplemental forces. Capture hoods are sensitive to external conditions, especially cross-drafts which may reduce the hood capture efficiency. Of the three hood types, capture hoods are the most commonly used. They are used when process requirements will not permit the obstruction of an enclosure. Capture hoods also require the most air to control a given process, making optimization of their performance an economic necessity. Slot hoods and side draft hoods are common types of capture hoods.

The hoods may be flanged or unflanged as shown on Figure 1.2. Flanged hoods are better because they eliminate air flow from ineffective zones where no contaminants exist. Increasing the hood effectiveness in this manner will usually reduce air requirements.

Air flow and particle movement in ducts, fans and filtration are relatively well developed. The hood may be considered the most important part in the local exhaust system. If the hood fails to capture the contaminants the efficiency of the system is meaningless as the main aim of a local exhaust system is to capture the contaminants produced in front of the hood.

The design of industrial ventilation has been neglected for a long time. The current design procedure for exhaust hoods is based on the selection of a proper capture or design velocity followed by the use of an equation to predict the actual velocity at the point of release as a function of hood air flow and distance along the hood centerline. The capture velocity is defined by the American Conference of Governmental Industrial Hygienists (2), as the velocity at any point in front of the hood necessary to overcome opposing currents and capture the contaminated air by causing it to flow into the hood. In this procedure the effect of cross-draft is not quantified and this is one of the problems which may face the

design engineer in choosing the proper capture velocity. The current increased demand to improve the workplace environment, means that more accurate techniques are required to solve the complex ventilation problems which are faced by industry.

The objective of this research was to develop, and validate experimentally, a model for predicting particle movement into flanged circular local exhaust hoods. The research project was divided into two steps:

1) Development of a theoretical model for predicting particle movement into a flanged circular hood in the presence of cross-drafts.

2) Validation of the theoretical model by comparing the theoretical particle trajectories with experimental trajectories.

1.2 REVIEW OF LOCAL EXHAUST HOOD DESIGN

The design of local exhaust hoods has been neglected for a long time. Dalla Valle's(3) doctoral thesis in 1930 and Silverman's(7) doctoral thesis in 1943 were the first work to predict air velocity in front of local exhaust hoods. Hemon in his book (plant and process ventilation,1963)(8) discussed the production and the motion of airborne contaminants using empirical equations to design local hoods. Fletcher(9,10) in 1977 developed empirical equations to predict air velocity in front of unflanged round, square, rectangular, and slot hoods. Garrison(11-13) in 1977 to 1983 conducted many experiments and developed empirical equations to predict air velocity in front of flanged and unflanged round ,square, rectangular, and slot hoods. The empirical models developed by Dalla Valle, Silverman, Fletcher, and Garrison are shown in Appendix A. These models predict the centerline velocity as a function of hood shape, air flow into the hood, distance of the source from the hood, and the hood area. The air flow necessary to obtain the desired capture velocity is calculated by using one of these models. The latter models developed by Fletcher and Garrison can be considered as refinments to the work

done by Dalla Valle and Silverman.

Bender(14) in 1979 developed a model technique to examine the performance of large industrial canopy fume hoods and the effect of cross-drafts on capturing the contaminants, and concluded that cross-draft is a very important factor which must be considered in designing canopy hoods.

Heinsohn, Johnson and Davis(15) in 1982 have examined the use of CAD system design for ventilation. This design has been used for designing a grinding booth for large castings, and they reported that there is good agreement between theoretical and experimental results.

Masood(16) in 1983 examined the parameters which will affect the capture of dust by hoods and found that the capture velocity is dependent on particle size, density, emission velocity, direction of emission, size of the emission source and the hood geometry, the empirical models developed by Masood are shown in section 1.6 in this chapter. Stewart(26) in 1985 examined existing guidelines for designing exhaust hoods. After discussing the design of canopies for cold and hot processes, he concluded that the heat released from hot sources must be considered in designing canopy hoods.

Flynn and Ellenbecker(17-19) in 1987; Conroy and Ellenbecker(20) in 1988; Conroy et al(21) in 1988 have used models to predict air flow into flanged circular and flanged rectangular slot hoods. These models can be used to quantify the effect of cross-drafts on hood air flow patterns and capture efficiency and are based on analytical solutions to Laplace's equation for frictionless, incompressible, and irrotational fluid flow. Alenius(22) in 1986 used numerical models to predict air flow into flanged circular, rectangular, and rectangular slot hoods. Alenius's models used numerical methods to solve Laplace's equation for frictionless, incompressible, and irrotational fluid flow. The theoretical models developed by

Flynn and Ellenbecker, and Alenius are shown in chapter 3.

When contaminant sources cover a considerable area or are subject to cross-drafts, the empirically predicted centerline velocity will not give an accurate prediction of hood performance. Velocity contours in front of hoods are elliptical in shape and an adequate capture velocity on the centerline at the edge of area source will result in lower, and perhaps inadequate velocities at the corners of the source.

A more quantitative index of hood performance is capture efficiency. Capture efficiency may be defined as the ratio between the contaminants captured by the hood to the generated contaminants. Ellenbecker et al(23) in 1983 have shown capture efficiency to be a function of hood air flow, hood area and geometry, distance from the hood, and the cross-draft velocity.

Theoretical models to predict the air flow in front of hoods would be very helpful for design engineers. These models must be examined experimentaly in the presence of cross-drafts before they are used in design applications. Existing empirical models are easier to use but they only predict the hood centerline velocity and they are valid to a certain limit. Most empirical models do not quantify the effect of cross-draft on hood design while it should be easy to quantify the effect of cross-draft on hood design given suitable theoretical models. Cross-draft is a very important factor which must be considered in designing hoods.

1.3 SOURCES OF CONTAMINANTS

Contaminants in a workplace can be found as solid particles or in form of vapours and gases. The two main mechanisms by which dust can be generated are pulvation and condensation. Pulvation is the prime mechanism of dust

generation in materials handling. Pulvation is a word coined by Hemon(8) and is defined as a non-molecular mechanical process whereby dust becomes suspended in air from a previous state of rest. Clouds of dust are formed as the result of two events in sequence. Firstly a mechanical or pneumatic action which projects particles into the air, and secondly air currents transport the dust particles from the place of generation.

The Warren Spring Laboratory(24) in Stevenage, U.K. introduced the pulvation equation for the aerodynamic seperation of particles from bulk materials. Consider a mass of particles subjected to an air stream from beneath in such a way that some of the top layers of particles become airborne. A particle in the top layer leaves the subtrate when the air velocity is such that the aerodynamic drag force on the particle overcomes the particle weight and the force of cohesion of the particle to those in the the layer beneath.

Aerodynamic Drag Force on Particle	>	Particle Weight	+	Force of Cohesion of Particle to Powder Bulk

The pulvation process produces different sizes of airborne particles. The large particles do not remain airborne for as long as small ones. These large particles have been termed inertials by Hemon(8). Examples of dust generation are grinding and handling of dry powder materials.

1.4 HAZARDS OF AIR CONTAMINANTS

Hazards of air contaminants in a workplace can be divided into two types; health hazards and hazards of fires and explosions. One of the greatest reasons for studying aerosol behavior is its relation to health. It is known that small particles contribute to respiratory disease. The contaminants enter the human body through the respiratory system. When these contaminants are breathed into the

respiratory system and retained in the body, they may cause different diseases. The link between disorders of the human body and specific contaminants has been difficult to recognise in most cases. However diseases of pneumoconiosis, emphesyma, and lung cancer represent classes of results from suspected chemical assaults. Viral and bacteriological links of infections have been established with influenza, bronchitis, pneumonia, and tuberculosis. Specific concentrations of contaminants are flammable or explosive.

1.5 THE PROBLEMS OF DESIGNING LOCAL EXHAUST HOODS

The current design procedure for exhaust hoods as described in the American Conference of Governmental Industrial Hygienists (Industrial Ventilation Manual) as shown in Figure 1.3 is based on the selection of a proper capture velocity dependent on the release velocity of the contaminants, the magnitude of disturbing air currents and the toxicity of the contaminants. The hood is then designed to produce this velocity at the point of release using an equation to predict velocity as a function of hood air flow, geometry and distance along the hood centerline.

DallaValle(3), Silverman(4-7), Garrison(11,13), and Fletcher(9,10) have presented empirical models(Appendix A) for centerline velocity as a function of hood shape, air flow into the hood, distance of the source from the hood, and the hood area. The air flow necessary to obtain the desired capture velocity is calculated by using one of these models. Hemon(8) describes the dust generation process as a kind of pulvation where particles are ejected from a mass of material and defines the null point for a particular particle as the point where it expends its energy and is then at the mercy of local air currents, the position of the null point can be determined by eye or by using a dust lamp. The capture of the dust cloud can be determined by ensuring that the air flow at the null point is directed towards the hood. Table 1.1 shows the capture velocities recommended by Hemon. A similar approach to that of Hemon is used by Alden and Kane(25)

and ACGIH(2), and their capture velocities are given in Table 1.2. For example Hemon recommended capture velocity of 0.3m/sec in case of contaminants released with practically no velocity into quiet air while the recommended capture velocity given by Alden and Kane is 0.5m/sec.

It can be seen that the latter capture velocities and volume exhaust rates are much higher than those recommended by Hemon in Table 1.1. These differences highlight the difficulties facing the design engineer to select a suitable capture velocity especially when energy considerations require that exhaust rates should be kept as low as possible. The difficulty with Hemon's approach is the difficulty of determining the null point, it is also difficult to judge what is meant by "moderately draughty" or "very draughty", "low toxicity" and "high toxicity". The recommended capture velocities for hoods given in Table 1.2 are also found in the American Society of Heating, Refrigerating and Air-Conditioning Engineers Handbook(27) and the Chartered Institute of Building Services Engineers Guide(28)

The procedure of the American Conference of Governmental Industrial Hygienists is very difficult to apply. In this procedure the release velocity of the contaminants is not quantified and the effect of cross-draft is not quantified even though cross-draft is a very important factor which must be considered in the design of exhaust hoods especially for particles smaller than 10 micron in diameter. The selection of the capture velocity is also dependent on other factors such as contaminant toxicity, contaminant production, and hood size. None of these factors are quantified.

Masood(16) has reported on results from an experimental program to study the parameters which affect the capture of dust by hoods. These parameters are, size of the particles to be captured, density of the material, emission velocity, direction of the emission, size of the emission source and the hood geometry.

The relationship obtained for unflanged square hood is given as:

$$(V_{cf}/V_j)^2 \ (V_t/V_j) = 11.7943 \exp(3.065 \ X/L) \qquad (1.1)$$

where

V_{cf} is the capture velocity at the face of the hood.

V_j is the emission velocity.

X is the distance measured from the hood face.

L is the hood length.

V_t is the terminal settling velocity of the particle.

Masood reported that a reduction of 37% in the capture velocity at the face of the hood is obtained by the flanged hood over the unflanged hood when the ratio between the distance of the release point from the face of the hood, to the hood length is between 0.25 and 1.25. The experimental program of Masood did not consider the effect of cross-draft on hood design.

The concept of flanged and unflanged is not well quantified. Fletcher(10) has shown that the optimum flange width is the square root of the hood area beyond which there is little further increase in velocity. Although the centerline velocity for a flanged hood may be more than 20% greater than for unflanged hood of the same dimensions the major advantage of a flanged hood that air is being pulled from the effective zone of the hood. Relationships between the width of the flange and the volume of exhaust air are not quantified.

The concept of capture efficiency is a good way to quantify hood performance. Capture efficiency is the fraction of contaminant generated which is captured directly by the hood. This concept gives a direct indication if the contaminant in front of the hood are captured or not, and the main aim of the hood is to capture the contaminants produced in front of it. In practice it may

easy to determine the captured contaminants, but on the other hand it is difficult to determine the generated contaminants with sufficient accuracy.

1.6 MODELLING METHODS FOR AIR FLOW IN FRONT OF LOCAL EXHAUST HOODS

Modelling air flow in front of local exhaust hoods can be divided into two types, experimental methods and theoretical methods. In experimental methods empirical equations of air flow in front of local exhaust hoods can be developed by doing a series of measurements of the parameters which influence the movement of air in front of these hoods. In theoretical methods, the approach can be achieved either by solving Navier–Stokes equation or by using potential flow theory for frictionless, incompressible, and irrotational fluid flow. These methods are examined in detail in chapter 3 of this thesis.

1.7 REFERENCES

1. Goodfellow, H.D.: Advanced design of ventilation systems for contaminant control. Imprint–Amsterdam Oxford C1985.

2. Industrial Ventilation– A Manual of Recommended Practice, 17th ed. American Conference of Governmental Industrial Hygienists, Committee on Industrial Ventilation, Lansing, MI (1982).

3. DallaValle, J.M.: Studies in the Design of Local Exhaust Hoods. Doctoral Thesis, Harvard University (1930).

4. Silverman, L.: Fundamental Factors in the Design of Lateral Exhaust Hoods for Industrial Tanks. The Journal of Ind. Hyg. and Tox. 23(5):187–226 (1941).

5. Silverman, L.: Centerline Velocity Characteristics of Round Openings Under Suction. The Journal of Ind. Hyg. and Tox. 24(9):259–266 (1942).

6. Silverman, L.: Velocity Characteristics of Narrow Exhaust Slots. The Journal of Ind. Hyg. and Tox. 24(9):267–276 (1942).

7. Silverman, L.: Fundamental Factors in the Design of Exhaust Hoods. Doctoral Thesis, Harvard University (1943).

8. Hemeon, W.C.L.: Plant and Process Ventilation, Industrial Press Inc., New York, N.Y.(1963).

9. Fletcher, B.: Centerline Velocity Characteristics of Rectangular Unflanged Hoods and Slots Under Suction. Ann. Occup. Hyg. 20:141–146 (1977).

10. Fletcher, B.: Effect of Flanges on the Velocity in Front of Exhaust Ventilation Hoods. Ann. Occup. Hyg. 21:265–269 (1978).

11. Garrison, R.P.: Nozzle Performance and Design for High Velocity/Low Volume Exhaust Ventilation. Doctoral Thesis, University of Michigan (1977).

12. Garrison, R.P.: Centerline Velocity Gradient for Plain and Flanged Local Exhaust Inlets. Am. Ind. Hyg. Assoc. J. 42(10):739–746 (1981).

13. Garrison, R.P.: Velocity Calculation for Local Exhaust Inlets–Empirical Design Equations. Am. Ind. Hyg. Assoc. J. 44(12):937–940 (1983).

14. Bender, M.: Fume Hoods, Open Canopy Type – Their Ability to Capture Pollutants in Various Environments. Am. Ind. Hyg. Assoc. J. 40(2):118–127 (1979).

15. Heinsohn, R.J., Johnson, D. and J.W. Davis: Grinding Booth for Large Casting. Am. Ind. Hyg. Assoc. J. 45(8):587-595 (1982).

16. Masood, T.: The Capture of Dust by Hoods, Dust and Material Handling, Report No. 13, Warren Spring Laboratory, Stevenage, U.K. (June 1983).

17. Flynn, M.R. and M.J. Ellenbecker: The Potential Flow Solution for Air Flow into a Flanged Circular Hood. Am. Ind. Hyg. Assoc. J. 46(6):318-322 (1985).

18. Flynn, M.R. and M.J. Ellenbecker: Capture Efficiency of Flanged Circular Exhaust Hoods. Ann. Occup. Hyg. 30(4):497-513 (1986).

19. Flynn, M.R. and M. J. Ellenbecker: Empirical Validation of Theoretical Velocity Fields into Flanged Circular Hoods. Am. Ind. Hyg. Assoc. J. 48(4):380-389 (1987).

20. Conroy, L. and M. Ellenbecker: Capture Efficiency of Flanged Slot Hoods under the Infuence of a Uniform Crossdraft, Doctoral Thesis, Harvard School of Puplic Health, Boston (1988).

21. Conroy, L., M. Ellenbecker, and M. Flynn: Prediction and Measurement of Velocity into Flanged Slot Hoods. Am. Ind. Hyg. Assoc. J. 49(5):226-234 (1988).

22. Alenius, S.: Calculation of air velocities outside exhaust openings with flange. Method and results. Undersokningsraport 1986:5. Arbetarskydsstyrelsen, FTV Solna, Sweden (1986).

23. Ellenbecker, M.J., R.E. Gempel, and W.A. Burgess: Capture Efficiency of Local Exhaust Ventilation Systems. Am. Ind. Hyg. Assoc. J. 44(10):752-755 (1983)

24. Mufitt, P.G.: Materials Properties and Dustiness, Report No.1, Dust and Materials Handling Research Project, Warren Spring Laboratory, Stevenage, U.K. (Oct. 1980).

25. Alden, J.L. and J.M. Kane: Design of Industrial Ventilation Systems. Industrial Press Inc.,New York, N.Y. (1982).

26. Stewart, L.J.: Design Guidelines for Exhaust Hoods, Technical Note TN 3/85, Building Services Research and Information Association, U.K. (1985).

27. American Society of Heating, Refrigerating and Air-Conditioning Engineers, Inc.: ASHRAE HANDBOOK, Heating, Ventilation, and Air-Conditioning Applications, U.S.A. (1991).

28. The Chartered Institution of Building Services Engineers: CIBSE GUIDE, Volume B, Instalation and Equipment Data, U.K. (1986).

CHAPTER 2 AEROSOL BEHAVIOR IN AIR

2.1 INTRODUCTION

An aerosol can be defined as solid or liquid particles suspended in a gas. These airborne particles vary greatly in their ability to affect not only visibility and climate but also our health and quality of life. Aerosols are two-phase systems, comprising both the particles and gas in which they are suspended. It is important to understand the properties of aerosols. Aerosol properties influence the production, and transport of atmospheric particulate pollutants. The measurement and control of particulate pollutants in the occupational and general environments require applications of this knowledge.

Aerosol technology grew in importance because of an increased environmental concern for the health effects arising from air pollution in community and occupational environments. It has become an important tool in understanding the effect we have on our environment and the impact of that environment on us. Aerosol technology is used in the fields of industrial hygiene, air pollution control, inhalation toxicology, atmospheric physics and chemistry, and radiological health.

2.2 AEROSOL CONCENTRATION

The most commonly measured aerosol property, and the most important one from the standpoint of health and environmental effects is mass concentration, the mass of particulate matter in a unit volume of aerosol. Common units are g/m^3, and mg/m^3.

Another common measure of concentration is number concentration, the number of particles per unit volume of aerosol. Common units are $number/m^3$. Unlike gaseous contaminants, volume ratio or mass ratio in parts per million(ppm)

are not used for aerosols because two phases are involved and aerosol concentrations are numerically very low when expressed in this way. Figure 2.1 shows the extremely wide range(from 0.001 to 1000 g/m^3) of aerosol concentration that one encounters in practice.

2.3 DRAG FORCE

The motion of particles is affected by the inertia of the particle and aerodynamic drag. When a particle moves through air the viscosity of the air produces a force on the particle in the opposite direction to the relative velocity. The drag force on a sphere(F_d) given by Stokes's Law is for Reynolds number$<<1$, but for different values of Reynolds number the drag force is given by Heinsohn(1) as:

$$F_d = - C_d \frac{1}{C} A_p \frac{\rho}{2} (V - U) |V - U| \qquad (2.1)$$

where

U is the air velocity.

V is the particle velocity.

C_d is the drag force factor.

C is the Cunningham slip correction factor.

(C is dependent of the particle size and on the mean free path of the molecules forming the air).

ρ is the air density.

A_p is projected particle area, perpendicular to the direction of relative motion to the air.

$(V-U)=V_r$ is the magnitude of the particle velocity (relative to the air).

$|V-U|$ is the particle velocity vector (relative to the air).

The drag force factor is dependent on the particle Reynolds number. Figure 2.2 shows the relationship between the drag force factor for a sphere and the Reynolds number. It is common practice to divide Figure 2.2 into three flow regimes:

Stokes flow regime: $Re < 1$, $C_d = \frac{24}{Re}$

Allen flow regime: $1 < Re < 10^3$, C_d = variable

Newtonian flow regime: $10^3 < Re < 10^5$, $C_d = 0.4$

In Industrial ventilation, the particle motion is in Allen flow regime. The relationship between the drag coefficient and Reynolds number for $0 < Re < 10^5$ is given by Heinsohn(1) by the following equation with an accuracy of 10% as,

$$C_d = 0.4 + \frac{24}{Re} + \frac{6}{(1 + Re^{0.5})} \qquad (2.2)$$

The particle Reynolds number for spherical particles is defined as:

$$Re = \frac{\rho D_p (V - U)}{\mu} \qquad (2.3)$$

For particles moving in motionless air, the relative velocity is the particle velocity.

The Cunningham slip correction factor for a particle is a correction for the surrounding air not being a truly homogeneous but a mixture of moving individual molecules. This correction is large if the particle size does not essentially exceed the mean free path of the molecules forming the air(0.06 micron at normal

pressure and temperature).

The Cunningham slip correction factor is given by Jenning(2) as:

$$C = 1 + \frac{\lambda}{D_p} \left[2.514 + 0.8 \exp \left[- \frac{0.55\ D_p}{\lambda} \right] \right] \qquad (2.4)$$

λ is the mean free path of the molecules forming the air.

2.4 PARTICLE MOTION

The motion of a particle in air is influenced by a gravity force, a drag force, and a buoyancy force. The particle motion can be described by Newton's Law of motion. The acceleration of a particle is proportional to the sum of the influencing forces divided by the mass of the particle. The acceleration vector is the second differentiation of the particle location vector with respect to time. Therefore it is possible to describe the motion of the particle as a particle trajectory with the locations as a function of the time elapsed. The motion of a particle through air can be considered to uneffected by other particles and not to affect the air velocity field if the number of particles per unit volume of air is less than a certain value as given by Hinds(3), (the average distance between particles should be at least 10 times the particle diameter). In industrial ventilation the particle concentration is hundreds of times less than this. The motion of a single spherical particle can be expressed as:

Mass X Acceleration = Drag Force + Gravity Force

+ Buoyancy Force

Using equation (2.1) for the drag force gives

$$\left[\frac{\pi\ D_p^3}{6}\right]\rho_p\ \frac{dV}{dt} = -\ \left[\frac{C_d\ \rho}{2\ C}\right]\left[\frac{\pi\ D_p^2}{4}\right](V-U)\,|V-U| - \left[\frac{\pi\ D_p^3}{6}\right]\rho_p\ g\ +$$

$$\left[\frac{\pi\ D_p^3}{6}\right]\ \rho\ g \qquad (2.5)$$

2.4.1 Particle Motion In moving Air

If we consider a spherical particle moving through a two dimensional air stream in which the air velocity(U) is variable as shown in Figure 2.3, then the particle acceleration motion can be expressed as:

$$\frac{dV}{dt} = -\ j\ g\ \left[1 - \frac{\rho}{\rho_p}\right] - \left[\frac{3\ C_d}{4\ C}\right]\ \left[\frac{\rho}{\rho_p\ D_p}\right]\ (V - U)\ |V - U|$$

(2.6)

where the relative velocity(V–U) is

$$(V - U) = i(V_x - U_x) + j(V_y - U_y)$$

$$= i\ V_{rx} + j\ V_{ry} \qquad (2.7)$$

where

V_{rx} is the particle relative velocity in horizontal direction.

V_{ry} is the particle relative velocity in vertical direction.

$$|V - U| = \left[V_{rx}^2 + V_{ry}^2 \right]^{\frac{1}{2}} \qquad (2.8)$$

where i and j are nodal coordinates.

Equation (2.6) can be expressed in differential way as:

$$\frac{dV_x}{dt} = \left[\frac{-3\ C_d}{4\ C}\right] \left[\frac{\rho}{\rho_p\ D_p}\right] V_{rx} \left[V_{rx}^2 + V_{ry}^2 \right]^{\frac{1}{2}} \qquad (2.9)$$

$$\frac{dV_y}{dt} = -g \left[1 - \frac{\rho}{\rho_p}\right] - \left[\frac{3\ C_d}{4\ C}\right] \left[\frac{\rho}{\rho_p\ D_p}\right] V_{ry} \left[V_{rx}^2 + V_{ry}^2 \right]^{\frac{1}{2}}$$

(2.10)

The Reynolds number can be expressed as:

$$Re = \rho\ D_p\ \frac{\left[V_{rx}^2 + V_{ry}^2 \right]^{\frac{1}{2}}}{\mu} \qquad (2.11)$$

If the motion of the particles is beyond the Stokes region, equations (2.9) and (2.10) have to be solved numerically to calculate the particle velocity and trajectory. In order to solve equations (2.9) and (2.10) numerically by writing them as:

$$\frac{dV_x}{dt} = A\ V_x + B \qquad (2.12)$$

$$\frac{dV_y}{dt} = A\ V_y + D \qquad (2.13)$$

where

$$A = -\left[\frac{3\ C_d}{4\ C}\right] \left[\frac{\rho}{\rho_p\ D_p}\right] \left[(V_x - U_x)^2 + (V_y - U_y)^2 \right]^{\frac{1}{2}} \qquad (2.14)$$

$$B = - A U_x \qquad (2.15)$$

$$D = - A U_y - g \left[1 - \frac{\rho}{\rho_p}\right] \qquad (2.16)$$

The equations can be solved numerically by computing the particle velocity and location at the end of a small interval of time δt. The velocity and location will be computed at the end of the first interval, $t_1 = \delta t$. If the velocity and location are known at t_1 as initial values, the velocity and location can be computed at the second time interval $t_2 = t_1 + \delta t$. The process can be repeated until the particle travels some prescribed distance or some prescribed time. The Runge-Kutta method (Appendix B) can be used.

2.5 REFERENCES

1. Heinsohn, R.J.: Industrial Ventilation Engineering Principles. Wiley Interscience Publications, New York (1990).

2. Jenning, S.G.: The Mean Free Path. Aerosol Sci., J. 19(2):159-166 (1988).

3. Hinds, W.C.: Aerosol Technology. Wiley Interscience Publications, New York (1982).

CHAPTER 3 MODELLING AIR FLOW FIELDS IN FRONT OF LOCAL EXHAUST HOODS

3.1 MODELLING METHODS

Modeling air flow in front of local exhaust hoods can be divided into two types Experimental methods and theoretical methods. In experimental methods empirical equations describing the air flow in front of local exhaust hoods can be developed by doing a series of measurements to quantify the parameters which influence the movement of air in front of these hoods. In theoretical methods, the approach can be either by solving Navier–Stokes and continuity equations or by using potential flow theory for frictionless, incompressible, and irrotational fluid flow. Prandtl and Tietjens(1) reported that specific air flow fields may, in principle, be determined by solving the Navier–Stokes and continuity equations. Rhyming(2) suggested that in practice there is no analytical solution to Navier–Stokes equations, and numerical procedures must be applied. Some General Fluid Dynamics Computer Codes for developing numerical solutions exist, such as Fluent, Phoenics and Teach–3D. These programs require knowledge of fluid mechanics, need a long time to compute the complicated equations used and the results are very sensitive to how the boundary conditions are defined. Potential flow theory was used in this thesis to model air flow in front of local exhaust hoods.

In modelling air flow in front of local exhaust hoods, Baturin, Dalla Valle, Engels and Willert, and Garrison (3,4,5,6) reported that the air flow fields generated by simple exhaust hoods of the same design may be assumed to have flow similarity. Therefore one model of the air flow field of an exhaust hood of a specific shape is sufficient regardless of the opening size or air flow rate. So the flow field modelling problem is simplified by assuming flow similarity for exhaust openings of the same geometrical design.

3.2 POTENTIAL FLOW THEORY AND THE NAVIER-STOKES EQUATION OF MOTION

The continuity equation for steady state, incompressible fluid flow states that the divergence of the velocity is zero :

$$\nabla.\vec{V} = 0 \qquad (3.1)$$

where

$\vec{V}$ is the velocity.

$\nabla.$ is the divergence of a vector.

If the flow is also irrotational and the viscosity is to be considered zero the result is Laplace's equation :

$$\nabla^2\Phi = 0 \qquad (3.2)$$

where

∇^2 is the Laplacian vector.

Φ is the scalar velocity-potential function.

Analysis of Laplace's equation is well developed by White (7) and is termed potential theory.

In potential flow the velocity at any point is the gradient of velocity-potential function :

$$\nabla \Phi = \vec{V} \qquad (3.3)$$

where ∇ is the gradient of a scalar.

In potential flow the fluid is considered incompressible and frictionless; i.e.,no shear forces were assumed to exist between fluid elements. This assumption holds well on fluids with low viscosity in many cases of practical importance but not in all. It is particulary poor in describing flow phenomena in the vicinity of solid bodies. The motion of incompressible viscous fluid is well described by the Navier–Stokes equation :

$$\frac{dv}{dt} = g - \frac{1}{\rho} \text{ grad } P + \frac{\mu}{\rho} \nabla^2 V \qquad (3.4)$$

where

g is the acceleration due to gravity.

P is the the fluid pressure.

ρ is the fluid density.

μ is the fluid dynamic viscosity.

Equation 3.4 was developed by Prandtl and Tietjens from Newton's fundamental law of mechanics :

Mass X Acceleration = Force

The fundamental difference between velocity–potential and Navier–Stokes equation for fluid is the friction term $(\mu/\rho)\ \nabla^2\ V$. Mathematically speaking, this point is very important, since the velocity–potential equation contains only the first derivative of velocity while the Navier–Stokes equation contains the second derivative of velocity in the friction term. In other words, this equation is of higher order. The need for a higher–order equation can also be explained on physical grounds by consideration of the boundary conditions which must be fulfilled at the interface between the viscous fluid and a solid body. The Navier–Stokes equation, the continuity equation, and the boundary conditions are necessary and sufficient to determine completely the motion of a viscous fluid. The mathematical difficulties involved in solving Navier–Stokes equation have

encouraged the use of the potential flow theory to describe the motion of fluid because it is easier to use mathematically.

It should be noted here that the friction term of the Navier–Stokes equation will not play an important part where potential flow can be assumed. This is true in practice for fluids of low viscosity (water, air) some distance away from the edges of fixed boundaries. Air is viscous and compressible but there are many industrial situations in which air behaves as if its viscosity is negligible and its density and temperature are constant. The region in the vicinity upstream of the exhaust hood(but not at the hood face), is a region where these conditions occur.

3.3 ANALYTICAL MODELS FOR AIR FLOW FIELDS INTO CIRCULAR FLANGED EXHAUST HOODS

Theoretical models of the three–dimensional velocity field into a flanged circular hood have been developed by Flynn and Ellenbecker(8), Ellenbecker et al(9), and Jansson(10).

The three models of air flow into flanged circular hoods developed by Flynn and Ellenbecker are described below. They were examined by the same authors and a final model with empirical modifications was selected which is also described.

Due to the axial symmetry, the cylindrical coordinate system(r,θ,z) will be used, where:

z is the axial distance along the hood centerline perpendicular to the hood face (The z–coordinate is directed from the exhaust opening centre point and outwards).

r is the radial distance perpendicular to z–axis in any direction (The r–coordinate axis is directed from the centreline of the opening, perpendicular to it and outwards) as shown in Figure 3.1.

θ is the angle that the r position vector makes with the reference base plane(θ=0, 180).

3.3.1 Model 1

The strict potential flow model (Model 1) of a flanged circular hood states that the total theoretical velocity(V_T) at any point (r,θ,z) is:

$$V_{T1} = \sqrt{(V_{R1})^2 + (V_{Z1})^2} \qquad (3.5)$$

where

V_R is the theoretical radial velocity.

V_Z is the theoretical axial(Z) velocity.

and there is no rotation about the hood centreline.

The numeric subscripts used with the velocities refer to the model being used. In this model,

$$V_{R1} = -\left[\frac{Q}{\pi}\right]\left[\frac{(a + r)\gamma 2 + (r - a)\gamma 1}{(\gamma 1 + \gamma 2)\gamma 1\gamma 2\sqrt{(\gamma 1 + \gamma 2)^2 - 4a^2}}\right] \qquad (3.6)$$

$$V_{Z1} = \frac{-Q\,Z}{\pi\,\gamma 1\,\gamma 2\sqrt{(\gamma 1 + \gamma 2)^2 - 4a^2}} \qquad (3.7)$$

$$\gamma 1 = \sqrt{z^2 + (a + r)^2} \qquad (3.8)$$

$$\gamma 2 = \sqrt{z^2 + (a - r)^2} \qquad (3.9)$$

where

Q is the hood flow.

a is the hood radius.

For any meridian plain the points (+a,0) and (−a,0) can be selected as foci on the r axis (see Figure 3.2). For any point P(r,z) the distance from −a to P is $\gamma 1$, and the distance from +a to P is $\gamma 2$. The theoretical tangential velocity is zero for all models, the angle (β) that the velocity vector makes with the hood centerline (z−axis) is :

$$\beta = \tan^{-1}\left[\frac{V_{R1}}{V_{Z1}}\right] \qquad (3.10)$$

3.3.2 Model 2

An alternative model was developed based on examinations of Dalla Valle's empirical results and on theoretical modifications to the strict potential flow solution. The modified potential flow solution (Model 2) gives the total theoretical velocity at any point (r,θ,z) as :

$$V_{T2} = \frac{\sqrt{3}\ Q\ \epsilon^2}{2\ \pi\ a^2\left[3 - 2\ \epsilon^2\right]^{\frac{1}{2}}} \qquad (3.11)$$

The quantity ϵ is called the eccentricity and it is the ratio of the hood diameter to the sum of the distances from the edges of the hood to any point in front of the hood and is given as :

$$\epsilon = \frac{2\ a}{\gamma 1 + \gamma 2} \qquad (3.12)$$

Model 2 predicts a different value for the velocity vector (as shown in the next page), but the direction is still given by (β) in equation 3.10. Therefore the velocities are given as :

$$V_{R2} = -\ V_{T2}\ (\sin\ \beta) \qquad (3.13)$$

$$V_{Z2} = -\ V_{T2}\ (\cos\ \beta) \qquad (3.14)$$

Model 1 and 2 derivations are found in reference (11).

3.3.3 Model 3

The third model is based on the fact that the total velocity at any point must equal the flow (Q) divided by the surface area inside the contour on which the point lies. The contours according to (Model 2) are half oblate ellipsoids (for the confocal ellipsoids that are the equipotential surfaces the gradient is not constant a long a given surface, the gradient becomes steeper near the flange. This difference in gradient is negligible far from the hood where the equipotential surfaces are nearly spheres, close to the hood face this difference is important) with surface areas (A_S) of :

$$A_S = \frac{1}{2}\left[2\pi c^2 + \pi \frac{d^2}{\epsilon} \text{Ln} \left[\frac{1+\epsilon}{1-\epsilon}\right] \right] \qquad (3.15)$$

where :

$$c = \frac{a}{\epsilon} \qquad (3.16)$$

$$d = \left[c^2 - a^2\right]^{\frac{1}{2}} \qquad (3.17)$$

The total theoretical velocity is given as :

$$V_{T3} = \frac{Q}{A_S} \qquad (3.18)$$

The direction of the velocity vector is predicted by equation 3.10, and the component velocities are given as :

$$V_{R3} = - V_{T3} (\sin \beta) \qquad (3.19)$$

$$V_{Z3} = - V_{T3} (\cos \beta) \qquad (3.20)$$

3.3.4 The Final Model

The first two models have particular singularities or inconsistencies. An inconsistent model is one that is not exact mathematically, while a singularity in a model refers to a region where unrealistic fluid behavior occurs. Model 1, the potential flow solution is a consistent but singular model. At the edges of the hood face (r=a,z=0), the predicted velocities are infinite, while at the center of the hood face(r=0,z=0), the theoretical velocity is $Q/2\pi a^2$ or half the average face velocity. The neglect of frictional forces by the potential theory and the boundary condition of constant potential at the hood face lead to these singularities which limit the utility of Model 1 near the hood face.

Model 2 is inconsistent, the velocity field does not integrate to give the specified flow of Q. This can be shown by solving equation 10 for velocity at the hood face (ϵ=1). The result is that the theoretical average face velocity is $3\ Q/(2\pi a^2)$ or 87% of the actual average face velocity. This iconsistency is the result of approximations in the derivation of the model; these approximations enable improvement over Model 1 in the ability to predict velocities, but create inconsistent Model 2. This inconsistency leads to empirical modification in the final model. Model 3 is neither singular nor inconsistent, but it suffers from complicated mathematics.

Experiments were conducted by Flynn and Ellenbecker to measure velocities in front of different flanged circular hoods. The results show that Model 2 and 3 are much better in predicting the velocities than Model 1. Further analysis of component velocities indicated that both Model 2 and 3 would require empirical modifications to their predicted velocities. Model 2 was selected as the best model because it was nearly as good as Model 3 at prediction and was easier to use mathematically. The analysis of component velocities in Model 2 indicated that the radial velocity increased more rapidly than predicted as $\epsilon \rightarrow 1$ (as the hood face

was approached). A radial correction factor (C_r) was determined which, when multiplied by the predicted radial velocity would more accurately reflect the true radial velocity, the factor (C_r) is given as :

$$C_r = 2.6\ \epsilon^{18} + 0.853 \qquad (3.21)$$

In addition, the theoretical axial velocities were adjusted by multiplying the experimentally calculated slope by 0.9. By adding both empirical corrections to Model 2, the final model is obtained :

$$V_T = \left[V_R^2 + V_Z^2\right]^{\frac{1}{2}} \qquad (3.22)$$

$$V_R = C_r\ V_{R2} \qquad (3.23)$$

$$V_Z = 0.9\ V_{Z2} \qquad (3.24)$$

The direction of the velocity vector in the final model is also predicted by equation 3.10.

The final model is in good agreement with previous investigations. In the 1930s, Dalla Valle(12) used empirical correlations to establish the centerline velocity gradient into a flanged circular hood :

$$100 - Y = \frac{100}{1 + e^{-3.5(\log x - \log x_0)}} \qquad (3.25)$$

$$\log x_0 = -0.624 + 1.09\ (\log d) \qquad (3.26)$$

where :

d is the the hood diameter in inches.

x is the centerline distance from the hood face in inches.

Y is the percentage of the hood face velocity.

Equations 3.25 and 3.26 are Dalla Valle,s exact formula that is usually approximated by :

$$V_{c1} = \frac{Q}{0.75\ (10\ x^2 + \pi a^2)} \qquad (3.27)$$

where :

x is the centerline distance in feet.

V_{c1} is the centerline velocity at x in feet/min.

Figure 3.3 shows the centerline predictions of the final model vs. Dalla Valle's exact formula. The two essentially are identical. Dalla Valle's work has been confirmed by Pruzner(13) and again by Fletcher(14). The only serious challenge came from Silverman(15) who did not agree with the method Dalla Valle used to calibrate the modified pitot tube used in his measurements. Silverman used thermometers approximately 0.5 inch long; in effect this size of sensor measures an integrated velocity and is not a good approximation of a point velocity. In fact, close to the face of a 2 inch hood, it represents a substantial portion of the hood area and may significantly perturb the flow field.

3.3.5 Jansson's Model

Another model was developed by Jansson (10) may be classified as a semi-empirical potential flow solution. The basis of the model is a potential flow solution for constant potential in the inlet plane. The flanges are assumed to be infinite. The resulting equal potential surfaces, constitute a family of surfaces of half oblate spheroids(rotated ellipses). An assumption that the velocity is perpendicular to the spheroid surfaces together with the continuity equation leads to the model presented. The absolute value of the air velocity is determined by setting the velocity times the spheroid surface area equal to the air flow rate. The value of the air velocity is calculated from the ellipse eccentricity(ϵ), which in turn is a function of the coordinates in space. The

description is two-dimensional and the third dimension is obtained by a rotation about the Z-axis (see Figure 3.4).

The model is presented as non-dimensional descriptions. The non-dimensional air velocity in the inlet plane becomes equal to 1 and it is perpendicular to the plane. Non-dimensional velocities are obtained by dividing any velocity by the opening mean face velocity(Uo), (Uo=exhaust opening flow rate/opening area). The expression for the non-dimensional velocity value, U', is given by :

$$U' = \epsilon^2 / \left[1 + \frac{1 - \epsilon^2}{2\epsilon} \text{Ln} \frac{1 + \epsilon}{1 - \epsilon} \right] = \frac{U}{Uo} \qquad (3.28)$$

where

$$\epsilon = 1/\left[\sqrt{z'^2 + (r' + 0.5)^2} + \sqrt{z'^2 + (r' - 0.5)^2} \right] \qquad (3.29)$$

$$r' = \sqrt{x'^2 + y'^2} \qquad (3.30)$$

Ln is the natural logarithm function.

Non-dimensional distances for circular hoods are obtained by dividing by the hood diameter, this is denoted by '.

The individual velocity components are given by :

$$U'_z = - U' \cos \beta \qquad (3.31)$$

$$U'_r = - U' \sin \beta \qquad (3.32)$$

$$U'_x = U'_r \cos \gamma \qquad (3.33)$$

$$U'_y = U'_r \sin \gamma \qquad (3.34)$$

where

$$\beta = \text{atan}\left[(1 - \epsilon^2)\ \ r'/z'\ \right] \tag{3.35}$$

$$\gamma = \text{atan}\ (\ y'/x'\ ) \tag{3.36}$$

atan is the arcus tangent function.

3.4 ANALYTICAL MODEL FOR AIR FLOW FIELDS OF RECTANGULAR FLANGED EXHAUST HOODS

A model for air flow fields of a rectangular flanged exhaust hood has been developed by Tyaglo and Shepleve(16), and then presented in a non-dimensional form by Jansson(10).

The expressions for the non-dimensional velocities are :

$$U'_x = -\frac{1}{2\pi}\ \text{Ln}\left[\left[\sqrt{Z^{*2}_{+} + X^{*2}_{-} + Y^{*2}_{+}} + Y^{*}_{-}\right]\left[\sqrt{Z^{*2} + X^{*2}_{+} + Y^{*2}_{-}} + Y^{*}_{-}\right]\right]$$

$$+\frac{1}{2\pi}\ \text{Ln}\left[\left[\sqrt{Z^{*2} + X^{*2}_{+} + Y^{*2}_{+}} + Y^{*}_{+}\right]\left[\sqrt{Z^{*2} + X^{*2}_{-} + Y^{*2}_{-}} + Y^{*}_{-}\right]\right] \tag{3.37}$$

$$U'_y = -\frac{1}{2\pi}\ \text{Ln}\left[\left[\sqrt{Z^{*2} + Y^{*2}_{-} + X^{*2}_{-}} + X^{*}_{-}\right]\left[\sqrt{Z^{*2} + Y^{*2}_{+} + X^{*2}_{-}} + X^{*}_{-}\right]\right]$$

$$+\frac{1}{2\pi}\ \text{Ln}\left[\left[\sqrt{Z^{*2} + Y^{*2}_{+} + X^{*2}_{+}} + X^{*}_{-}\right]\left[\sqrt{Z^{*2} + Y^{*2}_{-} + X^{*2}_{-}} + X^{*}_{-}\right]\right] \tag{3.38}$$

$$U'_z = -\frac{1}{2\pi}\left[\operatorname{atan}\frac{X^*_+\ Y^*_+}{Z^*\sqrt{Z^{*2}+X^{*2}_+ + Y^{*2}_+}} - \operatorname{atan}\frac{X^*_-\ Y^*_-}{Z^*\sqrt{Z^{*2}+X^{*2}_- + Y^{*2}_-}}\right.$$

$$\left. - \operatorname{atan}\frac{X^*_+\ Y^*_-}{Z^*\sqrt{Z^{*2}+X^{*2}_+ + Y^{*2}_-}} + \operatorname{atan}\frac{X^*_-\ Y^*_-}{Z^*\sqrt{Z^{*2}+X^{*2}_- + Y^{*2}_-}}\right]$$

(3.39)

$$U' = \sqrt{U'^2_x + U'^2_y + U'^2_z} = \frac{U}{Uo} \qquad (3.40)$$

where

$$X^*_+ = X^* + 0.5\sqrt{W/L} \qquad (3.41)$$

$$X^*_- = X^* - 0.5\sqrt{W/L} \qquad (3.42)$$

$$Y^*_+ = Y^* + 0.5\sqrt{L/W} \qquad (3.43)$$

$$Y^*_- = Y^* - 0.5\sqrt{L/W} \qquad (3.44)$$

W is the opening width in X-direction.

L is the opening length in Y-direction.

Non-dimensional distances for rectangular hoods are obtained by dividing by the square root of the hood area, this is denoted by *. Non-dimensional velocities are obtained by dividing any velocity by the opening mean face velocity (Uo), (Uo=exhaust opening flow rate/opening area).

3.5 A NUMERICAL METHOD TO CALCULATE AIR FLOW FIELDS OUTSIDE ARBITRARILY SHAPED FLANGED EXHAUST OPENINGS

The air velocity potential of a point sink is given by Alenius(17), as

$$\Phi(b) = k\ Q/b \qquad (3.45)$$

where

$K = 1/4\pi$ for a free (spherical), and $K = 1/2\pi$ for a flanged (half sphere) point sink.

b is the distance from the point sink to the point where the potential is $\Phi(b)$.

A real exhaust opening is not a point but covers an area. The velocity potential at a point outside a flanged exhaust opening with infinite flanges may be calculated by integrating the potential from infinitesimal point sinks covering the exhaust opening. For a flanged opening the distance from each infinitesimal point sink to the point where Φ is to be calculated can be defined. The flanges must be large enough to prevent air being sucked in from the region behined the flanges. Fletcher(18), has shown that centreline velocities are unaffected by flange widths larger than the square root of the exhaust opening area. However, velocities in other regions than on the centreline have not been examined. A flange width limitation will limit the size of the region in which the flanged opening model is valid.

The air velocity outside a flanged exhaust opening is given by Alenius as

$$\bar{U}(\bar{X}) = \frac{1}{2\pi}\,\mathrm{grad}\left[\int_S \frac{\bar{U}(d\bar{s})\,d\bar{s}}{b(\bar{x},d\bar{s})}\right] = \frac{1}{2\pi}\int_S \mathrm{grad}\left[\frac{\bar{U}(d\bar{s})\,d\bar{s}}{b(\bar{x},d\bar{s})}\right]$$

(3.46)

where

grad is the gradient operator ($\delta/\delta x$, $\delta/\delta y$, $\delta/\delta z$ in cartesian coordinates).

$\bar{U}(\bar{X})$ is the air velocity vector at the point $\bar{X}$.

$\bar{U}(d\bar{s})$ is the air velocity vector of the area element with the area vector $d\bar{s}$.

$\bar{U}(d\bar{s})\,d\bar{s}$ is the flow rate through the area element ds.

$d\bar{s}$ is the area vector of the infinitesimal area element considered to be a point sink.

s is the area defined by the exhaust hood.

$b(\bar{X},d\bar{s})$ is the distance from the point $\bar{X}$ to the infinitesimal sink $d\bar{s}$.

Flanged exhaust openings are usually plane and the air velocity in the opening may be assumed to be perpendicular to the opening plane. If the air velocity is to be considered constant in the opening, then

$\bar{U}(d\bar{s})$ $(ds/d\bar{s})$ is constant and equation 3.46 can be simplified to

$$\bar{U}(\bar{X}) = \frac{Uo}{2\pi} \int_{S} \text{grad} \left[\frac{1}{b\ (\bar{x},d\bar{s})} \right] ds \qquad (3.47)$$

where Uo is the opening mean face velocity.

Equation 3.47 can be used to predict the air velocity in front of circular and rectangular flanged openings.

3.6 A NUMERICAL METHOD TO CALCULATE AIR FLOW FIELDS OUTSIDE A CIRCULAR FLANGED EXHAUST OPENING

For a circular exhaust opening the air velocity field has a rotational symmetry, so only two coordinates are needed to describe the air velocity field. The r-coordinate axis is directed from the centreline of the opening, perpendicular to it and outwards. The z-coordinate is directed from the exhaust opening centre point and outwards. These directions make both the air velocity components negative. The air velocity components along the coordinates r and z are given by Alenius (17) as

$$U_r(r,z) = -\frac{Uo}{2\pi} \int_{\xi=0}^{R} \int_{\alpha=0}^{2\pi} \frac{\xi\ (r + \xi\ \cos(\alpha)\ )}{\left[z^2 + r^2 + \xi^2 + 2r\xi\cos(\alpha)\right]^{3/2}}\ d\alpha\ d\xi$$

(3.48)

$$U_z(r,z) = -\frac{Uo}{2\pi} \int_{\xi=0}^{R} \int_{\alpha=0}^{2\pi} \frac{\xi\ z}{\left[z^2 + r^2 + \xi^2 + 2r\xi\cos(\alpha)\right]^{3/2}}\ d\alpha\ d\xi$$

(3.49)

where

r is the perpendicular distance to the axis of symmetry.

z is the perpendicular distance to the opening surface (or flange).

R is the radius of the exhaust opening.

ξ, α are polar coordinates in the opening plane (z=0). With these coordinates $ds = d\alpha\ d\xi$ and

$$b(\bar{x},\ d\bar{s}) = \left[\ z^2 + r^2 + \xi^2 + 2r\ \xi\ \cos(\alpha)\ \right]^{\frac{1}{2}}.$$

The integrals are elliptical and numerical methods have to be used to solve the equations for a point, (r,z). Alenius found Romberg's method is suitable for solving these equations because it has a fast convergence in evaluating the integrals and evaluates the calculated value accurately.

3.7 A NUMERICAL METHOD TO CALCULATE AIR FLOW FIELDS OUTSIDE A RECTANGULAR FLANGED EXHAUST OPENING

In case of a rectangular flanged exhaust opening the air velocity is three-dimensional and three coordinates are needed to describe the air velocity field. The three coordinates can be chosen as follows: From the center of the opening along its width (x), along its length (y), and directed from the exhaust opening and outwards (z). The air velocity components are given by Alenius as

$$U_X(x,y,z)=-\frac{Uo}{2\pi}\int_{\xi=-w/2}^{w/2}\int_{\eta=-L/2}^{L/2}\frac{x-\xi}{\left[(x-\xi)^2+(y-\eta)^2+z^2\right]^{3/2}}d\eta\ d\xi$$

(3.50)

$$U_y(x,y,x)=-\frac{Uo}{2\pi}\int_{\xi=-w/2}^{w/2}\int_{\eta=-L/2}^{L/2}\frac{y-\eta}{\left[(x-\xi)^2+(y-\eta)^2+z^2\right]^{3/2}}d\eta\ d\xi$$

(3.51)

$$U_Z(x,y,z)=-\frac{Uo}{2\pi}\int_{\xi=-w/2}^{w/2}\int_{\eta=-L/2}^{L/2}\frac{z}{\left[(x-\xi)^2+(y-\eta)^2+z^2\right]^{3/2}}d\eta\ d\xi$$

(3.52)

where

x is the distance from the centreline along the opening width.

y is the distance from the centreline along the opening length.

z is the distance from the opening plane.

W is the opening width.

L is the opening length.

ξ, η are cartesian coordinates in the opening plane (z=0). With these coordinates $ds = d\eta\ d\xi$ and

$$b(\bar{x},d\bar{s}) = \left[\ (x-\xi)^2+(y-\eta)^2+z^2\ \right]^{\frac{1}{2}}$$

Equations 51, 52, 53 can be solved using the same numerical method as the equations for circular exhaust openings.

3.8 INFLUENCE OF CROSS-DRAFTS ON HOOD PERFORMANCE

The air movement around a local exhaust is controlled not only by the exhaust itself but also by other mechanisms. One type of air movement in an environment, in which the local exhaust is placed, can be approximated with a cross-draft near the exhaust. Such an air motion around a local exhaust normally decreases the capture of contaminants. The particles or gases are often transported away from the exhaust opening. The most important limitation of the capture velocity method of quantifying hood performance is its failure to account for the effects of cross-drafts. In the complete absence of cross-drafts, any exhaust hood will capture all contaminants given off within its area of influence. It is the action of cross-drafts and other air motions in the workplace that degrade the performance of exhaust hoods and make their design particulary difficult. For each operation being exhausted, a capture velocity must be selected to overcome the action of expected extraneous air flow patterns and direct the resultant velocity into the exhaust hood. Until considerably more work is done to quantify the effect of cross-drafts on hood capture efficiency, the selection of capture velocities sufficient to overcome extraneous air flows will remain an art rather than a science. Recent work done by Conroy(19); Conroy etal(20); Flynn and Ellenbecker(8); Ellenbecker etal(9); Alenius and Jansson(21) has resulted in models that can be used to quantify the effect of cross-drafts on hood air flow patterns and capture efficiency. To simulate a situation where two or more air velocity fields are involved it is necessary to combine the calculated air velocities. The air velocities can be added vectorially at the point where the resulting air velocity is to be calculated. This operation to combine airflows was used by Flynn and Ellenbecker, and they reported experimental results which confirmed that the concept of vector addition applies to the combined hood and cross-draft flows.

Alenius and Jansson suggested that the operation to combine airflows is physically not correct in general but may give a good approximation of the

resulting air velocity. All air velocities must be combined in the same coordinate system. To do that, all air fields have to be transformed into a global coordinate system before they are superimposed (added).

The linearity of Laplace's equation allows the addition of potentials, enabling the construction of more complex flows. So it is possible to add cross-drafts to potential functions, while it is not possible to use the addition or superposition with Stokes equation because it does not follow Laplace's equation.

3.9 DISCUSSION AND CONCLUSIONS

Six analytical and numerical models for air flow fields of circular and rectangular flanged exhaust openings have been presented. The models all used potential flow theory for frictionless, incompressible, and irrotational fluid flow. The final model developed by Flynn and Ellenbecker, and the non-dimensional model developed by Jansson were selected for prediction of particle trajectories and comparison with experimental trajectories. These two models are analytical and they do not require long computing time. Flynn and Ellenbecker described the final model as the best model to calculate the air distribution around a circular flanged hood. The numerical model developed by Alenius to calculate air flow fields outside a circular flanged hood was not used in the computer program because it used complicated equations. Rectangular hoods were not used in the experiments because there was not enough time to do experiments on them. Flynn and Ellenbecker's final model makes use of all three models they discussed. The sequence of calculations they recommended is:-

1) Calculate radial and axial velocities using model 1 (Equations 3.6 & 3.7)

2) Calculate angle (β) that the velocity vector makes with the hood centerline (z-axis), (Equation 3.10)

3) Calculate the total theoretical velocity using model 2 (Equation 3.11)

4) Calculate radial and axial velocities using model 2 (Equations 3.13 & 3.14)

5) Apply empirical corrections to calculate radial and axial velocities using (Equations 3.23 & 3.24)

3.10 REFERENCES

1. Prandtl, L and Tietjens. O. G.: Fundamentals of Hydro and Aerodynamics. Dover Publications, New York 1957.

2. Rhyming, I. L.: Dynamique des fluides. Presses Polytechnique Romandes, Lausanne 1985.

3. Baturin, W. W.: Fundamental of Industrial Ventilation. Pergamon Press, New York 1972.

4. Dalla Valle, J. M.: Exhaust Hoods. Industrial Press Inc., New York 1945.

5. Engels, L-H. and Willert. G.: Kriterien und Moglichkeiten Zur Erfassung Des Staubes in Industriebetrieben. Staub - Reinhalt. Luft 33(1973), 140-141.

6. Garrison, R. P.: Centerline Velocity Gradient for Plain and Flanged Local Exhaust Inlets. Am. Ind. Hyg. Assoc. J. 42(1981), 739-748.

7. White, F.: Fluid Mechanics. McGraw-Hill, New York (1982).

8. Flynn, M. R. and M. J. Ellenbecker: Empirical Validation of Theoretical Velocity Fields into Flanged Circular Hoods, Am. Ind. Hyg. Assoc. J. 48(4): 380-389 (1987).

9. Ellenbecker, M. J., R. E. Gempel and W. A. Burgess: Capture Efficiency of Local Exhaust Ventilation Systems. Am. Ind. Hyg. Assoc. J. 44(10): 752-755 (1983).

10. Jansson, A.: Description of Air Movement Outside Flanged Exhaust Openings. Part II: Air Velocity Fields. Solna, Sweden 1987.

11. Flynn, M. R. and M. J. Ellenbecker: The Potential Flow Solution for Air Flow into a Flanged Circular Hood. Am. Ind. Hyg. Assoc. J. 46(6):318-322 (1985).

12. Dalla Valle, J. M.: Studies in the Design of Local Exhaust Hoods. Doctoral Thesis, Harvard University, Boston, Mass.,1930.

13. Pruzner, A. S.: Flow Structure in the Zone of Action of Suction Apertures. Otopleniye i Ventilyatsiya 3:13–21 (1939).

14. Fletcher, B.: Centerline Velocity Characteristics of Rectangular Unflanged Hoods and Slots Under Suction. Ann. Occup. Hyg. 20:141–146 (1977).

15. Silverman, L.: Fundamental Factors in the Design of Exhaust Hoods. Doctoral Thesis, Harvard University (1943).

16. Tyaglo, I. G. and Shepeleve, I. A.: Air Movement Towards an Exhaust Opening (in Russian). Vodosnabzhenie i Sanitarnaya tekhnika (1970), 24–25.

17. Alenius, S.: Calculation of Air Velocities Outside Exhaust Openings With Flange. Method and Results. Solna, Sweden 1986.

18. Fletcher, B.: Effects of Flanges on the Velocity in Front of Exhaust Ventilation Hoods. Ann. Occup. Hyg. 21(1978), 265–269.

19. Conroy, M.: Capture Efficiency of Flanged Slot Hoods. Doctor of Science Thesis, Boston, 1988.

20. Conroy, L., M. Ellenbecker, and M. Flynn: Prediction and Measurement of Velocity Into a Flanged Slot Hood. Am. Ind. Hyg. Assoc. J. 49(5): 226–234 (1988).

21. Alenius, A. and A. Jansson: Air Flow and Particle Transport into Local Exhaust Hoods. Solna, Sweden 1989.

CHAPTER 4

A COMPUTER PROGRAM TO CALCULATE AND VISUALIZE PARTICLE MOVEMENT INTO A FLANGED CIRCULAR LOCAL EXHAUST HOOD

4.1 PARTICLE MOTION

The motion of a particle in air is influenced by a gravity force, a drag force, and a buoyancy force of the surrounding air. The particle can be described by Newton's law of motion. The acceleration of a particle is dependent on the sum of the forces acting on it divided by the mass of the particle.

MASS X ACCELERATION = DRAG FORCE + GRAVITY FORCE
+ BUOYANCY FORCE

A spherical particle moving through a two dimensional air flow was discussed in CHAPTER 2, and the general motion of a particle is described by differential equations (2.9) and (2.10). Therefore it is possible to describe the motion of the particle as a particle trajectory with the locations as a function of the time elapsed. The force of gravity is constant and directed vertically downwards. The force of buoyancy is directed upwards. The drag force is directed towards the particle (relative to the air)direction of motion. The drag force will generally change direction cotinuously along the particle trajectory. Analytical solutions to equations (2.9) and (2.10) are not possible and numerical solutions have to be applied. In order to solve these equations numerically, they have been rewritten as in equations (2.12 - 2.16). The equations can be solved numerically by computing the particle velocity and location at the end of a small interval of time δt. The velocity and location will be computed at the end of the first interval, $t_1=\delta t$. If the velocity and location are known at t_1 as initial values, the velocity and location can be computed at the second time interval $t_2=t_1+\delta t$. The process can be repeated until the particle travels some prescribed distance or some

prescribed time. The Rung Kutta Method (Appendix B) can be used.

4.2 AIR FLOW FIELDS OF A CIRCULAR FLANGED EXHAUST HOOD

Analytical models of air flow fields of a circular flanged exhaust hood have been discussed in CHAPTER 3. These models used potential flow theory for frictionless, incompressible, and irrotational fluid flow. In these models the air velocity in the horizontal and vertical direction can be calculated at any point in front of the hood. The final model developed by Flynn and Ellenbecker, and the non-dimensional model developed by Jansson are selected to be used on the computer program to calculate and visualize particle motion into a flanged circular hood. The final model equations used in the program are (3.5-3.9, 3.11-3.14, 3.23-3.24). Jansson's model equations used in the program are (3.28-3.36).

4.3 CROSS-DRAFTS

The air movement around a local exhaust is controlled not only by the exhaust itself but also by other mechanisms. One type of air movement in an environment, in which the local exhaust is placed, can be approximated with a cross-draft near the exhaust. Such an air motion around a local exhaust normally decreases the capture of contaminants. The effect of cross-drafts on the movement of a particle is going to be included in the computer program. The cross-draft is perpendicular to the hood centerline.

4.4 COMBINATION OF TWO OR MORE VELOCITY FIELDS

To simulate a situation where two or more air velocity fields are involved it is necessary to combine the air velocities in some way.

To combine two or more air velocity fields the air velocities at a point can be added vectorially to give the resulting air velocity at that point. The combination of air flows may give a good approximation of the resulting air velocity. The combination of air flows outside the exhaust hood may be justified by considering the the flow as a near potential flow. All air velocities must be combined in the same coordinate system. To do that all used fields (exhaust, cross-drafts) are transformed into a global coordinate system before they are superimposed (added).

4.5 COMPUTER PROCEDURE

Procedures for calculating air velocities outside a flanged circular hood, and particle trajectories in air flow have been described. To calculate particle trajectories outside a flanged circular hood two computer procedures have been developed in the language Basic. In order to calculate coordinate points along a particle trajectory, the user provides the following data: air pressure and temperature, hood diameter and flow rate, cross-draft velocity, particle starting point and velocity, particle diameter and density and calculation time step. The air flow field parameters are needed for calculating the air velocity at the particle locations along the trajectory. Either the final model developed by Flynn and Ellenbecker (the first and the second program) or Jansson's model (the third program) can be used to calculate the air velocities outside the hood. The cross-draft velocities and the air flow velocities outside the hood are added vectorially to calculate the combined air velocities in vertical and horizontal directions. The programs also calculate: particle relative velocity, Reynolds number, drag force coefficient, drag force, gravity force and buoyancy force. At the end of time step, the programs calculate new values of particle velocities and location. The location of the particle can be seen on the screen. The process of computing the velocity and location of the particle can be repeated until the particle reaches some prescribed position (the particle reach the x-axis). If the

distance of the particle from the y-axis when it reaches the x-axis is less than the radius of the hood, then the particle will be captured by the hood. If the particle is not captured by the hood, the user can change the input data and see if the particle is captured or not. Using the program in this way it is possible theoretically to design an exhaust able to capture contaminants under defined conditions. A flowchart of the computer program is shown on Figure 4.1, and a listing in APPENDIX C.

CHAPTER 5 EXPERIMENTAL WORK ON THE MOVEMENTS OF PARTICLES INTO A FLANGED CIRCULAR HOOD

5.1 INTRODUCTION

Flow visualization is an important tool in experimental aerodynamic research. It can give directly the details of complex flow patterns which otherwise must be found indirectly through tedious point by point measurements. The methods for flow visualization have improved little over the past several decades despite the progresses in experimental techniques. Smoke is the most commonly used flow tracer. The individual smoke particles follow the air motion because they are extremely small, but they must be concentrated to be visible, and also there is a problem of diffusion.

Soap bubbles as aerodynamic flow tracers have been used since the birth of aviation as mentioned by Lock (1) in 1928. In 1961 Johnson (2) generated small bubbles with a concentric arrangement of two fine tubes and examined the flow in a cylindrical vortex tube. In 1971 Hale, Stowell and Ordway (3) of SAGE Action, Inc. puplished a paper on the developement of an integrated system for flow visualization in air using neutrally buoyant helium filled soap bubbles. With their arrangement bubbles could be produced at rates up to 500/sec in air at velocities up to 65m/sec. The National Institute of Agricultural Engineering (4) in U.K. conducted several experiments to study the characteristics of soap bubbles. In these experiments, the rate and diameters of bubbles produced were determined by means of high speed cine photography. In 1989 Kic (5) used soap bubbles to visualize the air flow for designing and assessment of ventilation systems in livestock barns.

Our investigation utilised bubbles as particles to test a computer model for calculating particle trajectories outside a flanged circular local exhaust hood. This

is somewhat different to their use to visualize air flows as described above. The experimental results are in good agreement with the model results. The method used is simple and easy, not expensive.

5.2 EXPERIMENTAL EQUIPMENT

Refering to Figure 5.1, air is blown by the centrifugal fan 1, through the perforated gauze flow equaliser 2 (make the air flow in the tunnel uniform), into the wind tunnel 6. The air velocity in the wind tunnel is regulated by changing the speed of the fan, and is measured by using a hotwire anemometer. The bubbles formed by the bubble generator 3 are carried by the air in the wind tunnel and some of them may be caught by the exhaust hood 9. The rate of flow in the duct 10 can be calculated easily by using the orifice plate 11. The light from the motor car fog lamps 7, and the stroboscope 8 illuminate the bubbles. Photographs are taken by a conventional camera. Time exposures show the trajectories of individual bubbles. Figure 5.2 is a sketch of a short length of a bubble trajectory and the photograph in Figure 5.11shows the trajectory of a bubble captured by the hood. The continuous lines are produced by reflections on the bubble surface of light from the lamps shining upwards. The pairs of dots are reflections of the stroboscope flashes.

The dimensions of the wind tunnel are 400cm long, 43cm high and 65cm wide. The bottom and front face of the tunnel are plexiglas while the top and back face are wood painted black. All other surfaces were painted black to minimize reflections and maximize bubble visibility. The flanged exhaust hood was fixed on the center of the top side of the tunnel at 180cm away from the bubble generator. The lighting arrangement was achieved by having two sources of light. The first source consists of four 50 watt motor car fog lamps. These lamps were put inside black wooden boxes, an opening 5cm in width along the box is made on the center of the top side of the box to allow a flat beam of light to pass to

the tunnel. The box was put under the tunnel and the light is directed upwards to illuminate the vertical plane along the center line of the tunnel. An other sheet of black wood with one centimeter wide slot along its center is put on the bottom side of the tunnel to reduce the illuminated area in the tunnel. The second source of light is the stroboscope which produces flashes at time intervals. This stroboscope is put inside the tunnel 120cm downstream from the exhaust hood and flashes in the horizontal direction. The flashes from the stroboscope, the light from the motor car fog lamps and the Camera are mutually perpindicular. Photographs were taken with medium speed* black and white film using a PRAKTICA Super TL Camera. * (ISO 125/22°)

5.3 A BUBBLE GENERATOR

A bubble generator is a device for producing soap film bubbles. The bubbles are formed by extruding a tubular film from an annular orfice, the film breaking up into bubbles many of which last several minutes and have terminal velocities low enough to enable them to be used in visualization of the air movement. The device shown on the diagram of Figure 5.3 was taken from the National Institute of Agriculture Engineering(4) and it consists of a chamber C into which the bubble blowing liquid is run via the feed tube F. An air tube A passes through the chamber and terminates in the nozzle N. The end die D is dimensioned so as to leave a narrow annular gap between the outside of the Nozzle and the die. The fine thread on the inlet end of the air tube enables it to be positioned relative to the end die and locked in position by the Locknut L against the end of the liquid chamber. Size and number of bubbles produced by this generator were large which make it difficult to get good photographs for individual bubbles.

A local made bubble generator was developed during the research. Figure 5.4 shows this generator. It consists of a plastic tube B joined with a circular flat plastic plate C which has four small holes, an other plastic tube N is fixed at the

top of plate C. Tube B is for compressed air and tube N for bubble liquid. The bubbles are formed when the compressed air breaks up the film liquid at holes. This bubble generator was used in the experiments because it produces very small bubbles.

5.4 BUBBLE GENERATOR LIQUID

Hyamine 2389 is the registered trade name for the liquid which is used to produce bubbles by the generator. Hyamine consists of 40 percent methyle dodecyl benzyl trimethyl ammonium chloride, 10 percent methyle dodecyl xylylene bis (trimethyl ammonium chloride) and 50 percent water. This liquid is safe to use for producing bubbles but it becomes dangerous if it is used for drink.

5.5 BUBBLE PARAMETERS

The parameters which influence the movement of any particle are particle diameter, density and velocity. If these parameters can be determined for an individual bubble, it will be possible to calculate the trajectory of that bubble. In our experiments we succeeded in calculating the diameter, density, and velocity of individual bubbles from photographs taken of these bubbles.

The techniques for measuring bubble parameters is achieved by putting a grid inside the tunnel at the center of the exhaust hood. This grid is used as a reference for measuring bubble parameters. The distance of the Camera from the grid is kept constant when the photographs are taken and the enlarger kept at a fixed position when the photographs are printed. The scale factor is then known and constant. The bubble diameter can be measured from the photograph by using a traversing microscope with cross line sighting. Distances between consecutive flashes are proportional to bubble velocities. At a large enough distance from both the bubble generator and the hood, it is safe to assume that

the bubble is moving in the horizontal direction at a velocity equal to the cross wind velocity and moving in the vertical direction at a velocity equal to the settling velocity of that bubble. The cross wind velocity can be measured by hotwire anemometer. The vertical and horizontal distances between consecutive flashes are measured directly from the photograph and the bubble settling velocity can be calculated. The density of the bubble can be calculated from the bubble settling velocity.

5.5.1 Bubble Diameter

One of the main difficulties of using bubbles as particles is the difficulty of determining individual bubble diameter. The National Institute of Agriculture Engineering (4) in U.K conducted experiments to measure bubbles diameters, but in these experiments the average diameter of groups of bubbles was determined. The illumination arrangement which is shown on Figure 5.1, enables the diameter of individual bubbles to be ascertained.

When the stroboscope flashes two pin points of light are recorded on the film in the camera as it is shown on the photograph in Figure 5.11. These are the reflections on the front and rear surfaces of the bubble. Ideal, i.e stroboscope and camera at infinite distances from bubble, light paths are shown in Figure 5.5. From this figure it can be seen that the bubble diameter is equal to $\sqrt{2}$ X the distance between the two reflections.

The procedure used to scale distances as recorded on the photographic prints up to full size is described later in Table 5.1. The distance between simultaneous reflections on photographs was measured using a traversing microscope with cross line sighting . A micrometer moved the microscope from one sighting to its partner, the difference between the micrometer readings being the distance between the images of the reflections.

5.5.2 Bubble Velocity

It is safe to assume that at some distance from the bubble generator and the exhaust hood that the bubble is moving in a horizontal direction with a velocity equal to the cross wind velocity and in the vertical direction with a velocity equal to the settling velocity. These velocities can be measured from the photograph, far away from the exhaust hood, the effect of the exhaust hood is very small and can be neglected. At that distance the initial bubble velocity in X and Y direction is equal to the cross wind and the settling velocity. From Figure 5.6

$$\tan\alpha = \frac{\text{settling velocity}}{\text{cross wind velocity}}$$

$$= \frac{\text{measured distance in vertical direction}}{\text{measured distance in horizontal direction}}$$

The cross wind velocity is known (measured by hotwire anemometer) and is equal to bubble velocity in horizontal direction. Distances between consecutive flashes are bubble velocities. The vertical and horizontal distances between consecutive flashes are measured directly from the photograph, then the bubble settling velocity is calculated. The errors from assuming at some distance from the bubble generator and the exhaust hood that the bubble is moving in the horizontal direction at a velocity equal to cross wind velocity and in the vertical direction at a velocity equal to settling velocity are very small and can be neglected.

5.5.3 Bubble Density

The bubbles produced by the bubble generator are about 1.8 meter away from the exhaust hood, the air velocity from the bubble generator is less than 6m/sec, the diameters of bubbles formed are between (2-8)mm, so it is safe to

assume at some distance from the bubble generator and the exhaust hood that the bubble is moving in the horizontal direction at a velocity equal to the cross wind velocity and moving in moving in the vertical direction at a velocity equal to the settling velocity of that bubble. The settling velocity for a bubble can determined as described above.

The settling velocity occurs when,

Drag Force + Buoyancy Force = Gravitional Force

but drag force F_d,

$$F_d = \frac{1}{2} \rho C_d A_p V^2 \qquad (5.1)$$

For a spherical particle

$$A_p = \frac{\pi D_p^2}{4}$$

and

$$F_d = \frac{1}{8} \rho C_d \pi D_p^2 V^2$$

so that

$$\frac{1}{8} \rho C_d \pi D_p^2 V^2 + \left[\frac{\pi D_p^3}{6}\right] \rho g = \left[\frac{\pi D_p^3}{6}\right] \rho_p g \qquad (5.2)$$

simplifying and rearranging

$$\frac{1}{8} \rho C_d V^2 = \left[\frac{D_p}{6}\right] (\rho_p - \rho) g$$

and

$$V = V_t = \frac{4 D_p g}{3 \rho C_d} (\rho_p - \rho) \qquad (5.2)$$

If we assume the flow is in Allen region, in this region the drag force coefficient is given by Busnaina (6) as

$$C_d = \frac{24}{Re^{0.646}} \qquad \text{for} \qquad 1 < Re \leqslant 400 \qquad (5.3)$$

The Reynolds number Re, is equal to

$$Re = \frac{V_t \ D_p \ \rho}{\mu} \qquad (5.4)$$

where

ρ is the air density.

μ is the air dynamic viscosity.

V_t is the bubble terminal velocity.

g is the acceleration due to gravity.

D_p is the bubble diameter.

ρ_p is the bubble density.

A_p is the projected bubble area.

The density of the bubble can be determined from equation(5.2), as the diameter and the settling velocity are measured from the photograph.

5.5.4 Bubble Position

The initial bubble position far away from the exhaust hood while it moves in the horizontal direction with a velocity equal to the cross wind velocity and in the vertical direction with a velocity equal to the settling velocity can be measured from the photograph. The bubble position at any time can also be measured from the photograph.

5.5.5 Bubble Trajectory

The bubble position on the bubble trajectory at any time can be measured from the photograph by knowing the number of flashes per second which is produced by the stroboscope.

5.6 COMPARISON BETWEEN THEORETICAL AND EXPERIMENTAL TRAJECTORY

The computer model developed through the research can calculate the position of a particle on the trajectory at any time in front of a flanged circular local exhaust hood. From a photograph, the trajectory for a bubble is known, so the theoretical trajectory for a bubble with same diameter, density and velocity from the same position can be calculated.

The error at time t_i between two points on the experimental and calculated trajectory is E_i , as shown on Figure 5.7,

$$E_i = \sqrt{(X_i - x_i)^2 + (Y_i - y_i)^2} \qquad (5.5)$$

where

X_i is calculated distance from y–axis at t_i.

x_i is experimental distance from y–axis at t_i.

Y_i is calculated distance from x–axis at t_i.

y_i is experimental distance from x–axis at t_i.

The mean error $\bar{E}$, is

$$\bar{E} = \frac{\sum E_i}{n} \qquad (5.6)$$

The standard error of deviation S, is

$$S = \sqrt{\frac{\sum (E_i - \bar{E})^2}{n}} \qquad (5.7)$$

where n is the number of error values.

Trajectories with smallest values of $\bar{E}$ and S are the best fit.

5.7 PHOTOGRAPHIC MEASUREMENTS AND ERRORS

For measuring the bubble position, diameter and velocity from the photographs, a grid (71.4 X 40.8)cm was put inside the tunnel at the center of the exhaust hood at 50 cm from the camera. The grid was divided to squares (5.1 X 5.1)cm, this grid was used as a reference for measuring the bubble position, diameter and velocity from the photographs. Figure 5.12 shows the photograph of this grid.

5.7.1 Grid Error

Figure 5.8 shows the actual dimensions(direct measured dimensions) of the grid in X and Y directions. During dividing the grid into squares, the squares may be not equal.

The actual grid length in x – direction is

5.1 X 8 + 5.05 X 6 = 71.1 cm

The theoretical grid length in x – direction is

5.1 X 14 = 71.4 cm

The percentage error measurement in x – direction

$$= \frac{\text{theoretical grid length - actual grid length}}{\text{theoretical grid length}}$$

$$= \frac{71.4 - 71.1}{71.4} = 0.42\ \%$$

The actual grid length in y – direction is

5.1 X 6 + 5.05 X 2 = 40.7 cm

The theoretical grid length in y – direction is

5.1 X 8 = 40.8 cm

The percentage error measurement in y – direction

$$= \frac{\text{theoretical grid length - actual grid length}}{\text{theoretical grid length}}$$

$$= \frac{40.8 - 40.7}{40.8} = 0.25\ \%$$

5.7.2 Parallax Error

The width of the light coming from the motor car fog lamps is 8 cm, the streak of bubbles which we will get from the photograph will be at distance between (46–54) cm from the camera as shown on Figure 5.9.

The maximum percentage of Parallax Error

$$= \frac{\text{Theoretical camera distance - Actual camera distance}}{\text{Theoretical camera distance}}$$

$$= \mp \frac{4}{50} = \mp\ 8\ \%$$

The percentage of parallax error in photographs can be reduced either by reducing the light width which is coming from the motor car fog lamps or by puting the camera at further distance from the center of the hood. The cross–wind velocity in the wind tunnel is measured by hotwire anemometer and it is made the basis for considering if there is parallax error or not. There is no parallax error if this velocity is equal to the bubble velocity measured from the photograph.

5.7.3 Errors From Considering The Stroboscope And The Camera As A Point Source And A point Sink

At ideal situation we assumed that the stroboscope and the camera are far away from the bubble, so in this case all beams of light falling from the stroboscope on the bubble will be parallel and also all beams of light reflecting from the bubble and falling on the camera will be parallel.

At actual situation as shown on Figure 5.10, the stroboscope was put at 1.2 meter from the bubble and the camera was put at 0.5 meter from the bubble, in this case beams of light falling from the stroboscope on the bubble will not be parallel, also beams of light reflecting from the bubble and falling on the camera will not be parallel. At ideal situation the measured distance CB is equal AB, while at actual situation the measured distance CK,is

$$CK = CB - KB$$

$$KB = AB \times \tan \alpha$$

Percentage of Error

$$= \frac{\text{Ideal measured distance - Actual measured distance}}{\text{Ideal measured distance}}$$

$$= \frac{CB - CK}{CB} = \frac{KB}{CB} = \frac{AB \times \tan \alpha}{CB} = \tan \alpha$$

If the maximum bubble diameter is assumed to be 8 mm, in the case of considering α as the angle between the beam light reflecting from the bubble surface to the camera and the bubble center, in this situation

$$\tan \alpha = \frac{0.004}{0.5} = 0.008$$

percentage of error $= \tan \alpha = 0.008\ \%$

This error is negligable, also the angle between the light falling from the stroboscope on the surface of the bubble and the bubble center will be smaller than α and the error is negligable also.

5.8 EXTRACT FLOW MEASUREMENT

The flow rate measurement in the exhaust duct 10, as shown on Figure 5.1 was made according to British Standard Code B.S. 1042 by using an orifice plate with D and D/2 tappings. The diameter of the orifice plate is 10.7 cm and the

diameter of the plastic duct is 15 cm. A straight duct for two meters upstream of the orifice plate and one meter downstream from it was used to measure the flow rate in the duct. The expected accuracy of measurement of an orifice and manometer is about 1% .

5.9 EXPERIMENTAL PROCEDURE

A series of experiments were performed to test the theoretical computer models. A 15 cm circular flanged hood diameter with face velocities equal to 3 and 2 m/sec were used. The cross wind velocity in the tunnel was between 0.53 and 1 m/sec, the stroboscope was set up to produce 20 flashes/sec, the camera was put in front of the tunnel at 50 cm from the center of the tunnel, the camera exposure was put on one second, and the bubble generator was put at the center of the tunnel at 1.8 meter from the exhaust hood. Figure 5.1 shows the experimental equipment. The experimental procedure can be described as follows:

1) Turn on the exhaust fan 13 and measure the flow rate in the exhaust duct 10 using an orifice plate 11.
2) Turn off the exhaust fan 13.
3) Turn on the blowing fan 1 and measure the velocity in the wind tunnel using a hotwire anemometer.
4) Turn on the exhaust fan While the blowing fan is on.
5) Turn on the stroboscope and the motor car fog lamps.
6) Turn on the bubble generator.
7) Photograph the bubbles while they are moving into the exhaust hood.
8) Turn off the exhaust fan 13 and change the velocity in the tunnel.
9) Turn on the exhaust fan 13 and photograph the bubbles while they are moving into the exhaust hood.
10) Put the grid in the center of the exhaust hood and photograph it.

The velocity at the face of the hood can be changed and the experimental procedure can be repeated when the velocity in the tunnel is set at different values.

5.10 RESULTS

Experimentaly measured x and y values were compared with values predicted from two theoretical computer models. The mean error E, and the standard error of deviation S were determined for different trajectories. Trajectories with smallest values of E and S are the best fit. Table 5.1 displays the values of E, S, x, and y for thirteen experimental and theoretical trajectories. Table 5.2 shows comparison between the mean error and the standard error of deviation for these two models. In Tables 5.1 and 5.2 there are seven trajectories without correction (no parallax error), and six trajectories with correction (corrected due to parallax error). It is clear from Table 5.2 that model 1 is better than model 2. A multiple regression between hood face velocity, cross wind velocity, bubble diameter and mean error indicated that the value of the multiple correlation coefficient is very low, which means a bad fit (insignificant relation) between hood face velocity, cross wind velocity, bubble diameter and mean error.

5.11 DISCUSSION

The computer program developed used two different models to calculate the distribution of air round a circular flanged hood. Model 1, the final model developed by Flynn and Ellenbecker (7) used an approximate solution with equipotential surfaces coincident with equal velocity surfaces. This model seems to give the best estimates of velocity as suggested by the authors because it includes correction for frictional forces near the hood face and the assumed constant potential at the hood face. Model 2 developed by Jansson (8) is a semi-empirical potential flow solution, the model uses surfaces of oblate spheroids (rotated ellipse)

for describing surfaces of equal air velocity. The magnitude of the air velocity is calculated from the ellipse eccentricity, which in turn is a function of the coordinates in space. This model is not as good as model 1 because this model assumed the velocity to be constant over the inlet plane and vena contracta effect in the opening is not considered.

5.12 REFERENCES

1. Lock, C.N.H.: Photographs of Streamers Illustrating the Flow Around an Airscrew in the "Vortex Ring State", ARC Reports and Memoranda No.1167, April 1928.

2. Owen, F.S., Hale, R.W., Johnson, B.V. and A. Travers: Experimental Investigation of Characteristics of Confined Fet-Driven Vortex Flows, United Aircraft Research Laboratories, Report R-2494-2, November 1961.

3. Hale, R.W., Tan, P., Stowell, R.C. and D.E. Ordway: Developement of an Integrated System for Flow Visualization of Air Using Neutrally-Buoyant Bubbles, Sage Action Inc., SAI-RR 7107, December 1971.

4. A Device for Producing Small Bubbles for use in the Visualization of Air Movement, Departmental note DN/FB/035/3020, National Institute of Agricultural Engineering, Wrest Park, Silsoe, Bedford, U.K.

5. Kic, P.: Stable Microclimate in Cattle Breeding Houses, Zemed, Techn., 35, 1989(1):39-51.

6. Ahmed Busnaina: Computer Modeling of Air Flow in Clean Rooms. A short Course for Presentation at the 20 th Annual Meeting of the Fine Particle Society, Boston, Massachusetts, August, 1989.

7. Flynn, M.R. and M.J. Ellenbecker: Empirical Validation of Theoretical Velocity Fields into Flanged Circular Hoods. Am. Ind. Hyg. Assoc. J. 48(4): 380–389 (1987).

8. Jansson, A.: How to Model Air Flow Fields Outside Flanged Exhaust Openings, Staub–Reinh, Sweden, Luft 49:11–16 (1989).

CHAPTER 6 DISCUSSION AND CONCLUSION

6.1 DISCUSSION

The current practices for designing local exhaust hoods are largely based on coarse rules and on personal experience. In most design schemes empirical equations are used to calculate contaminant capture velocity at the hood centerline. The present work describes a theoretical model to predict particle movement into a flanged circular exhaust hood and explains a method to compare theoretical trajectories with experimental trajectories by using soap bubbles.

The motion of gaseous and vapor contaminants is affected by the velocity field of the air through which they move. The motion of particle contaminants on the other hand is also affected by the inertia of the particle and aerodynamic drag. If the average distance between particles is at least 10 times the particle diameter, it is safe to assume that particles move through the carrier gas independently of each other and that the particles do not influence the gas velocity field. For most problems in air pollution and industrial ventilation the average distance between particles is hundreds of times larger than this. So the motion of carrier gas is independent of the motion of particles. To describe the motion of an aerosol, one must first compute the velocity field of the carrier gas and then compute the motion of the particle.

Modelling air flow in front of local exhaust hoods can be achieved either by experimental or theoretical methods. In experimental methods empirical equations describing air flow in front of local exhaust hoods can be developed by doing a series of measurements to quantify the parameters which influence the movement of air in front of these hoods. In theoretical methods, the approach can be either by solving Navier–Stokes and continuity equations or by using potential flow theory for frictionless, incompressible, and irrotational fluid flow. The mathematical

difficulties involved in solving Navier-Stokes equations have encouraged the use of the potential flow theory to describe the motion of fluid because it is easier to use mathematically.

In the present work more complex flow configurations can be approximately modelled by superposing several flow fields. Superpositioning is attractive because it is a simple technique to model more complex configurations. It was first suggested more than 40 years ago by Dalla Valle(1), but application was hard without computers. Alenius and Jansson(2) suggested that it is physically incorrect but may be justified by the near potential flow behavior of exhaust hood flow. Another method to model complex flow configurations is to solve Navier-Stokes equations using general fluid dynamics programs. With the limited storage capablities of small computers this does not seem possible at present on personal computers. The use of general fluid dynamics computer programs, requires extensive computing facilities, extensive experience of the programs and knowledge of fluid dynamics. This situation is changing and fluid dynamics programs for PC's are now becoming available.

The computer programs developed to calculate particle trajectory in front of a flanged circular exhaust hood used potential flow theory and the superposition technique to calculate the air distribution around the hood, the programs are written in basic and are easy to run on a personal computer.

Soap bubbles have been used to produce experimental trajectories. This is believed to be the first time that soap bubbles have been used as particles. In the past soap bubbles have been used only for visualizing air movement, and the bubble density was assumed equal to that of air. The lighting technique used in the experiments increased the information contained in bubble trace photographs. This made it possible to calculate the diameter and density of individual bubbles. Some very small bubbles, may be 1mm in diameter or less, were produced in

these experiments but the simple photographic facilities which were available did not allow taking clear photographs of these bubbles. More elaborate cameras would enable smaller bubbles to be photographed over a wider field of view.

The present technique of using soap bubbles to simulate particles could be used successfully to validate theoretical models describing particle movement in air. Although the bubble sizes are much larger and densities lower than the particles found in industrial applications, this will not reduce the validity of using bubbles as particles because the movement of bubbles and particles are governed by the same laws of motion. Drag forces are affected by size and shape and it is possible that these are less accurately described.

The accuracy needed for modelling contaminant movement into local exhaust hoods may be argued. Data on validation of contaminant movement into local exhaust hoods is rare. Besides what has been presented here, Alenius and Jansson have developed a computer program to predict particle movement into local exhaust hoods and they reported that there is a good agreement between theoretical and experimental trajectories for particles moving into flanged circular hoods. It is quite difficult to compare the present model for predicting particles movement into local exhaust hoods with models developed in the past. In the past empirical models were used to calculate the capture velocity at the hood center line necessary to direct the particles into the hood. In these models neither the particle release velocity nor the cross wind velocity are quantified. In the present model, the particle release velocity and the cross wind velocity are quantified, and it is possible to predict the particle movement at any point in front of the hood as well as along the centerline.

A good agreement was found between theoretical predictions and actual particle movement for particles moving into a flanged circular local exhaust hood. The results indicated that values of the mean error and the standard error of deviation for theoretical and experimental trajectories are small. The effect of

these errors are very small in case of using the program for design processes.

Particle movement in air is governed by well known physical processes. Therefore straight forward modelling ought to give correct descriptions. Real industrial local exhaust hoods are different from the ideal shapes of the models, the disturbances from the surrounding of an exhaust must be taken into account. Surfaces, moving objects, air movement and particle sources create complex disturbances. Failure in predicting actual particle movement may be due to failure in describing the actual flow fields and particle sources in real industrial processes rather than errors in the modelling.

The presented modelling method could be used for other shapes of local exhaust hoods and theoretical trajectories can be compared easily with experimental trajectories by using soap bubble method described earlier. The model may seem very limited in its application. However, it could be a useful tool for industrial hygienists and design engineers in predicting particle movement for similar situations.

The work reported here was conducted in the laboratory under controlled conditions. The greatest limitation on the use of the model is the variation of industrial cross-drafts. Field validation of the model, both for larger flanged circular exhaust hoods and for less steady cross-drafts is necessary.

6.2 CONCLUSION

The main objectives of this research were to develop and validate a model for predicting the movement of particles into a flanged circular exhaust hood in the presence of a uniform cross-draft. The model was developed in two stages, each of which could improve the development of local exhaust ventilation design.

The first stage of the research was the development of a model to predict the velocity of a particle in front of a flanged circular exhaust hood. With this model the particle velocity at any point in front of a flanged circular hood can be predicted. Until now the basis for most exhaust hood designs have been empirical models for centerline velocity. Empirical models are not necessarily valid outside of the range of conditions for which they were developed, while a theoretical model can be used for conditions other than those tested with more confidence than the empirical models currently used. The developed model is important not only because it can be used to predict the particle velocity at any point but also because it is a theoretical model developed from a solution to Laplace's equation and Newton's second law of motion.

Cross-drafts can be added vectorially to the local exhaust air velocity field generated by the hood. The superposition technique seems to work well outside local exhaust hoods.

The second stage of the research was the development of an experimental method to test the theoretical model. In this method, soap bubbles were used to simulate particles. As well as the usual bubble trajectories, time exposure photographs showed the position of bubbles at discrete time intervals and enabled the bubble diameter and density to be deduced.

The model has been validated for one hood size, several hood face velocities, and several cross-draft velocities. A good agreement was found between theoretical prediction and experimental bubble trajectories moving into a flanged circular hood. The face velocities and cross-draft velocities used are typical of industrial situations but the experimental hood was smaller than those typically found in industrial settings. The experimental apparatus limited the size of the hood which could be used.

The developed model is an improvement over the current design technique for local exhausts in that it provides a quantitative index of hood performance, i.e, capture efficiency, rather than a wide range index, such as control or capture velocity. The effects of cross-drafts are also quantified replacing the qualitative descriptions used previously. The designer can use the model by choosing different release points from the particle source and run the program to see if the released particles are captured by the hood. If some of the released particles are not captured, the designer may have to increase the hood flow rate or the hood size until all released particles are captured.

The model was developed using cross-drafts which were uniform in direction and magnitude. Cross-drafts in industrial situations are unlikely to be uniform over a long time period such as several hours or even minutes. The greatest limitation on the use of the model is the variation of industrial cross-drafts. The cross-drafts may have a distribution of magnitudes and directions. If these parameters can be quantified, they could be very useful for hood design engineers. Designers will have to take care in using the model. Cross-drafts should be measured around the area where the exhaust hood is going to be installed in order to include this value in the computer program to calculate the required flow rate to capture the contaminants. The exhaust system will have to be tested after installing and when in use.

Validation of the model in the field is important in order to determine the accuracy when scaled up to larger hoods as well as to determine the effects of worker activity on the efficiency of local exhaust hoods. Further research is also required to validate the model on different sizes and densities of particles.

The developed model for predicting the movement of a particle into a flanged circular hood has been programmed in basic. The program takes 2-5 minutes to run on a standard personal computer. The program calculates the location of a

particle at selected time intervals.

The importance of local exhaust hoods is to protect workers from hazardous materials. An accurate model for capturing particles should result in more effective protection and economic local exhaust hood design.

6.3 REFERENCES

1. Dalla Valle, J.M.: Exhaust Hoods. Industrial Press, New York 1945

2. Alerius, A. and A. Jansson: Air Flow and Particle Transport into Local Exhaust Hoods. Solna, Sweden 1989.

TABLE 1.1

Hemeon's Recommended Capture Velocities (ref.8)

Draught Characteristics	Lower Safety Factor (Non-toxic dusts or toxic at small emission rates)	Higher Safety Factor (Toxic dusts, large emission rates of non-toxic dusts)
	Controlling velocities at farthest null point fpm ($m\ s^{-1}$)	
Draughtless	40 - 50 fpm (0.2 - 0.25 $m\ s^{-1}$)	50 - 60 fpm (0.25 - 0.30 $m\ s^{-1}$)
Moderately Draughtly	50 - 60 fpm (0.25 - 0.30 $m\ s^{-1}$)	60 - 70 fpm (0.30 - 0.36 $m\ s^{-1}$)
Very Draughty	70 - 80 fpm (0.36 - 0.41 $m\ s^{-1}$)	75 - 100 fpm (0.38 - 0.51 $m\ s^{-1}$)

TABLE 1.2

Recommended Capture Velocities - ACGIH (ref.2) and Alden and Kane (ref.25)

Condition of Dispersion of Contaminant	Examples	Capture Velocity, $m\ s^{-1}$
Released with practically no velocity into quiet air.	Evaporation from tanks; degreasing, etc.	0.25-0.5
Released at low velocity into moderately still air.	Spray booths; intermittent container filling; low speed conveyor transfers; welding; plating; pickling.	0.5-1.0
Active generation into zone of rapid air motion	Spray painting in shallow booths; barrel filling; conveyor loading; crushers	1.0-2.
Released at high initial velocity into zone of very rapid air motion.	Grinding; abrasive blasting; tumbling.	2.5-10

In each category above, a range of capture velocity is shown. The proper choice of values depends on several factors:

Lower End of Range

1. Room air currents minimal or favourable to capture.
2. Contaminants of low toxicity or of nuisance value only.
3. Intermittent, low production.
4. Large hood - large air mass in motion.

Upper End of Range

1. Disturbing room air currents.
2. Contaminants of high toxicity.
3. High production, heavy use.
4. Small hood - local control only.

TABLE 5.1

Comparison between experimental and theoretical trajectories for two models.

Photograph 1 bubble NO(1)

D=0.15 M	Q=.0529305 M3/S	Vc (anemo) =0.55 M/S
Db =3.643 mm	Vt=0.009 M/S	Vc (photo) =0.556 M/S
Rb=1.229 KG/M3	Vb.h=0.55 M/S	

MEASUREMENTS		MODEL 1		MODEL 2	
X	Y	X	Y	X	Y
41.84	-13.10	41.84	-13.10	41.84	-13.10
39.06	-13.15	39.10	-13.09	38.44	-12.87
36.16	-13.23	36.28	-13.05	34.70	-12.50
33.12	-13.27	33.43	-13.00	30.84	-12.07
30.20	-13.27	30.55	-12.92	26.88	-11.54
27.10	-13.23	27.63	-12.82	22.79	-10.90
23.96	-13.12	24.66	-12.67	18.55	-10.07
20.86	-12.95	21.63	-12.47	14.13	-8.96
17.60	-12.62	18.53	-12.18	9.54	-7.37
14.25	-12.10	15.33	-11.76	5.02	-4.92
10.90	-11.33	12.01	-11.12	1.34	-1.57
7.45	-9.92	8.54	-10.09	-0.1	-0.1
3.83	-7.51	4.96	-8.33		
0.48	-2.43	1.43	-4.94		
		M=0.92		M=6.8	
		S=0.63		S=4.33	

TABLE 5.1 Continued

Photograph 1 bubble NO(2)
D=.15 M Q=0.0529305 M3/S Vc =0.55 M/S (anemo)
Db=5.117 mm Vt=0.045 M/S Vc =0.562 M/S (photo)
Rb=1.349 KG/M3 Vb.h=0.55 M/S

MEASUREMENTS		MODEL 1		MODEL 2	
X	Y	X	Y	X	Y
42.87	-16.20	42.87	-16.20	42.87	-16.20
40.06	-16.43	40.16	-16.37	39.68	-16.15
37.00	-16.58	37.38	-16.50	36.09	-15.92
34.25	-16.81	34.56	-16.62	32.38	-15.62
31.28	-16.92	31.72	-16.72	28.57	-15.22
28.54	-17.18	28.85	-16.97	24.68	-14.72
25.61	-17.28	25.96	-16.82	20.70	-14.06
23.03	-17.32	23.03	-16.82	16.62	-13.18
20.17	-17.19	20.07	-16.75	12.47	-12.01
17.29	-17.08	17.07	-16.61	8.30	-10.41
14.42	-16.74	14.03	-16.36	4.27	-8.20
11.70	-16.53	10.97	-15.97	0.7	-5.27
9.04	-15.97	7.89	-15.39	-2.3	-1.91
6.45	-15.18	4.84	-14.95	-4.46	-0.2
3.67	-14.17	1.86	-13.50		
1.23	-12.92	-0.9	-12.09		
-0.95	-11.23	-3.51	-10.32		
-2.80	-9.05	-5.67	-8.19		
-4.00	-5.79	-7.25	-5.64		
-3.73	-0.57	-7.78	-2.51		
		M=1.36		M=8.54	
		S=1.21		S=6.10	

TABLE 5.1 Continued

Photograph 2 bubble NO(1)

D=.15 M Q=.0529305 M3/S Vc =0.67 M/S (anemo)

Db=2.972 MM Vt=0.0326 M/S Vc =0.74 M/S (photo)

Rb=1.436 KG/M3 Vb.h=0.67 M/S

MEASUREMENTS		MODEL 1		MODEL 2	
X	Y	X	Y	X	Y
40.80	-14.39	40.80	-14.39	40.80	-14.39
37.08	-14.57	37.46	-14.49	36.77	-14.21
33.52	-14.55	34.05	-14.55	32.41	-13.87
30.14	-14.56	30.60	-14.58	27.94	-13.44
26.18	-14.51	27.1	-14.58	23.35	-12.86
22.64	-14.41	23.56	-14.53	18.63	-12.07
19.02	-14.18	19.97	-14.40	13.79	-10.95
15.30	-13.75	16.3	-14.14	8.87	-9.30
11.64	-13.18	12.55	-13.70	4.15	-6.84
7.68	-12.42	8.74	-12.97	1.6	-3.53
4.04	-10.83	4.93	-11.80	-3.23	-0.3
0.36	-8.37	1.25	-9.96		
-2.55	-3.94	-2.02	-7.14		
		M=1.15		M=6.02	
		S=0.73		S=3.93	

TABLE 5.1 Continued

Photograph 3 bubble NO(1)

D=0.15 M Q=0.0529305 M3/S Vc =0.67 M/S (anemo)

Db=4.426 MM Vt=0.022 M/S Vc =0.696 M/S (photo)

Rb=1.273 KG/M3 Vb.h=0.67 M/S

MEASUREMENTS		MODEL 1		MODEL 2	
X	Y	X	Y	X	Y
43.05	-10.66	43.05	-10.66	43.05	-10.66
39.57	-10.77	39.75	-10.72	39.16	-10.55
35.93	-10.88	36.36	-10.76	34.86	-10.32
32.28	-10.92	32.93	-10.78	30.41	-10.01
28.80	-11.06	29.45	-10.78	25.81	-9.61
25.16	-11.10	25.91	-10.74	21.05	-9.07
21.55	-10.94	22.31	-10.64	16.09	-8.29
17.73	-10.79	18.6	-10.45	10.89	-7.09
13.56	-10.20	14.76	-10.10	5.63	-5.04
9.26	-9.29	10.72	-9.43	1.15	-1.89
4.86	-7.17	6.46	-8.10	-1.49	0.2
0.36	-1.97	2.12	-5.21		
		M=1.15		M=5.35	
		S=0.91		S=3.57	

TABLE 5.1 Continued

Photograph 4 bubble NO(1)

D=0.15 M Q=0.0529305 M3/S Vc =0.92 M/S (anemo)

Db=4.41 MM Vt=0.04 M/S Vc =0.98 M/S (photo)

Rb=1.36 KG/M3 Vb.h=0.92 M/S

MEASUREMENTS		MODEL 1		MODEL 2	
X	Y	X	Y	X	Y
39.72	-11.12	39.72	-11.12	39.72	-11.12
34.82	-11.33	35.19	-11.25	34.85	-11.04
29.86	-11.56	30.56	-11.35	28.98	-10.79
25.04	-11.60	25.85	-11.40	23.17	-10.39
20.17	-11.48	21.05	-11.37	17.15	-9.74
15.30	-11.09	16.13	-11.21	10.93	-8.63
10.20	-10.42	11.03	-10.75	4.72	-6.63
4.98	-8.47	5.77	-9.67	-0.60	-3.51
-0.12	-4.29	0.60	-7.41	-5.45	-0.20
		M=1.14		M=4.13	
		S=0.82		S=2.54	

TABLE 5.1 Continued

Photograph 5 bubble NO(1)

D=0.15 M Q=0.0363864 M3/S Vc =0.53 M/S (anemo)

Db=3.643 MM Vt=0.077 M/S Vc =0.464 M/S (photo)

Rb=1.74 KG/M3 Vb.h=0.53 M/S

MEASUREMENTS		MODEL 1		MODEL 2	
X	Y	X	Y	X	Y
41.61	-11.00	41.61	-11.00	41.61	-11.00
39.29	-11.34	38.99	-11.34	38.59	-11.20
36.48	-11.56	36.31	-11.65	35.29	-11.32
34.01	-11.78	33.61	-11.96	31.90	-11.39
31.05	-12.01	30.89	-12.26	28.44	-11.40
28.49	-12.19	28.15	-12.53	24.93	-11.34
25.72	-12.35	25.38	-12.78	21.34	-11.17
23.16	-12.46	22.57	-12.99	17.68	-10.87
20.30	-12.60	19.73	-13.14	13.95	-10.36
17.53	-12.50	16.85	-13.23	10.19	-9.57
14.60	-12.44	13.92	-13.22	6.50	-8.39
11.84	-12.24	10.96	-13.07	3.04	-6.75
8.91	-11.67	7.98	-12.74	0.03	-4.72
6.04	-10.76	5.03	-12.17	-2.69	-2.58
3.23	-9.44	2.15	-11.32	-5.49	-0.6
0.6	-7.42	-0.5	-10.17		
-1.57	-4.01	-3.01	-8.7		
		M=1.26		M=6.84	
		S=1.19		S=3.93	

TABLE 5.1 Continued

Photograph 6 bubble NO(1)

D=0.15 M	Q=0.0363864 M3/S	Vc (anemo) =0.53 M/S
Db=5.177 MM	Vt=0.014 M/S	Vc (photo) =0.534 M/S
Rb=1.223 KG/M3	Vb.h=0.53 M/S	

MEASUREMENTS		MODEL 1		MODEL 2	
X	Y	X	Y	X	Y
42.42	-9.24	42.42	-9.24	42.42	-9.24
39.75	-9.17	39.83	-9.19	39.47	-9.12
36.97	-9.17	37.18	-9.17	36.23	-8.96
34.19	-9.06	34.51	-9.15	32.88	-8.77
31.36	-9.06	31.80	-9.13	29.45	-8.55
28.52	-9.02	29.07	-9.10	25.93	-8.29
25.50	-8.95	26.31	-9.05	22.32	-7.95
22.58	-8.75	23.50	-8.98	18.60	-7.52
19.47	-8.57	20.63	-8.87	14.74	-6.94
16.34	-8.23	17.69	-8.70	10.73	-6.11
12.86	-7.70	14.64	-8.43	6.66	-4.81
9.26	-6.95	11.45	-7.97	2.94	-2.81
5.34	-4.86	8.07	-7.15	-0.08	-0.61
		M=1.15		M=3.88	
		S=0.99		S=2.42	

TABLE 5.1 Continued

Photograph 7 bubble NO(1)

D=0.15 M Q=0.0529305 M3/S Vc =0.92 M/S (anemo)

Db=7.846 MM Vt=0.071 M/S Vc =1.012 M/S (photo)

Rb=1.337 KG/M3 Vb.h=0.92 M/S

MEASUREMENTS		MODEL 1		MODEL 2	
X	Y	X	Y	X	Y
43.06	-11.72	43.06	-11.72	43.06	-11.72
38.00	-12.11	38.59	-12.03	38.24	-11.90
32.89	-12.46	34.04	-12.30	32.98	-11.90
27.9	-12.80	29.43	-12.54	27.47	-11.77
22.69	-12.98	24.76	-12.73	21.77	-11.50
17.37	-13.04	20.02	-12.86	15.89	-10.97
11.87	-12.80	15.18	-12.86	9.86	-10.03
6.40	-12.19	10.23	-12.63	3.89	-8.39
0.90	-10.81	5.22	-12.01	-1.55	-5.88
-3.91	-8.59	0.30	-10.84	-6.70	-2.87
-7.41	-5.56	-4.31	-9.05	-12.87	-0.30
		M=2.91		M=3.37	
		S=1.45		S=2.41	

TABLE 5.1 Continued

Photograph 7 bubble NO(1)

Correction to Vb.h for extract is about + 0.04 M/S

Parallax Error 5.1%

Corrected Values

Db=7.445 MM Vt=0.074 M/S Vc =0.96 M/S (photo)

Rb=1.358 KG/M3 Vb.h=0.96 M/S

MEASUREMENTS		MODEL 1		MODEL 2	
X	Y	X	Y	X	Y
40.86	-11.12	40.86	-11.12	40.86	-11.12
36.06	-11.49	36.24	-11.44	35.26	-10.76
31.21	-11.82	31.61	-11.72	29.51	-10.31
26.48	-12.15	26.94	-11.97	23.57	-9.68
21.53	-12.32	22.21	-12.14	17.38	-8.78
16.48	-12.37	17.39	-12.22	10.92	-7.28
11.26	-12.15	12.45	-12.11	4.68	-4.54
6.07	-11.57	7.40	-11.66	-0.10	-1.18
0.85	-10.26	2.34	-10.63	-2.38	-0.10
-3.71	-8.15	-2.45	-8.85		
-7.03	-5.27	-6.60	-6.39		
		M=0.93		M=6.61	
		S=0.44		S=3.83	

TABLE 5.1 Continued

Photograph 8 bubble NO(1)

D=0.15 M Q=0.0529305 M3/S Vc =0.67 M/S (anemo)

Db=2.908 MM Vt=0.0276 M/S Vc =0.767 M/S (photo)

Rb=1.395 KG/M3 Vb.h=0.67 M/S

MEASUREMENTS		MODEL 1		MODEL 2	
X	Y	X	Y	X	Y
38.83	-13.67	38.83	-13.67	38.83	-13.67
35.00	-13.83	35.48	-13.73	34.75	-13.43
31.13	-13.61	32.04	-13.76	30.33	-13.05
27.40	-13.54	28.56	-13.75	25.78	-12.55
23.48	-13.45	25.03	-13.70	21.10	-11.88
19.64	-13.07	21.44	-13.58	16.28	-10.94
15.53	-12.64	17.77	-13.36	11.32	-9.58
11.72	-12.12	14.01	-12.97	6.37	-7.52
8.30	-10.99	10.16	-12.30	1.93	-4.48
3.40	-8.88	6.24	-11.16	-1.61	-1.07
-0.36	-5.22	2.39	-9.27	-3.26	0.10
		M=2.15		M=4.66	
		S=1.24		S=3.02	

TABLE 5.1 Continued

Photograph 8 bubble NO(1)

Correction to Vb.h for extract is about + 0.04 M/S

Parallax Error 7.4%

Corrected Values

Db=2.693 MM Vt=0.03 M/S Vc =0.71 M/S (photo)

Rb=1.448 KG/M3 Vb.h=0.71 M/S

MEASUREMENTS		MODEL 1		MODEL 2	
X	Y	X	Y	X	Y
35.96	-12.65	35.96	-12.65	35.96	-12.65
32.41	-12.80	32.51	-12.72	31.74	-12.39
28.82	-12.60	29.03	-12.73	27.22	-11.97
25.37	-12.53	22.49	-12.70	22.55	-11.39
21.74	-12.46	21.88	-12.61	17.72	-10.58
18.18	-12.10	18.19	-12.41	12.73	-9.39
14.38	-11.70	14.39	-12.04	7.66	-7.56
10.85	-11.22	10.47	-11.36	2.97	-4.71
7.68	-10.18	6.44	-10.15	-0.70	-1.31
3.15	-8.22	2.44	-7.93	-2.37	0.00
-0.33	-4.83	-1.07	-3.55		
		M=0.52		M=6.25	
		S=0.44		S=3.82	

TABLE 5.1 Continued

Photograph 9 bubble NO(1)

D=0.15 M Q=0.0363864 M3/S Vc =0.73 M/ (anemo)

Db=4.762 MM Vt=0.035 M/S Vc =0.836 M/S (photo)

Rb=1.32 KG/M3 Vb.h=0.73 M/S

MEASUREMENTS		MODEL 1		MODEL 2	
X	Y	X	Y	X	Y
41.61	-12.10	41.61	-12.10	41.61	-12.10
37.43	-11.90	37.99	-12.04	37.70	-11.95
33.27	-11.83	34.36	-12.11	33.48	-11.82
28.94	-11.80	30.70	-12.19	29.14	-11.65
24.69	-11.78	27.00	-12.26	24.70	-11.40
20.28	-11.65	23.26	-12.29	20.17	-11.03
15.87	-11.47	19.47	-12.27	15.55	-10.49
11.53	-11.22	15.61	-12.15	10.84	-9.66
7.16	-10.42	11.68	-11.88	6.17	-8.39
2.75	-9.22	7.68	-11.36	1.79	-6.57
-1.21	-7.30	3.69	-10.45	-2.09	-4.34
-4.12	-4.05	-0.1	-9.02	-5.96	-2.01
		M=3.55		M=1.4	
		S=1.85		S=1.1	

TABLE 5.1 Continued

Photograph 9 bubble NO(1)

Correction to Vb.h for extract is about + 0.03 M/S

Parallax Error 9%

Corrected Values

Db=4.333 MM Vt=0.038 M/S Vc =0.76 M/S (photo)

Rb=1.356 KG/M3 Vb.h=0.76 M/S

MEASUREMENTS		MODEL 1		MODEL 2	
X	Y	X	Y	X	Y
37.86	-11.01	37.86	-11.01	37.86	-11.01
34.06	-10.82	34.20	-11.15	33.81	-11.00
30.27	-10.76	30.52	-11.27	29.48	-10.87
26.33	-10.73	26.81	-11.35	25.03	-10.66
22.46	-10.72	23.06	-11.40	20.48	-10.34
18.45	-10.60	19.24	-11.39	15.81	-9.83
14.44	-10.43	15.35	-11.27	11.06	-9.04
10.49	-10.21	11.37	-10.98	6.32	-7.78
6.51	-9.48	7.30	-10.37	1.90	-5.91
2.50	-8.39	3.24	-9.26	-1.95	-3.64
-1.10	-6.64	-0.60	-7.46	-5.76	-1.36
-3.75	-3.68	-3.92	-4.77	-9.00	0.00
		M=0.95		M=3.76	
		S=0.27		S=2.36	

TABLE 5.1 Continued

Photograph 10 bubble NO(1)

D=0.15 M Q=0.0363864 M3/S Vc =0.73 M/ (anemo)

Db=2.492 MM Vt=0.037 M/S Vc =0.788 M/S (photo)

Rb=1.57 KG/M3 Vb.h=0.73 M/S

MEASUREMENTS		MODEL 1		MODEL 2	
X	Y	X	Y	X	Y
40.80	-9.80	40.80	-9.80	40.80	-9.80
36.85	-10.00	37.19	-9.94	36.68	-9.79
32.55	-10.08	33.53	-10.06	32.32	-9.71
28.75	-10.20	29.83	-10.17	27.87	-9.57
24.92	-10.20	26.09	-10.24	23.31	-9.33
20.86	-10.10	22.29	-10.27	18.64	-8.95
16.80	-9.97	18.41	-10.23	13.83	-8.33
12.54	-9.52	14.43	-10.04	8.93	-7.29
8.09	-8.50	10.31	-9.60	4.23	-5.58
3.88	-6.60	6.09	-8.65	1.86	-3.31
-0.12	-2.55	1.94	-6.78	-3.44	-1.12
		M=1.87		M=2.6	
		S=1.19		S=1.54	

TABLE 5.1 Continued

Photograph 10 bubble NO(1)

Correction to Vb.h for extract is about + 0.03 M/S

Parallax Error 3.7%

Corrected Values

Db=2.399 MM Vt=0.04 M/S Vc =0.76 M/S (photo)

Rb=1.644 KG/M3 Vb.h=0.76 M/S

MEASUREMENTS		MODEL 1		MODEL 2	
X	Y	X	Y	X	Y
39.29	-9.43	39.29	-9.43	39.29	-9.43
35.48	-9.63	35.63	-9.58	35.11	-9.43
31.34	-9.70	31.95	-9.72	30.72	-9.35
27.68	-9.82	28.23	-9.83	26.22	-9.21
24.00	-9.82	24.47	-9.91	21.62	-8.95
20.08	-9.72	20.63	-9.93	16.88	-8.52
16.18	-9.60	16.70	-9.85	12.01	-7.80
12.07	-9.16	12.64	-9.59	7.11	-6.55
7.79	-8.18	8.44	-8.96	2.61	-4.57
3.73	-6.35	4.17	-7.60	-1.18	-2.28
-0.11	-2.45	0.10	-4.96	-4.80	-0.30
		M=0.84		M=3.66	
		S=0.62		S=2.14	

TABLE 5.1 Continued

Photograph 11 bubble NO(1)

D=0.15 M	Q=0.0363864 M3/S	Vc (anemo) =1.00 M/S
Db=2.951 MM	Vt=0.0416 M/S	Vc (photo) =1.10 M/S
Rb=1.532 KG/M3	Vb.h=1.00 M/S	

MEASUREMENTS		MODEL 1		MODEL 2	
X	Y	X	Y	X	Y
39.24	-7.45	39.24	-7.45	39.24	-7.45
33.73	-7.68	34.33	-7.62	33.82	-7.49
28.17	-7.75	29.34	-7.76	28.09	-7.45
22.30	-8.05	24.27	-7.87	22.20	-7.31
16.11	-8.18	19.10	-7.90	16.12	-6.98
9.73	-8.12	13.75	-7.78	9.84	-6.25
3.52	-7.28	8.11	-7.17	3.70	-4.65
-2.43	-4.98	2.34	-5.22	-1.57	-2.40
-6.22	-0.23	-2.58	-0.50	-6.57	-0.30
		M=2.97		M=1.25	
		S=1.47		S=0.97	

TABLE 5.1 Continued

Photograph 11 bubble NO(1)

Correction to Vb.h for extract is about + 0.03 M/S

Parallax Error 6.4%

Corrected Values

Db=2.762 MM Vt=0.042 M/S Vc =1.03 M/S (photo)

Rb=1.575 KG/M3 Vb.h=1.03 M/S

MEASUREMENTS		MODEL 1		MODEL 2	
X	Y	X	Y	X	Y
36.72	-6.97	36.72	-6.97	36.97	-6.97
31.57	-7.18	31.74	-7.14	31.21	-7.00
26.36	-7.25	26.71	-7.27	25.40	-6.93
20.87	-7.53	21.59	-7.36	19.41	-6.74
15.08	-7.65	16.32	-7.33	13.20	-6.29
9.11	-7.60	10.78	-7.02	6.84	-5.22
3.29	-6.82	4.90	-5.73	1.09	-3.17
-2.27	-4.66	-0.70	-1.89	-3.90	-1.02
-5.82	-0.21	-2.97	-0.1	-6.38	-0.10
		M=1.53		M=2.18	
		S=1.03		S=1.42	

TABLE 5.1 Continued

Photograph 12 bubble NO(1)

D=0.15 M Q=0.0363864 M3/S Vc =1.00 M/S (anemo)

Db=4.410 MM Vt=0.032 M/S Vc =1.068 M/S (photo)

Rb=1.32 KG/M3 Vb.h=1.00 M/S

MEASUREMENTS		MODEL 1		MODEL 2	
X	Y	X	Y	X	Y
42.42	-10.93	42.42	-10.93	42.42	-10.93
37.08	-11.10	37.55	-11.05	37.17	-10.93
31.75	-11.22	32.62	-11.15	31.61	-10.81
26.58	-11.15	27.64	-11.22	25.91	-10.61
21.32	-10.99	22.61	-11.24	20.08	-10.28
16.23	-10.53	17.49	-11.19	14.12	-9.72
11.07	-9.86	12.25	-10.97	8.08	-8.74
5.88	-8.54	6.91	-10.39	2.27	-7.08
0.60	-6.26	1.59	-9.21	-2.94	-4.88
-3.60	-2.20	-3.33	-7.29	-8.38	-2.61
		M=1.89		M=2.18	
		S=1.53		S=1.56	

TABLE 5.1 Continued

Photograph 12 bubble NO(1)

Correction to Vb.h for extract is about + 0.03 M/S

Parallax Error 3.5%

Corrected Values

Db=4.255 MM Vt=0.034 M/S Vc =1.03 M/S (photo)

Rb=1.338 KG/M3 Vb.h=1.03 M/S

MEASUREMENTS		MODEL 1		MODEL 2	
X	Y	X	Y	X	Y
40.93	-10.54	40.93	-10.54	40.93	-10.54
37.78	-10.71	35.98	-10.67	35.61	-10.54
30.63	-10.82	31.02	-10.77	30.00	-10.43
25.64	-10.75	26.02	-10.84	24.25	-10.21
20.57	-10.60	20.95	-10.86	18.37	-9.84
15.65	-10.16	15.78	-10.77	12.35	-9.18
10.67	-9.51	10.49	-10.46	6.31	-8.03
5.67	-8.24	5.09	-9.68	0.60	-6.16
0.58	-6.04	-0.10	-8.14	-4.48	-3.87
-3.47	-2.12	-4.83	-5.79	-10.26	-1.76
		M=1.18		M=3.4	
		S=1.14		S=2.2	

TABLE 5.1 Continued

D=HOOD DIAMETER IN METER.

Q=HOOD SUCTION VOLUME IN M3/S.

Db=BUBBLE DIAMETER IN MM.

Rb=BUBBLE DENSITY IN KG/M3.

Vt=BUBBLE SETLING VELOCITY IN M/S.

Vc (anemo) =CROSS-WIND VELOCITY (M/S) IN HORIZONTAL DIRECTION

MEASURED BY AN ANEMOMETER.

Vc (photo) =CROSS-WIND VELOCITY (M/S) IN HORIZONTAL DIRECTION

MEASURED FROM A PHOTOGRAPH.

Vb.h=VELOCITY OF A BUBBLE (M/S) IN HORIZONTAL DIRECTION.

X=BUBBLE LOCATION IN THE X-DIRECTION IN CENTIMETER.

Y=BUBBLE LOCATION IN THE Y-DIRECTION IN CENTIMETER.

MODEL 1 = FINAL MODEL DEVELOPED BY FLYNN AND ELLENBECKER.

MODEL 2 = JANSSON'S MODEL.

M=MEAN ERROR; S=STANDARD ERROR OF DEVIATION.

TABLE 5.2

RESULTS OF COMPARING TRAJECTORIES FOR TWO MODELS AND THE EFFECT OF PARALLAX ERROR

			RESULTS WITHOUT CORRECTION					RESULTS WITH CORRECTION				
NO	Vf	Vc	Db	M1	S1	M2	S2	Db	M1	S1	M2	S2
1	3	0.55	3643	0.92	0.63	6.8	4.33					
2	3	0.55	5117	1.36	1.21	8.54	6.1					
3	3	0.67	2972	1.15	0.73	6.02	3.93					
4	3	0.67	4426	1.15	0.91	5.35	3.57					
5	3	0.92	4410	1.14	0.82	4.13	2.54					
6	2	0.53	3643	1.26	1.19	6.48	3.93					
7	2	0.53	5177	1.15	0.99	3.88	2.42					
8	3	0.92	7846	2.91	1.45	3.37	2.41	7445	0.93	0.44	6.61	3.83
9	3	0.67	2908	2.15	1.24	4.66	3.02	2693	0.52	0.44	6.25	3.82
10	2	0.73	4762	3.55	1.85	1.40	1.10	4333	0.95	0.27	3.76	2.36
11	2	0.73	2492	1.87	1.19	2.60	1.54	2399	0.84	0.62	3.66	2.14
12	2	1.00	2951	2.97	1.47	1.25	0.97	2762	1.53	1.03	2.18	1.42
13	2	1.00	4410	1.89	1.33	2.18	1.56	4255	1.18	1.14	3.40	2.20

Vf=HOOD FACE VELOCITY IN M/S;Vc=CROSS-WIND VELOCITY IN M/S;

Db=BUBBLE DIAMETER IN MICRON ;M=MEAN ERROR;

S=STANDARD ERROR OF DEVIATION;

WITHOUT CORRECTION=NO PARALLAX ERROR;

WITH CORRECTION=CORRECTION DUE TO PARALLAX ERROR;

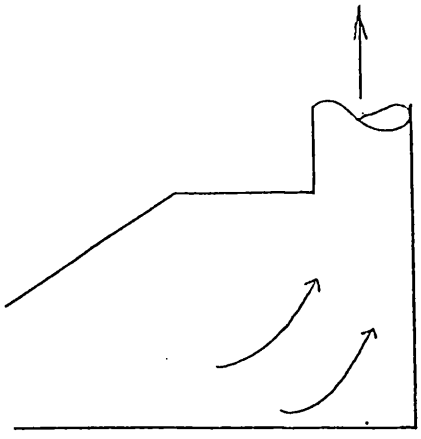

Enclosure Type – Laboratory Hood

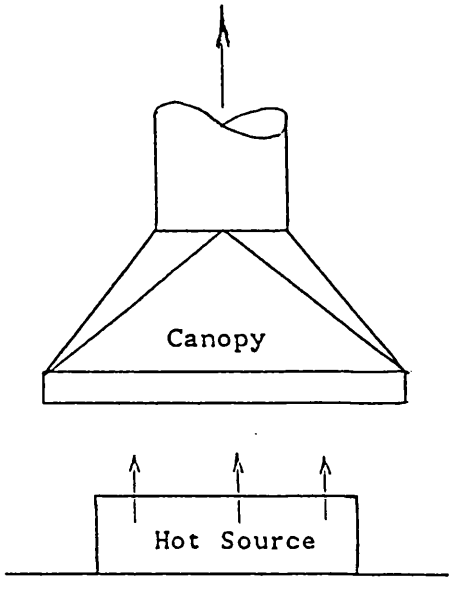

Recieving Type – Canopy Hood

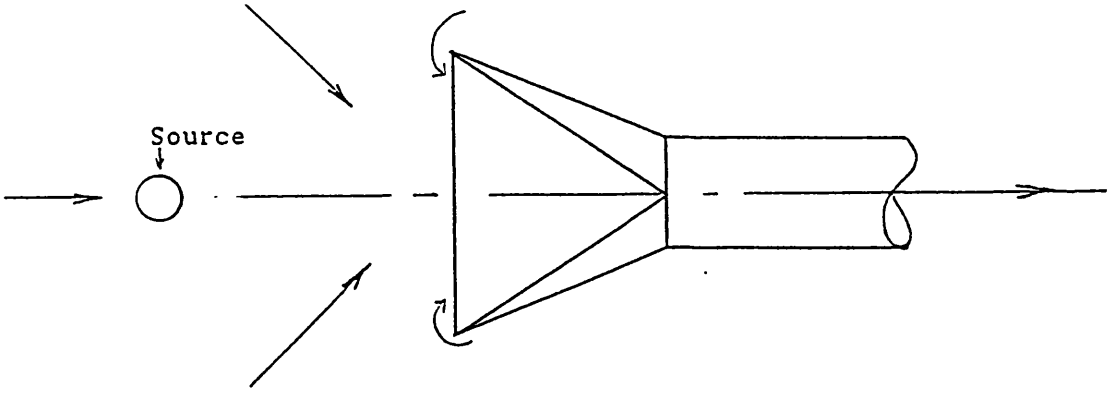

Capturing Type – Side Draft Hood

Fig. 1.1 Types of Hoods

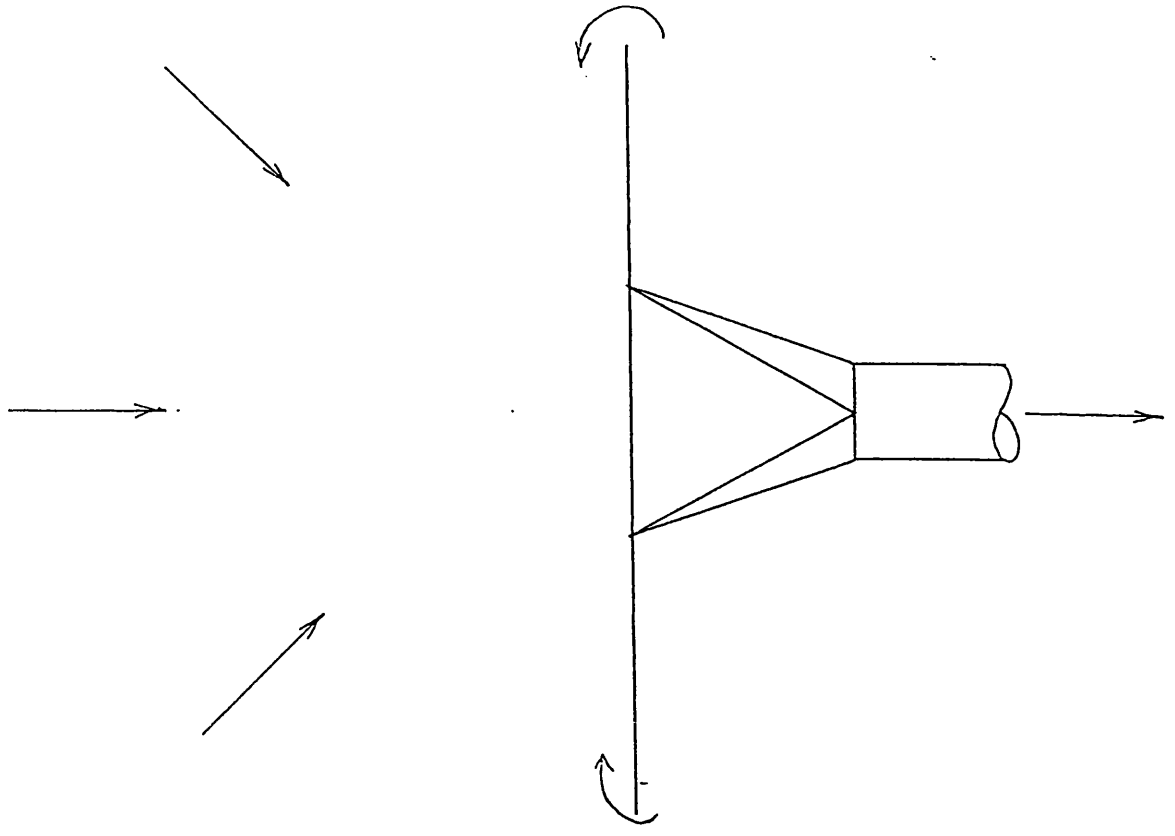

Flanged Hood

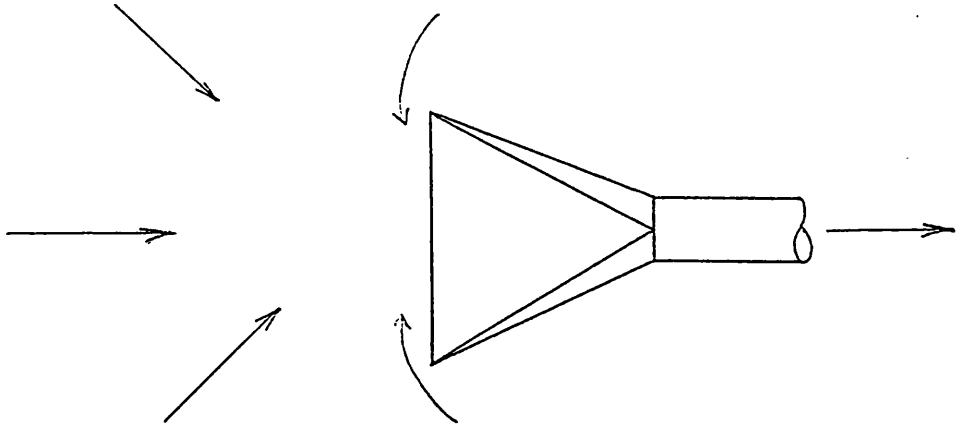

Unflanged Hood

Fig. 1.2 Flanged and Unflanged Hood

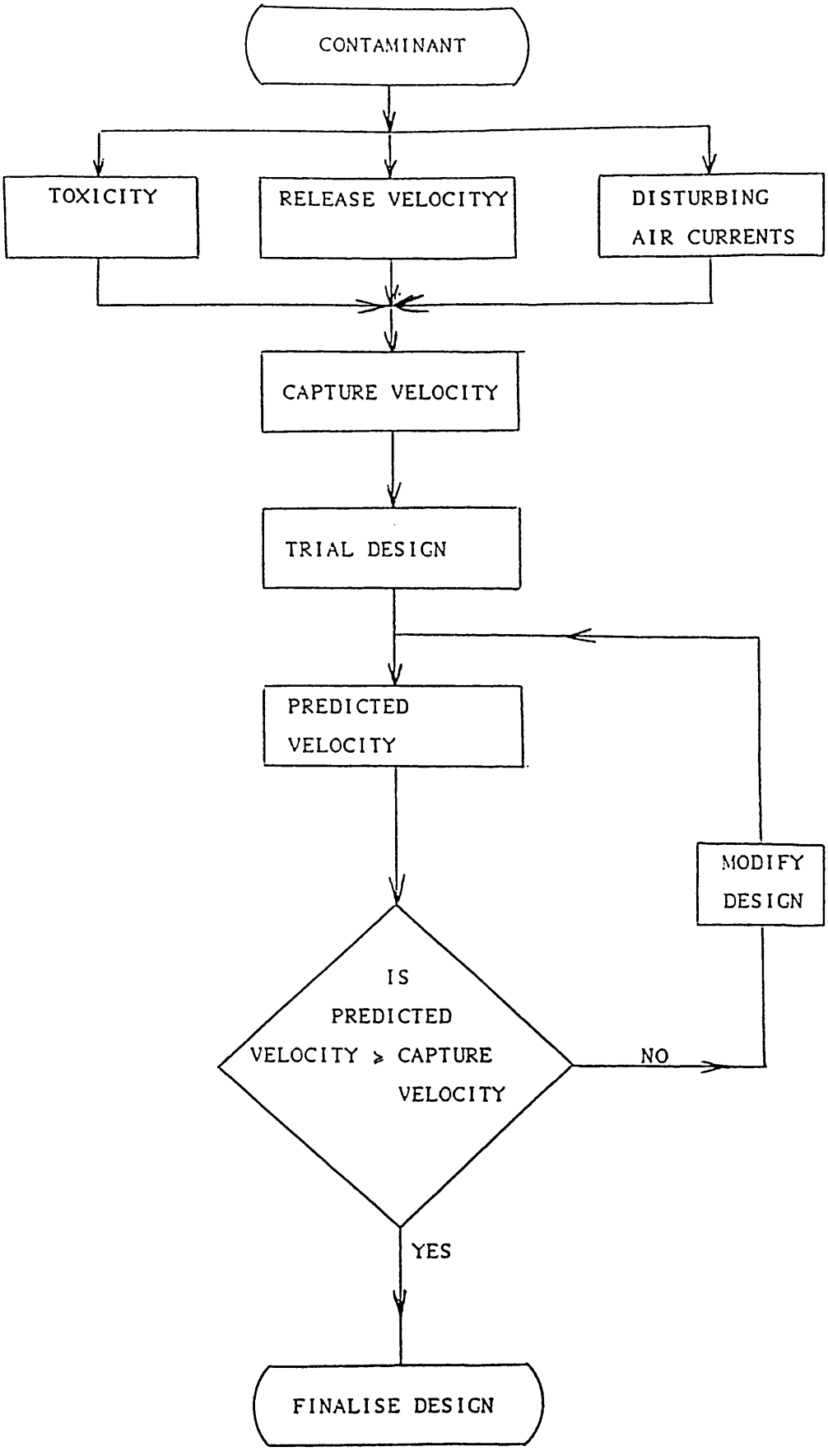

FIG. 1.3 DESIGN PROCEDURE FOR EXHAUST HOODS

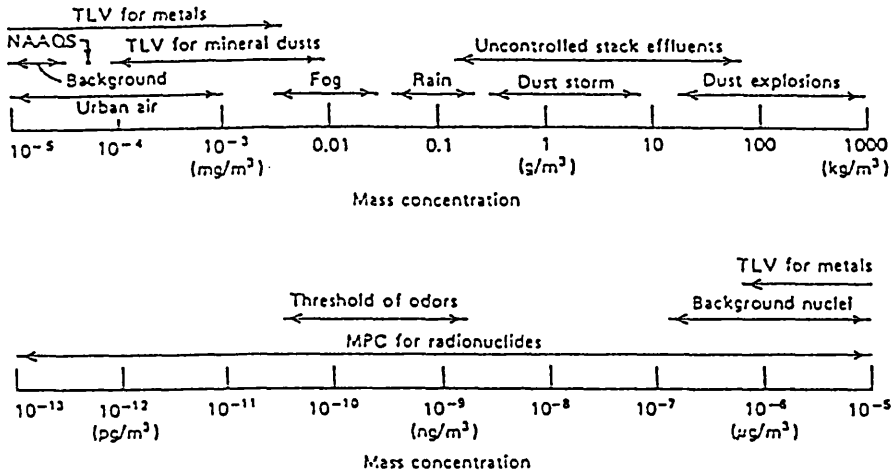

Fig. 2.1 Range of aerosol concentration.

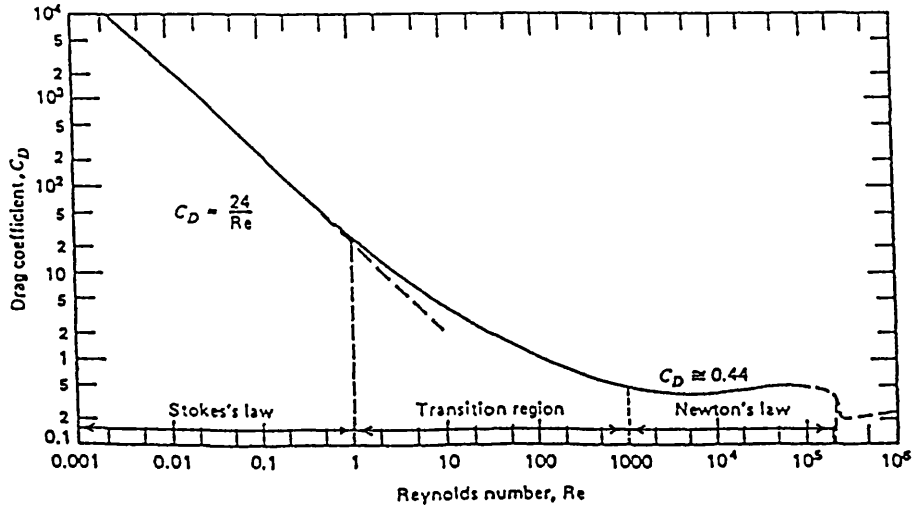

Fig. 2.2 Drag coefficient versus Reynolds number for spheres.

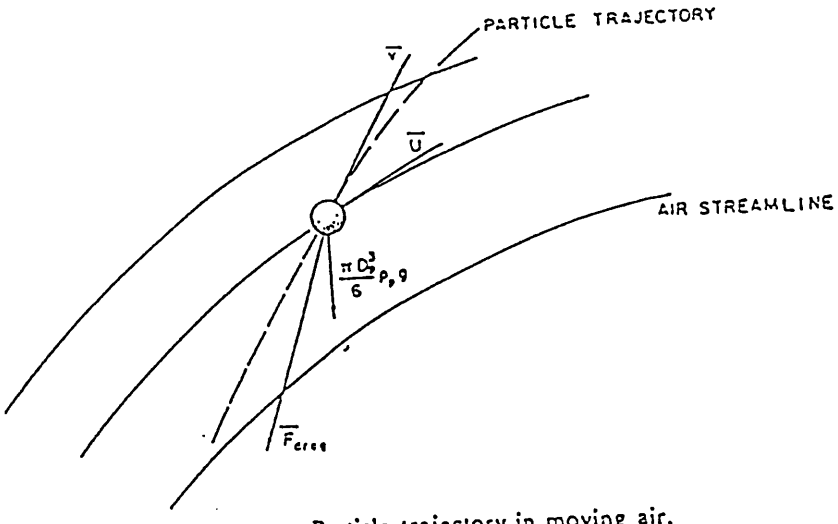

Fig. 2.3 Particle trajectory in moving air.

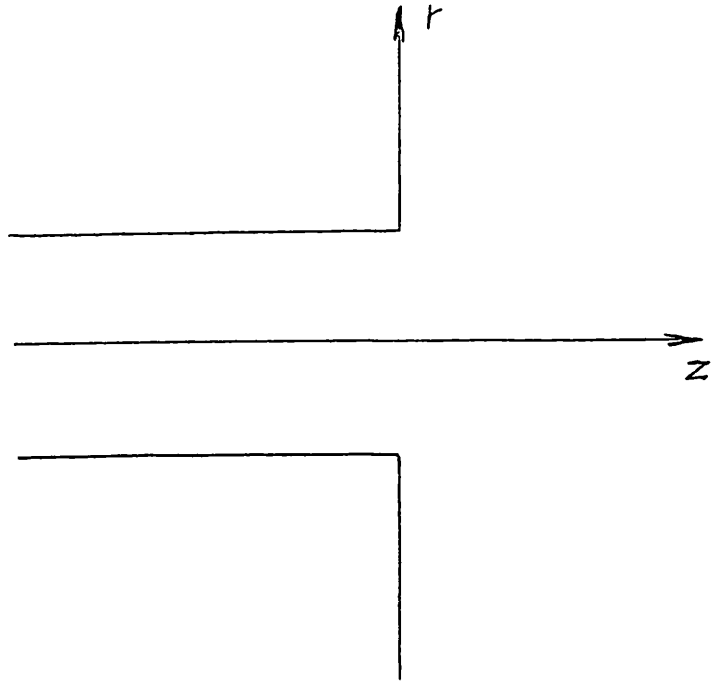

Fig. 3.1 Coordinate system for a flanged circular hood.

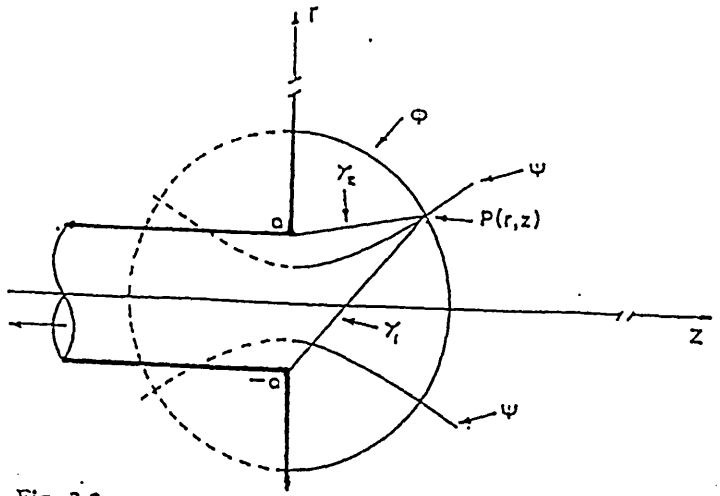

Fig. 3.2 Theoretical potential lines and streamlines for a flanged circular hood.

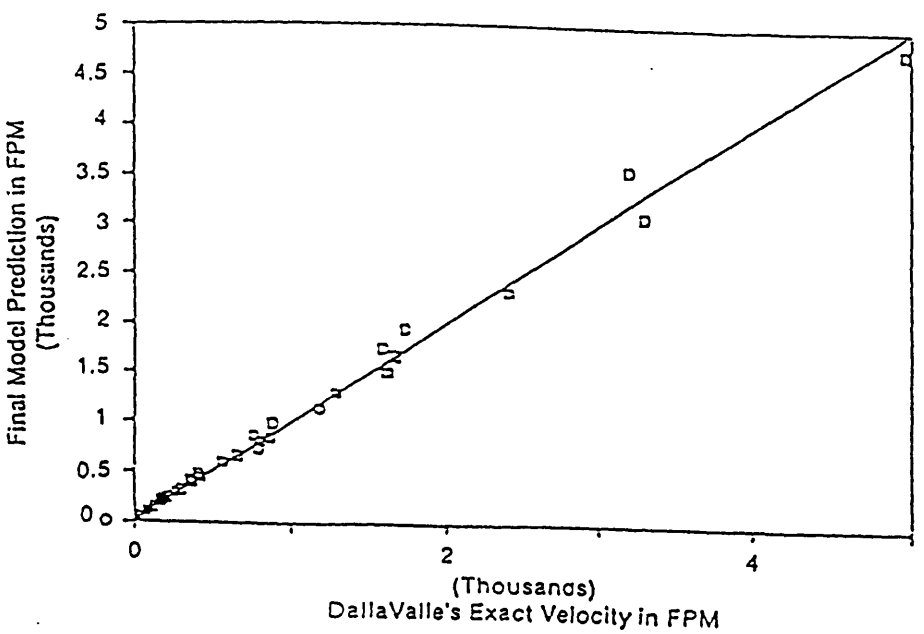

Fig. 3.3 Centerline velocities, final model *vs.* DallaValle's exact prediction.

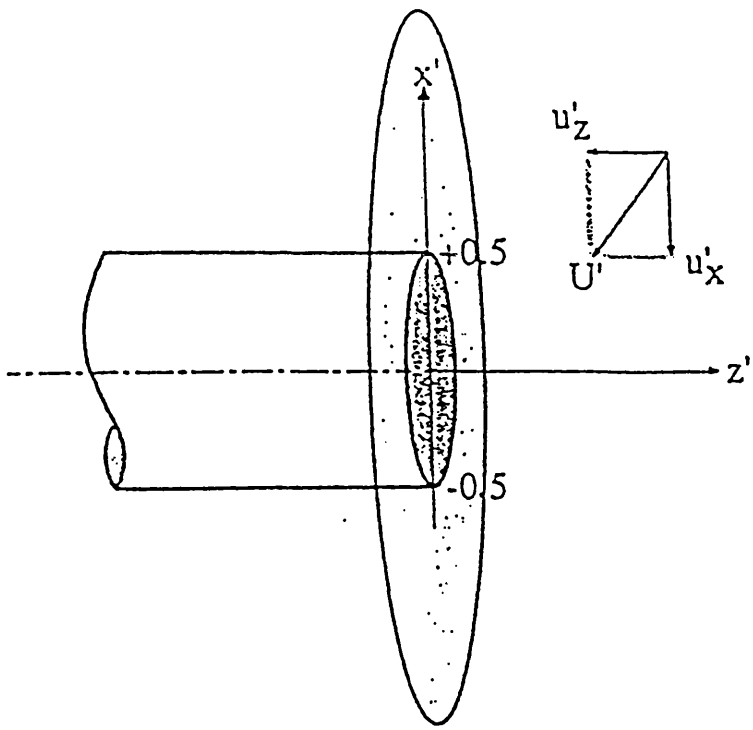

Fig. 3.4 Coordinate system and notations for circular openings

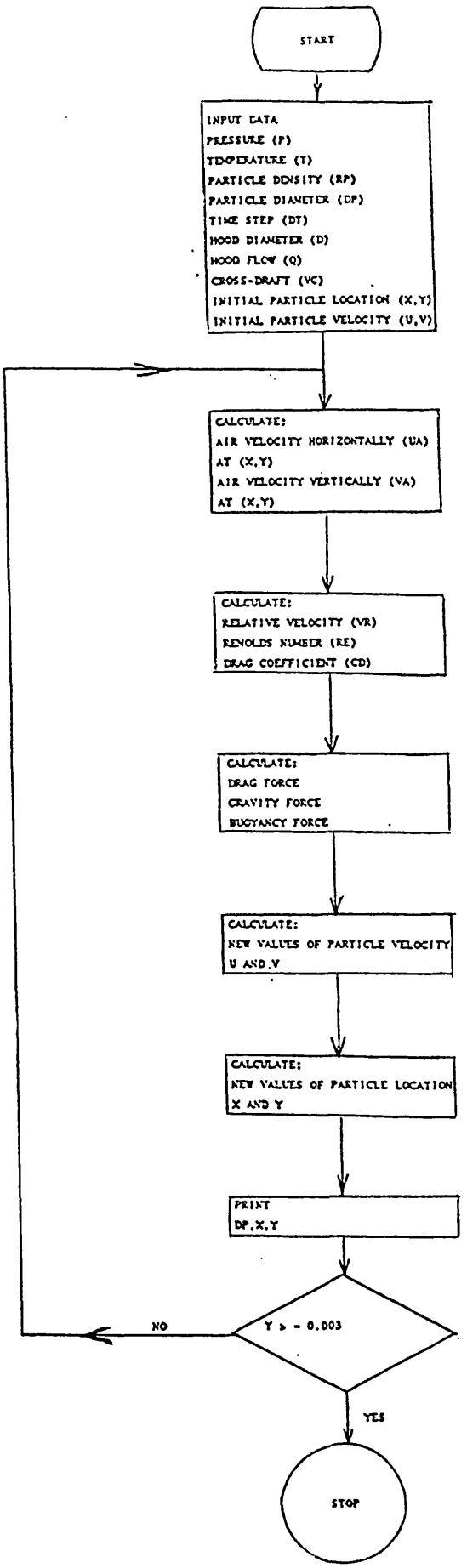

FIG. 4.1 COMPUTER PROGRAM FLOWCHART

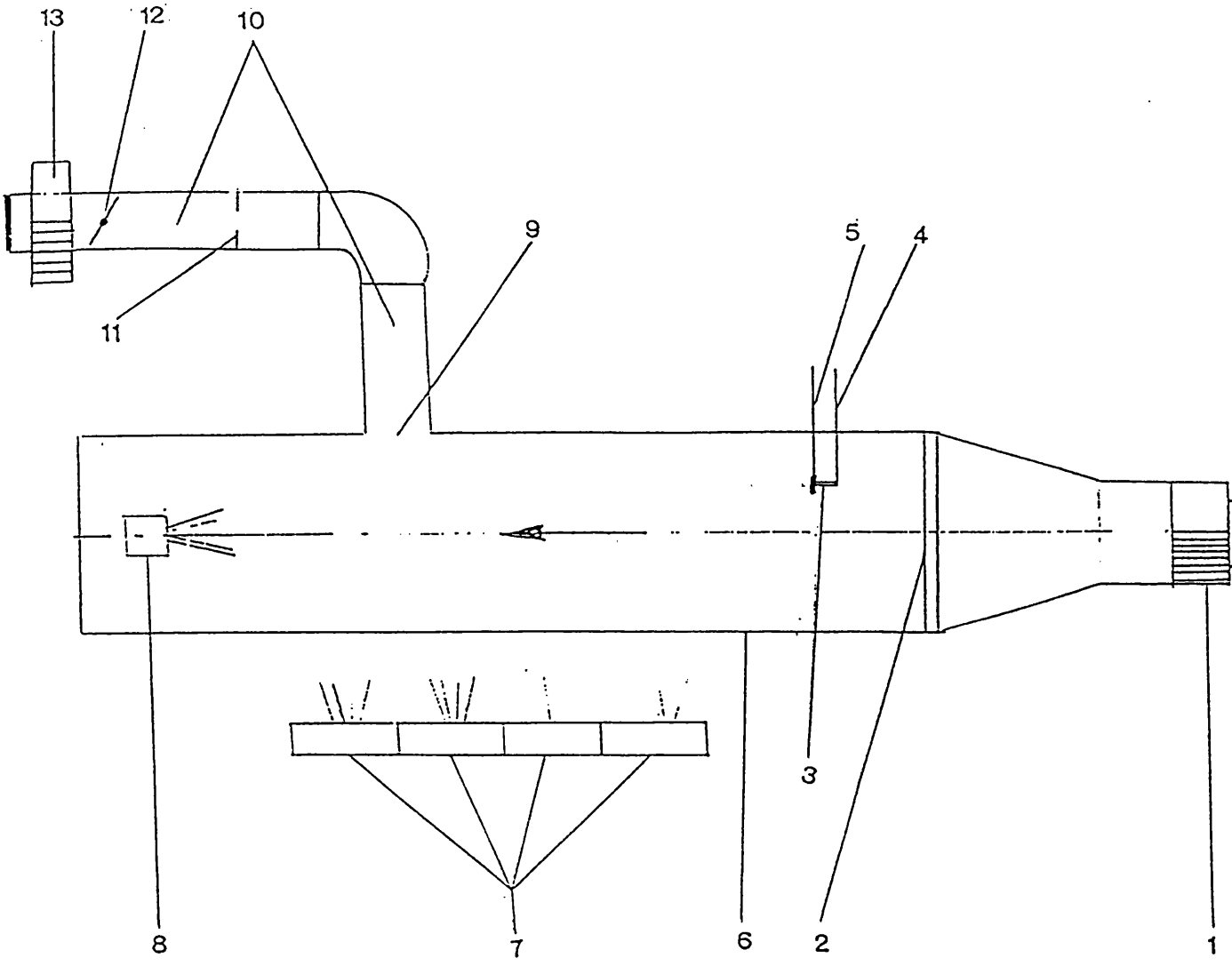

Fig. 5.1 Sketch Of the experimental equipment

1. Variable speed centrifugal fan
2. Perforated gauze flow equliser
3. Bubble generator
4. Compressed air hose
5. Liquid hose
6. Wind tunnel
7. Motor car fog lamps
8. Stroboscope
9. Exhaust hood
10. Air duct
11. Orifice plate
12. Damper
13. Centrifugal fan

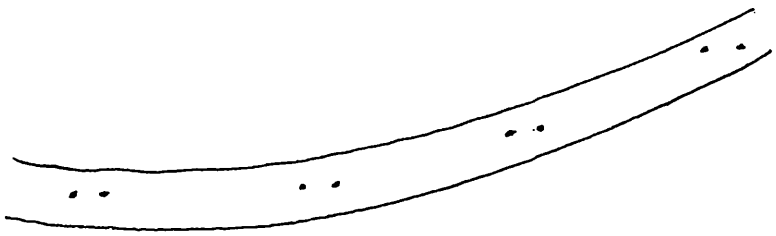

Fig. 5.2 Sketch of a bubble trajectory

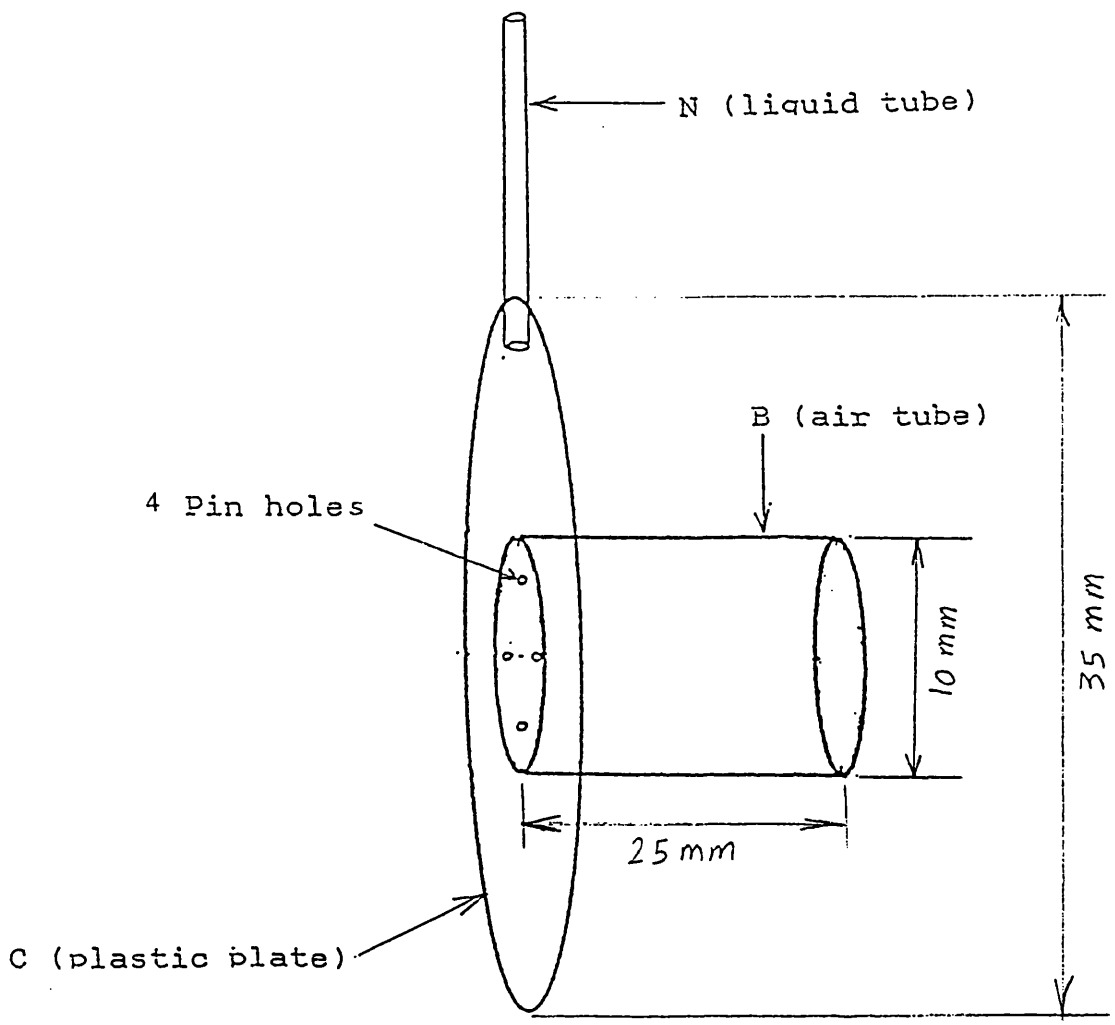

Fig. 5.4 Local made bubble generator

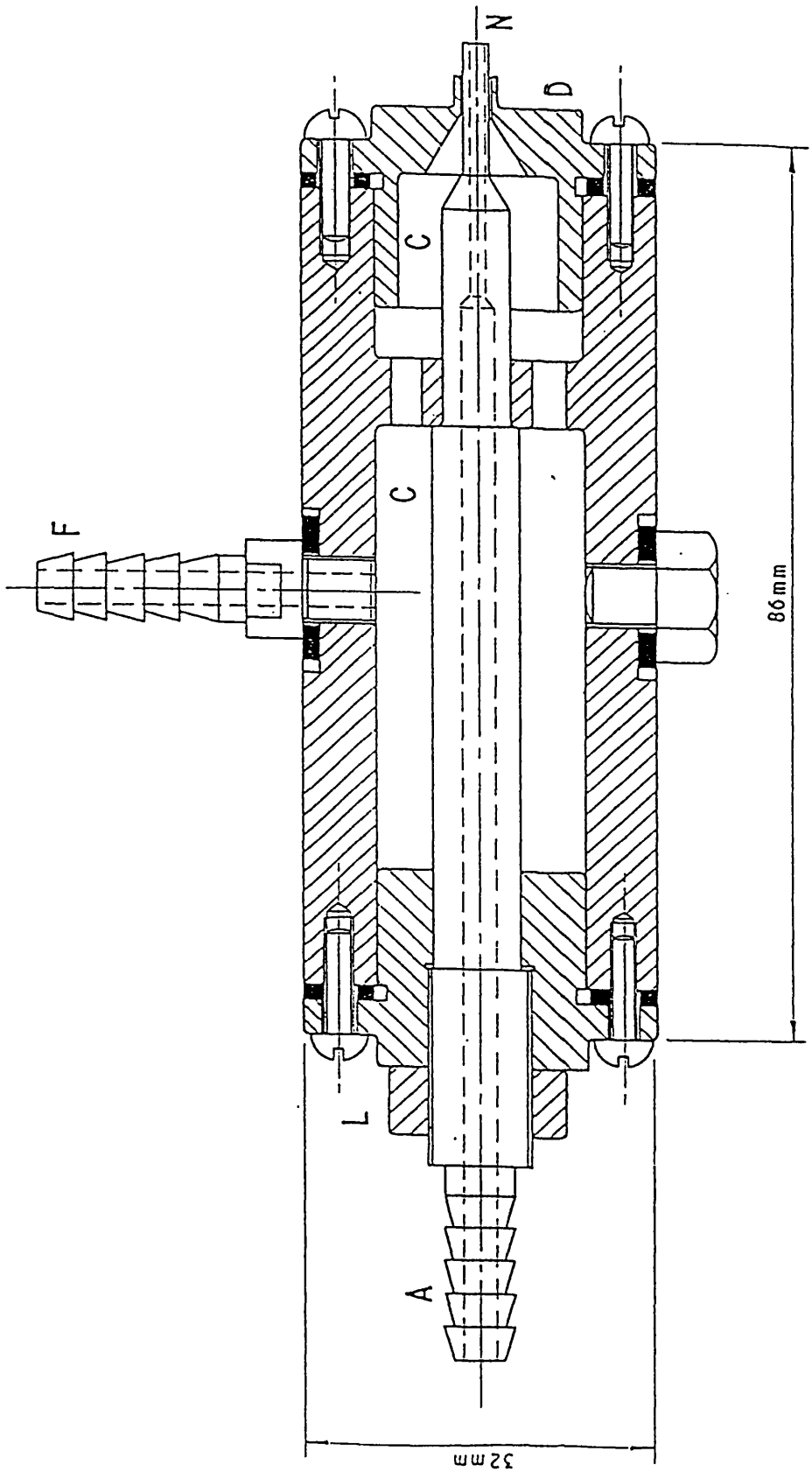

Fig. 5.3. Sectional View of Jet Device

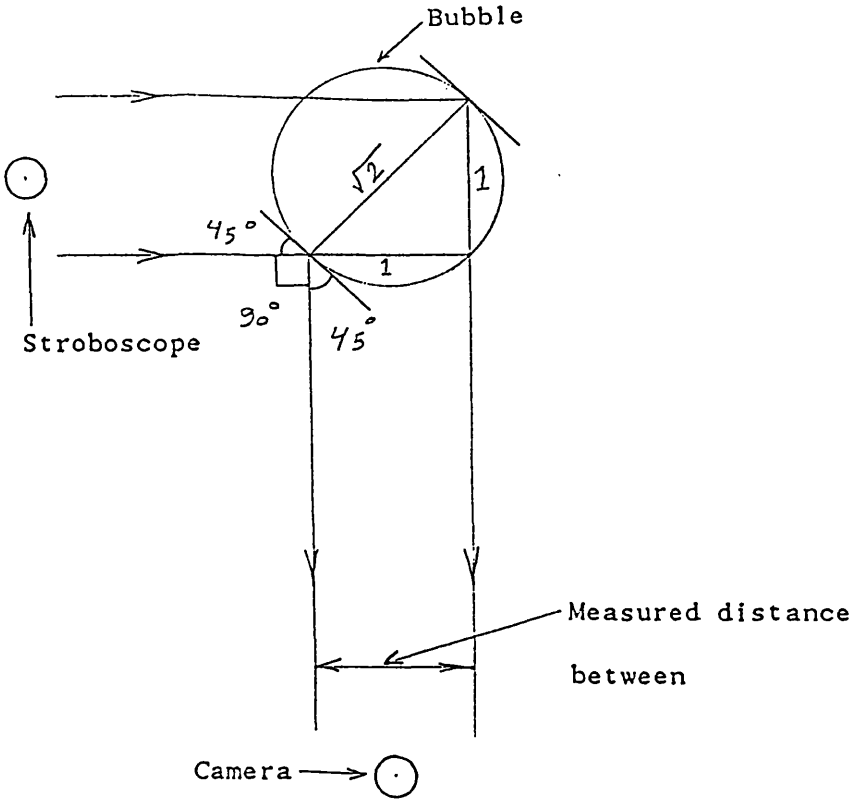

Fig. 5.5 Reflection of light beams falling on the bubble from the stroboscope

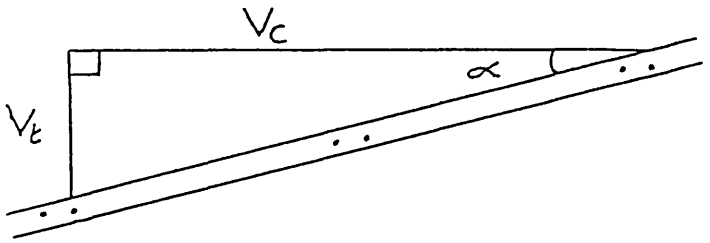

Fig. 5.6 Bubble velocity in vertical and horizontal direction

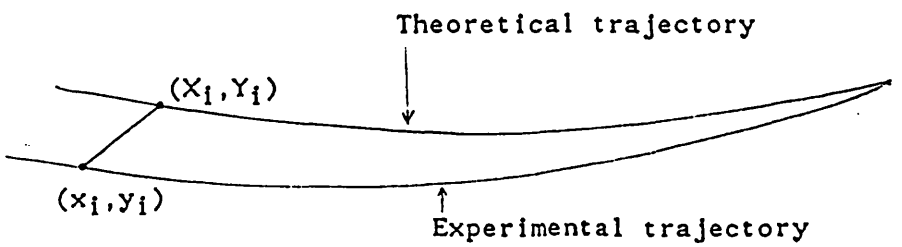

Fig. 5.7 Experimental and theoretical trajectory

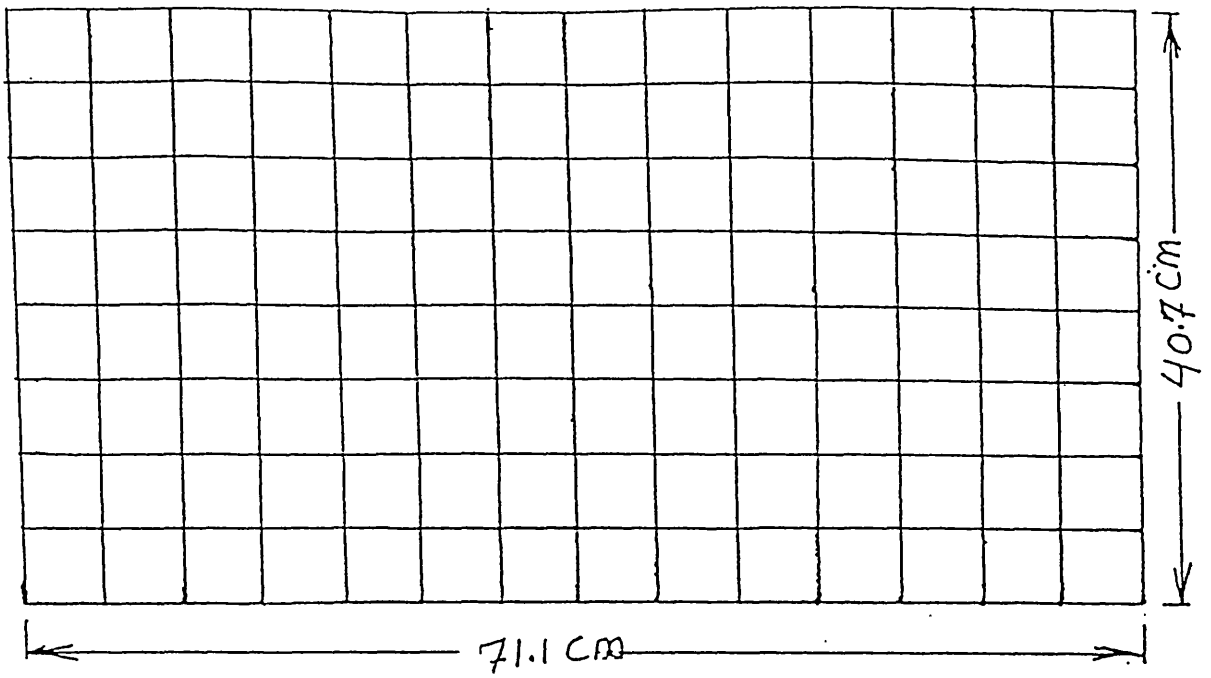

Fig. 5.8 The actual grid dimensions

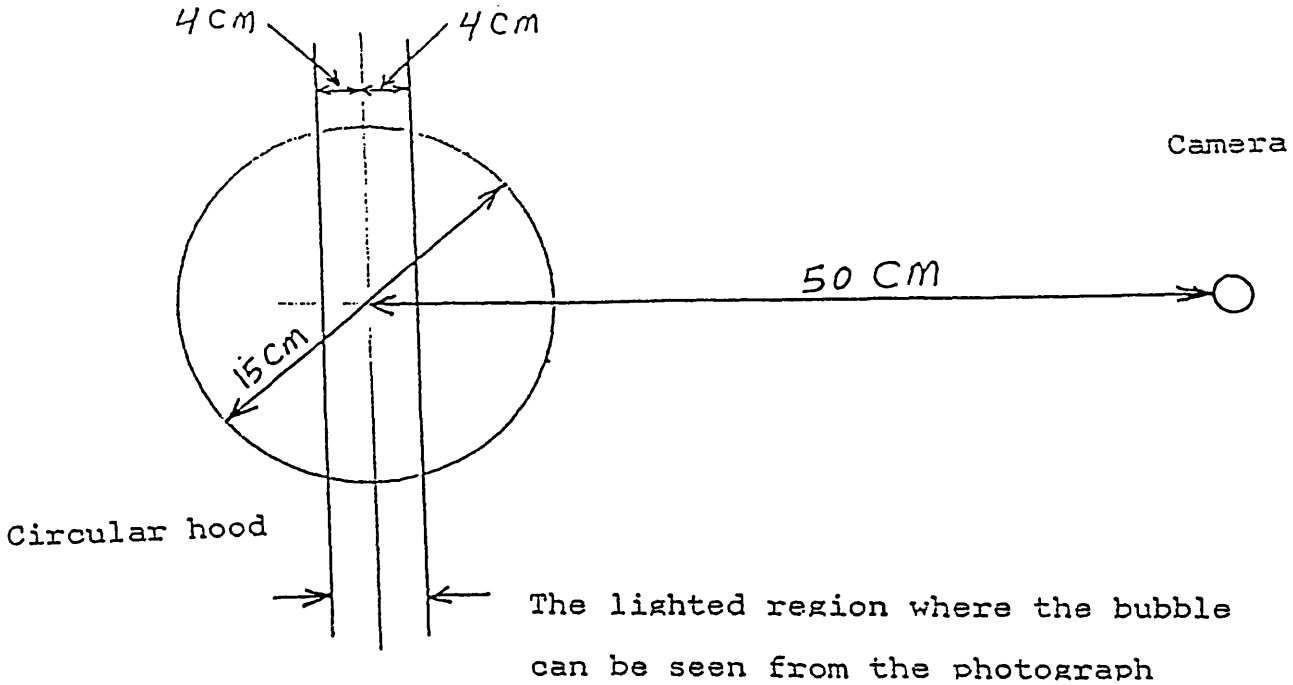

Fig. 5.9 The range of bubbles distance from the camera

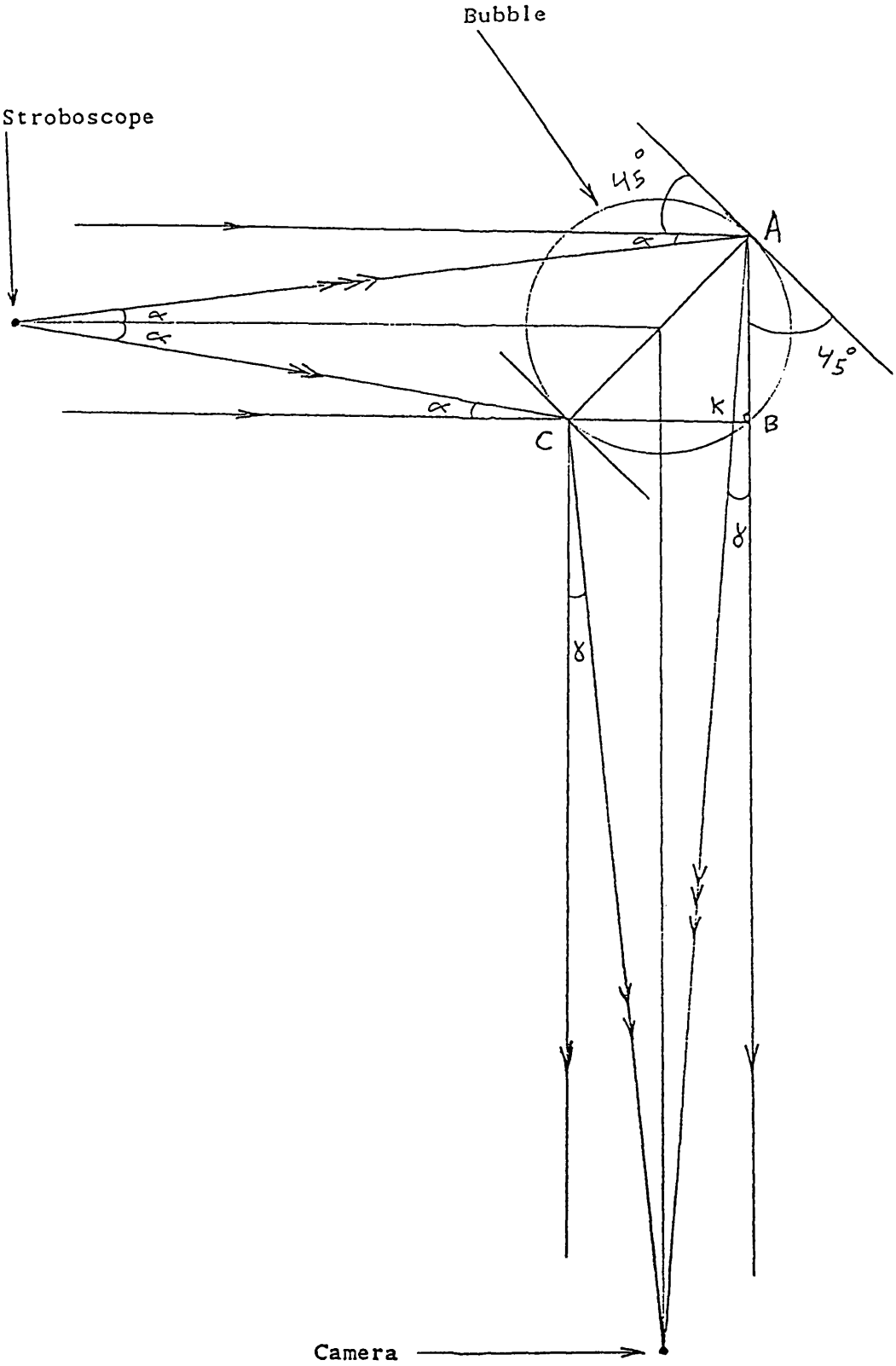

Fig. 5.10 The stroboscope and the camera as a point source and a point sink

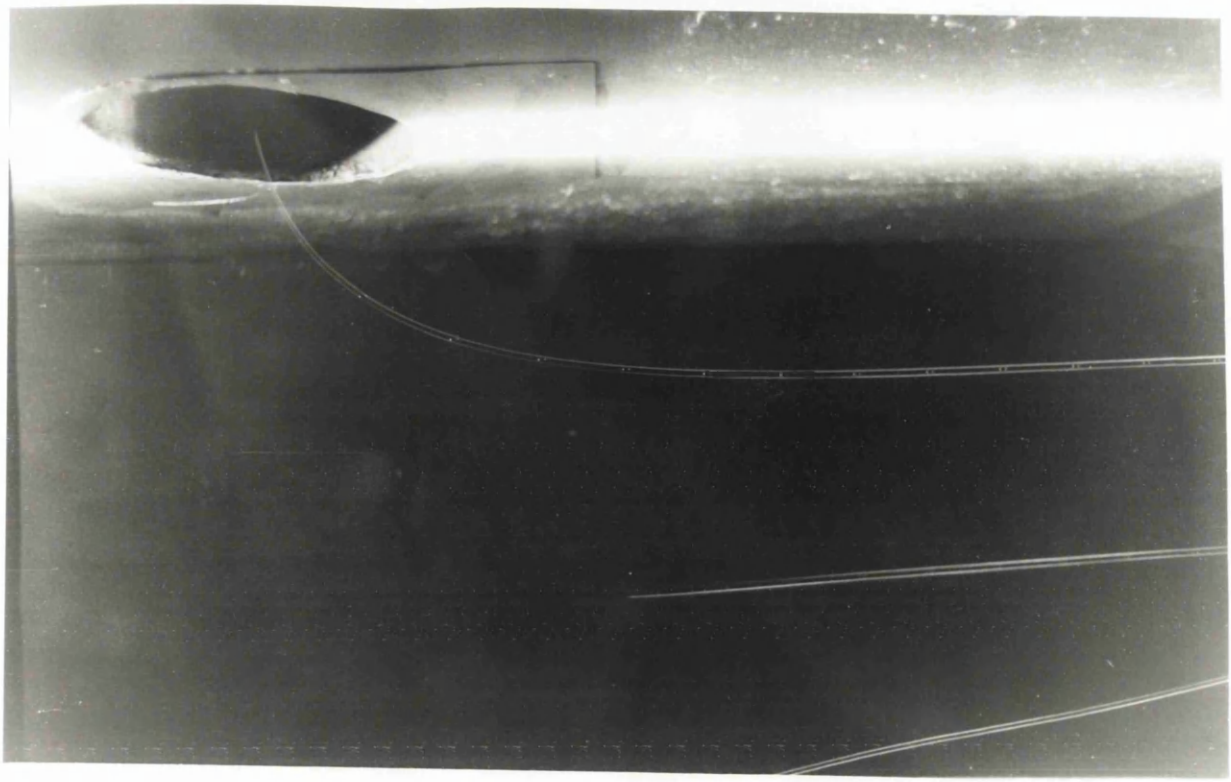

Figure 5.11 A trajectory of bubble captured by the hood

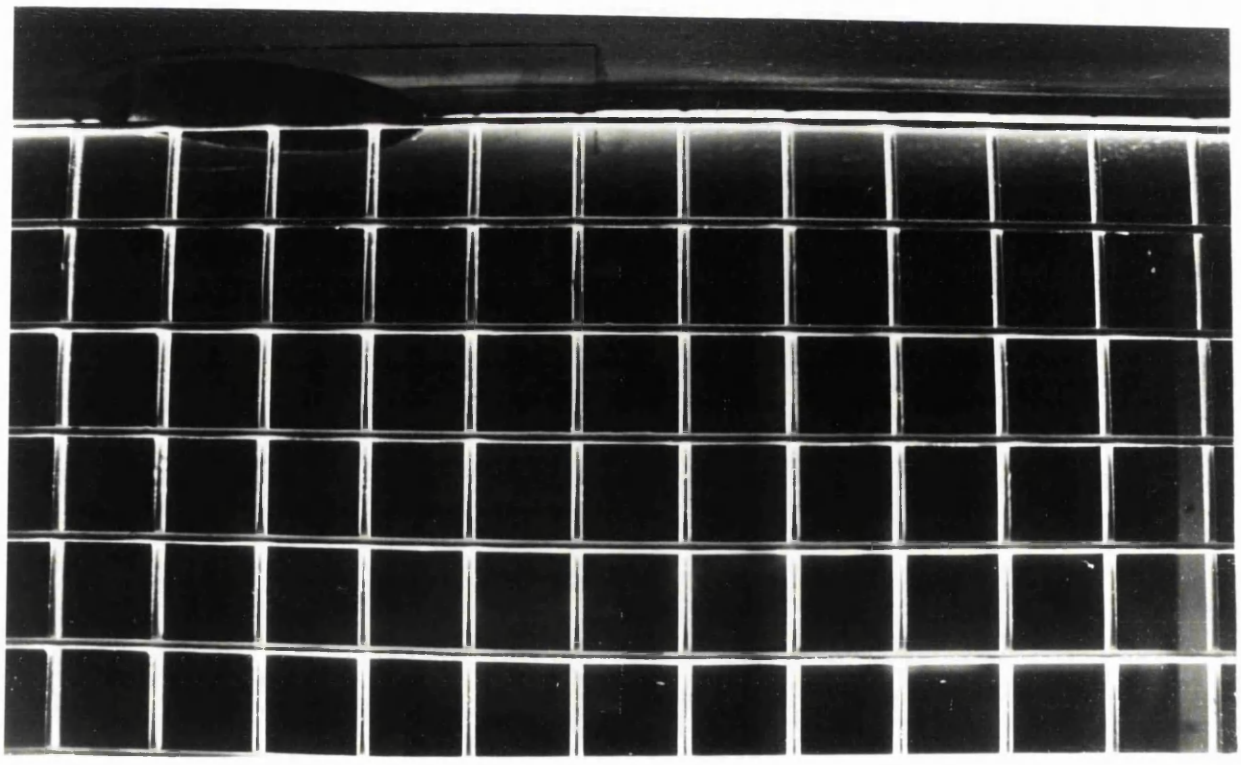

Figure 5.12 Photograph of the grid used in the experiments

APPENDIX A: EXHAUST HOOD CENTERLINE VELOCITY MODELS

Applicable Range	Equation	Equation Number
	Round Hoods, Unflanged	
DALLAVALLE		
$0 < \frac{X}{D} < \infty$	$\frac{V}{V_f} = \frac{1}{12.7(X/D)^2 + 1}$	(1)
FLETCHER		
$0 < \frac{X}{D} < \infty$	$\frac{V}{V_f} = \frac{1}{10.9(X/D)^2 + 1}$	(2)
GARRISON		
$0 < \frac{X}{D} < 0.5$	$\frac{V}{V_f} = 1.1(0.06)^{X/D}$	(3)
$0.5 \leqslant \frac{X}{D} \leqslant 1.5$	$\frac{V}{V_f} = 0.08 \left[\frac{X}{D}\right]^{-1.7}$	(4)
	Round Hoods, Flanged	
DALLAVALLE		
$0 < \frac{X}{D} < \infty$	$\frac{V}{V_f} = \frac{1}{9.6(X/D)^2 + 0.75}$	(5)
GARRISON		
$0 < \frac{X}{D} < 0.5$	$\frac{V}{V_f} = 1.1\ (0.07)^{X/D}$	(6)
$0.5 \leqslant \frac{X}{D} \leqslant 1.5$	$\frac{V}{V_f} = 0.10 \left[\frac{X}{D}\right]^{-1.6}$	(7)
	Square Hoods, Unflanged(side=a)	
DALLAVALLE		
$0 < \frac{X}{a} < \infty$	$\frac{V}{V_f} = \frac{1}{10(X/a)^2 + 1}$	(8)
FLETCHER		
$0 < \frac{X}{a} < \infty$	$\frac{V}{V_f} = \frac{1}{8.6(X/a)^2 + 0.93}$	(9)
GARRISON		
$0 < \frac{X}{a} < 0.5$	$\frac{V}{V_f} = 1.07\ (0.09)^{X/a}$	(10)
$0.5 \leqslant \frac{X}{a} \leqslant 1.5$	$\frac{V}{V_f} = 0.10 \left[\frac{X}{a}\right]^{-1.7}$	(11)
	Square Hoods, Flanged	
DALLAVALLE		
$0 < \frac{X}{a} < \infty$	$\frac{V}{V_f} = \frac{1}{7.5(X/a)^2 + 0.75}$	(12)
GARRISON		
$0 < \frac{X}{a} < 0.5$	$\frac{V}{V_f} = 1.07\ (0.11)^{X/a}$	(13)

Applicable Range	Equation	Equation Number
	Square Hoods, Flanged	
GARRISON		
$0.5 \leqslant \frac{X}{a} \leqslant 1.5$	$\frac{V}{V_f} = 0.12 \left[\frac{X}{a}\right]^{-1.6}$	(14)
	Rectangular Hoods, Unflanged ($0.2 < W/L < 1$)	
DALLAVALLE		
$0 < \frac{X}{W} < \infty$	$\frac{V}{V_f} = \frac{1}{10(X^2/WL) + 1}$	(15)
FLETCHER		
$0 < \frac{X}{W} < \infty$	$\frac{V}{V_f} = \frac{1}{8.58\ \alpha^2 + 0.93}$	(16)
	$\alpha = \frac{X}{(WL)^{\frac{1}{2}}} \left[\frac{W}{L}\right]^{-\beta}$	
	$\beta = 0.2\left[\frac{X}{(WL)^{\frac{1}{2}}}\right]^{1/3}$	
GARRISON*		
At $W/L = 0.5$:		
$0 < \frac{X}{W} < 0.5$	$\frac{V}{V_f} = 1.07(0.14)^{X/W}$	(17)
$0.5 \leqslant \frac{X}{W} < 1.0$	$\frac{V}{V_f} = 0.18 \left[\frac{X}{W}\right]^{-1.2}$	(18)
$1.0 \leqslant \frac{X}{W} \leqslant 2.0$	$\frac{V}{V_f} = 0.18 \left[\frac{X}{W}\right]^{-1.7}$	(19)
At $W/L = 0.25$:		
$0 < \frac{X}{W} < 0.5$	$\frac{V}{V_f} = 1.07(0.18)^{X/W}$	(20)
$0.5 \leqslant \frac{X}{W} < 1.0$	$\frac{V}{V_f} = 0.23 \left[\frac{X}{W}\right]^{-1.0}$	(21)
$1.0 \leqslant \frac{X}{W} \leqslant 2.5$	$\frac{V}{V_f} = 0.23 \left[\frac{X}{W}\right]^{-1.5}$	(22)

APPENDIX A: (Continued)

Applicable Range	Equation	Equation Number
	Rectangular Hoods, Flanged	
DALLAVALLE		
$0 < \frac{X}{W} < \infty$	$\frac{V}{V_f} = \frac{1}{7.5\ X^2/WL}$	(23)
GARRISON		
For W/L = 0.5:		
$0 < \frac{X}{W} < 0.5$	$\frac{V}{V_f} = 1.07(0.17)^{X/W}$	(24)
$0.5 \leq \frac{X}{W} < 1.0$	$\frac{V}{V_f} = 0.21 \left[\frac{X}{W}\right]^{-1.1}$	(25)
$1.0 \leq \frac{X}{W} \leq 2.0$	$\frac{V}{V_f} = 0.21 \left[\frac{X}{W}\right]^{-1.6}$	(26)
For W/L = 0.25:		
$0 < \frac{X}{W} < 0.5$	$\frac{V}{V_f} = 1.07(0.22)^{X/W}$	(27)
$0.5 \leq \frac{X}{W} < 1.0$	$\frac{V}{V_f} = 0.27 \left[\frac{X}{W}\right]^{-0.9}$	(28)
$1.0 \leq \frac{X}{W} \leq 3.0$	$\frac{V}{V_f} = 0.27 \left[\frac{X}{W}\right]^{-1.4}$	(29)
	Slot Hoods, Unflanged	
SILVERMAN		
$0 < \frac{X}{W} < \infty$	$\frac{V}{V_s} = 0.27 \left[\frac{X}{W}\right]^{-1.0}$	(30)
GARRISON		
$0 < \frac{X}{W} < 0.5$	$\frac{V}{V_s} = 1.07(0.19)^{X/W}$	(31)
$0.5 \leq \frac{X}{W} < 1.0$	$\frac{V}{V_s} = 0.24 \left[\frac{X}{W}\right]^{-1.0}$	(32)
$1.0 \leq \frac{X}{W} \leq 3.5$	$\frac{V}{V_s} = 0.24 \left[\frac{X}{W}\right]^{-1.2}$	(33)

APPENDIX A: (Continued)

Applicable Range	Equation	Equation Number
FLETCHER		
$0 < \frac{X}{W} < \infty$	$\frac{V}{V_s} = \frac{1}{8.58\ \alpha^2 + 0.93}$	(34)
	$\alpha = \frac{X}{(WL)^{\frac{1}{2}}} \left[\frac{W}{L}\right]^{-\beta}$	
	$\beta = 0.2\left[\frac{X}{(WL)^{\frac{1}{2}}}\right]^{1/3}$	
	Slot Hoods, Flanged	
SILVERMAN		
$0 < \frac{X}{W} < \infty$	$\frac{V}{V_s} = 0.36\ \left[\frac{X}{W}\right]^{-1.0}$	(36)
GARRISON		
$0 < \frac{X}{W} < 0.5$	$\frac{V}{V_s} = 1.07(0.22)^{X/W}$	(37)
$0.5 \leqslant \frac{X}{W} < 1.0$	$\frac{V}{V_s} = 0.29\ \left[\frac{X}{W}\right]^{-0.8}$	(38)
$1.0 \leqslant \frac{X}{W} \leqslant 4.0$	$\frac{V}{V_s} = 0.29\ \left[\frac{X}{W}\right]^{-1.1}$	(39)

* Empirical coefficient were calculated only at W/L = 0.5 and W/L=0.25.

ref. Burgess, W.A., M.J. Ellenbecker and R.D. Treitman: Ventilation for Control of the Work Environment. Wiley – Interscience Publication, New York (1989).

APPENDIX B. (Heinsohn (ref.4) in CHAPTER 2)

Runge–Kutta Methods for Solving First-order Differential Equations

Suppose one wants to find the value of the continuous function $U(t)$ at arbitrary values of t where the function satisfied the nonlinear differential equation,

$$\frac{dU}{dt} = UA(t) + B(t) \tag{A-12.1}$$

and the quantities A and B are known analytical functions of t. Assume that the initial value of $U(0)$ is known, i.e.

$$U(t_0) = U(0) = \text{known} \tag{A-12.2}$$

Express the function $U(t)$ as a Taylor series,

$$U(t + \delta t) = U(t) + U'(t)\,\delta t + U''(t)\,\frac{\delta t^2}{2} + \ldots \tag{A-12.3}$$

Where the function $U(t)$ and its derivatives $U'(t)$ and $U''(t)$ are evaluated at time t and δt is a small increment of time. Eliminate the second, third, and all higher order derivatives and replace the first derivative by Eq. A-12.1

$$U(t + \delta t) = U(t) + \delta t[U(t)A(t) + B(t)] \tag{A-12.4}$$

Since dropping the higher-order derivatives introduces error, replace $U(t)$ inside the brackets on the right-hand side by the average value of the function between (t) and $(t + \delta t)$,

$$U(t + \delta t) = U(t) + \delta t\left[A(t)\frac{[U(t) + U(t + \delta t]}{2} + B(t)\right] \tag{A-12.5}$$

Rearrange and obtain

$$U(t + \delta t) = \frac{\left\{U(t)\left[1 + \left(\frac{\delta t}{2}\right)A(t)\right] + \delta t\, B(t)\right\}}{M(t)}$$

$$M(t) = 1 - \left(\frac{\delta t}{2}\right)A(t) \tag{A-12.6}$$

To obtain the value of U at the end of a time period t_n, that is, $U(t_n)$, begin by evaluating Eq. A-12.6 at t_1:

$$t_1 = t_0 + \delta t$$

$$U(t_1) = \frac{\left\{U(t_0)\left[1 + \left(\frac{\delta t}{2}\right)A(t_0)\right] + (\delta t)B(t_0)\right\}}{M(t_0)}$$

$$M(t_0) \doteq 1 - \left(\frac{\delta t}{2}\right)A(t_0) \qquad \text{(A-12.7)}$$

Now evaluate Eq. A-12.6 at t_2 but use $U(t_1)$, $A(t_1)$, and $B(t_1)$ on the right hand-side of Eq. A-12.6,

$$t_2 = t_1 + \delta t$$

$$U(t_2) = \frac{\left\{U(t_1)\left[1 + \left(\frac{\delta t}{2}\right)A(t_1)\right] + (\delta t)B(t_1)\right\}}{M(t_1)}$$

$$M(t_1) = 1 - \left(\frac{\delta t}{2}\right)A(t_1) \qquad \text{(A-12.8)}$$

Repeat the process until you have computed $U(t_n)$

$$t_n = t_{n-1} + \delta t \qquad \text{(A-12.9)}$$

The quantity δt is the time step; its magnitude is selected by the user. The value should be small such that

$$\left(\frac{\delta t}{2}\right)A(t) < 1 \qquad \text{(A-12.10)}$$

Fourth-order Runge–Kutta Method

More accuracy can be obtained using Runge–Kutta methods of higher order (196). In such methods estimates are made at intermediate values between t and $t + \delta t$. A commonly used expression is the Runge-Kutta fourth-order method. Begin by expressing the differential equation as,

$$\frac{dU}{dt} = f(U, t) \qquad \text{(A-12.11)}$$

It will be presumed that the value of U is known at the initial time t_1, that is

$$U_1 = U(t_1) \qquad \text{(A-12.12)}$$

The value of U at the end of the time step δt, that is,

$$U(t + \delta t) = U_{i+1} \qquad \text{(A-12.13)}$$

is given by

$$U_{i+1} = U_i + \delta t\left[\frac{f_i}{6} + \frac{f_1}{3} + \frac{f_2}{3} + \frac{f_3}{6}\right] \qquad \text{(A-12.14)}$$

where the functions f_i, f_1, f_2, and f_3 are given by

$$f_i = f(t_i, U_i) \qquad \text{(A-12.15)}$$

$$t_1 = t_i + \frac{\delta t}{2} \qquad \text{(A-12.16)}$$

$$U_1 = U_i + \left(\frac{\delta t}{2}\right) f_i \qquad \text{(A-12.17)}$$

$$f_1 = f(t_1, U_1) \qquad \text{(A-12.18)}$$

$$U_2 = U_i + \left(\frac{\delta t}{2}\right) f_1 \qquad \text{(A-12.19)}$$

$$f_2 = f(t_1, U_2) \qquad \text{(A-12.20)}$$

$$U_3 = U_i + (\delta t) f_2 \qquad \text{(A-12.21)}$$

$$t_2 = t_i + \delta t \qquad \text{(A-12.22)}$$

$$f_3 = f(t_2, U_3) \qquad \text{(A-12.23)}$$

Simultaneous Ordinary Differential Equations

If one is asked to solve a simultaneous set of ordinary differential equations of the form

$$\begin{aligned} \frac{dp}{dt} &= f(p, q, \ldots, z, t) \\ \frac{dq}{dt} &= g(p, q, \ldots, z, t) \\ &\vdots \\ \frac{dz}{dt} &= h(p, q, \ldots, z, t) \end{aligned} \qquad \text{(A-12.24)}$$

Equations A-12.14 to A-12.23 can also be used. Each intermediate functions f_1, f_2, f_3; g_1, g_2, g_3; and so on involves intermediate values of time t_1 and t_2 and intermediate values of the variables. Since there are several independent variables, each variable has intermediate values noted by subscripts 1, 2, and 3. Thus before intermediate function f_1, $g_1, \ldots, h_1$ are computed, users will have to compute p_1, q_1, $r_1, \ldots, z_1$. Similarly p_2, q_2, $r_2, \ldots, z_2$ will have to computed before the functions f_2, $g_2, \ldots, h_2$ are found. Lastly, p_3, q_3, $r_3, \ldots, z_3$ will have to be computed before functions f_3, $q_3, \ldots, h_3$ are found.

APPENDIX C Computer Programs to Calculat and Visualize Particles Movement into a Flanged Circular Local Exhaust Hood

INTRODUCTION

This appendix provides the computer programs developed throughout the research project. The appendix is divided into two parts, one for calculating the particle trajectories and the other one for plotting it in front of a flanged circular hood.

The first part lists three programs to calculate particle trajectories in front of a flanged circular hood. The first and second program used the final model developed by Flynn and Ellenbecker to calculate the air distribution around the hood. In the first program the face of the flanged hood is horizontal and the hood face is over the released particles, while in the second program the face of the flanged hood is vertical. The third program used used the non-dimensional model developed by Jansson to calculate the air distribution around the hood, the face of the flanged hood is horizontal and the hood face is over the released particles.

The second part lists three programs to plot particle trajectories in front of a flanged circular hood. The first and second program used the final model developed by Flynn and Ellenbecker to calculate the air distribution around the hood. In the first program the face of the flanged hood is horizontal, and the hood face is over the released particles, while in the second program the face of the hood is vertical. The third program used the non-dimensional

model developed by Jansson to calculate the air distribution around the hood, the face of the flanged hood is horizontal and the hood face is over the released particles.

PART 1

FIRST PROGRAM

```
10 REM FILE NAME----------CAPTURE----------
20 REM  PROGRAM  COMPUTES  PARTICLE TRAJECTORIES  IN  FRONT
   OF A CIRCULAR FLANGED HOOD.
30 REM  THE  FACE OF THE  FLANGED  HOOD IS  HORIZONTAL  AND
   THE  PARTICLES  ARE  RELEASED  IN  FRONT  OF  THE  HOOD
   (THE HOOD FACE IS OVER THE RELEASED PARTICLES).
40 REM THE VALUE OF Y IS NEGATIVE IN THE INPUT DATA Y (-) .
50 REM  LINES  90-220  ARE  INPUT  STATEMENTS  FOR  VALUES
   PROVIDED BY THE USER.
60 REM VARIABLES: RA IS THE AIR DENSITY IN (KG/M3).
                  MU IS THE AIR VISCOSITY IN (KG/M S).
                  RE IS THE REYNOLDS NUMBER.
70 REM VARIABLES: UF,VF ARE PARTICLE  VELOCITY  AT  END  OF
                  TIME STEP IN (M/S).
                  X,Y ARE PARTICLE LOCATION AT END OF  TIME
                  STEP IN (M).
                  TI,DT ARE ELAPSED  TIME  AND  TIME  STEPS
                  IN (S).
80 REM VARIABLES: RP IS THE PARTICLE DENSITY IN (KG/M3).
                  DP IS THE PARTICLE DIAMETER IN (MICRON).
                  P IS THE AIR PRESSURE IN (ATM).
                  T IS THE AIR TEMPERATURE IN (K).
                  D IS THE HOOD DIAMETER IN (M).
                  Q IS THE HOOD FLOW IN (M3/S).
```

```
                    VC IS THE CROSSDRAFT VELOCITY IN (M/S).
                    V IS THE PARTICLE VELOCITY IN VERTICAL
                    DIRECTION IN (M/S).
                    U IS THE PARTICLE VELOCITY IN HORIZONTAL
                    DIRECTION IN (M/S).
90 INPUT "AIR PRESSURE IN (ATM)=";P
100 INPUT "AIR TEMPERATURE IN (K)=";T
110 INPUT "PARTICLE DENSITY IN (KG/M3)=";RP
120 INPUT "TIME STEP IN (SECONDS)=";DT
130 INPUT "PARTICLE DIAMETER IN (MICROMETERS)=";DP
140 INPUT "HOOD DIAMETER IN (M)=";D
150 INPUT "HOOD FLOW IN (M3/S)=";Q
160 REM THE CROSSDRAFT IS IN HORIZONTAL DIRECTION.
170 INPUT "CROSSDRAFT VELOCITY IN (M/S)=";VC
180 REM INPUT INITIAL PARTICLE LOCATION AND VELOCITY.
190 INPUT "INITIAL PARTICLE DISTANCE FROM Y-AXIS IN (M)=";X
200 INPUT "INITIAL PARTICLE DISTANCE FROM X-AXIS IN (M)=";Y
210 INPUT "INITIAL PARTICLE VELOCITY IN VERTICAL DIRECTION
    IN (M/S)=";V
220 INPUT "INITIAL PARTICLE VELOCITY IN HORIZONTAL DIRECTION
    IN (M/S)=";U
230 PRINT "DP (MICROMETER)     X (M)          Y (M)       "
240 PRINT "-------------    ------------    --------------"
250 REM K IS A COUNTER.
260 K=0
270 RA=P*100/(.287*T)
280 MU=(13.554 + .6738*T - (3.808*T*T/10000) + (1.183*T*T*T/
10000000))/10000000
```

```
290 TI=0
300 REM  A  IS THE RADIUS OF THE HOOD.
310 A=D/2
320 PI=3.1415927
330 REM LINES 340-550 CALCULATES THE VELOCITY IN FRONT OF
    A CIRCULAR FLANGED HOOD A CCORDING TO THE FINAL MODEL
    DEVELOPED BY FLYNN AND ELLENBECKER.
340 GAMMA1=SQR(Y^2+(A+X)^2)
350 GAMMA2=SQR(Y^2+(A-X)^2)
360 REM  ECC  IS THE ECCENTRICITY.
370 ECC=(2*A)/(GAMMA1+GAMMA2)
380 ECC2=ECC^2
390 T1=A+X
400 T2=X-A
410 T3=GAMMA1+GAMMA2
420 T4=GAMMA1*GAMMA2
430 T5=4*A^2
440 T6=SQR(T3^2-T5)
450 T7=-Q/PI
460 T8=(T1*GAMMA2)+(T2*GAMMA1)
470 T9=T3*T4*T6
480 VR1=(T8/T9)*T7
490 VZ1=(T7*Y)/(T4*T6)
500 V1=SQR(VR1^2+VZ1^2)
510 VTF=(Q*ECC2*SQR(3))/(2*PI*A^2*SQR(3-2*ECC2))
520 VR2=(VR1/V1)*VTF
530 VZ=.9*((VZ1/V1)*VTF)
540 VA=VZ
550 VRTOT=(2.6*ECC^18+.853)*VR2+VC
```

```
560 UA=VRTOT
570 TI=TI+DT
580 REM CALCULATE: RELATIVE VELOCITY  (VR)
                   REYNOLDS NUMBER (RE)
                   DRAG COEFFICIENT (CD)
590 VR=SQR((U-UA)*(U-UA)+(V-VA)*(V-VA)
600 RE=RA*DP*VR/(MU*1000000)
610 CD=(24/RE ^0.646)
620 REM  LAM IS THE MEAN FREE PATH FOR AIR IN (MICRON).
630 LAM=.0667
640 REM  C  IS THE SLIP FACTOR ALSO CALLED THE CUNNINGHAM
        CORRECTION FACTOR.
650 C=1+(LAM/DP)*(2.514+.8*EXP(-.55*DP/LAM))
660 REM CALCULATE PARTICLE VELOCITY AND POSITION AT END OF
       TIME STEP.
       CALCULATE A1,B,AND D1 IN RUNGE-KUTTA METHOD.
670 F=RA/RP
690 A1=-.75*CD*VR*RA/(RP*DP*C/1000000)
700 B=-A1*UA
710 REM G IS THE EARTH GRAVITY ACCELERATION FIELD IN (M/S2)
720 G=9.8
730 N=1-F
740 D1=-(A1*VA)-G*N
750 UF=(U*(1+A1*DT/2)+B*DT)/(1-A1*DT/2)
780 VF=(V*(1+A1*DT/2)+D1*DT)/(1-A1*DT/2)
790 REM PRINT X AND Y EVERY 25 ITERATIONS
800 K=K+1
810 IF K=25 GOTO 880
```

```
820 REM CALCULATE NEW VALUES OF X AND Y AND RESET INITIAL
        VALUES OF U AND V.
830 X=X+DT*(UF+U)/2
840 Y=Y+DT*(VF+V)/2
850 U=UF
860 V=VF
870 GOTO 340
880 PRINT DP,X,Y
890 K=0
900 REM CALCULATE THE PARTICLE LOCATION  WHEN  THE  PARTICLE
        IS VERY NEAR TO X-AXIS IN ORDER TO FIND THE DISTANCE
        OF THE PARTICLE FROM Y-AXIS.
910 IF Y>=-.003 OR X<=-5*D THEN GOTO 930
920 GOTO 340
930 PRINT
940 REM IF THE VALUE OF X IS LESS THAN THE RADIUS OF THE
        HOOD THEN THE PARTICLE WILL BE CAPTURED.
950 END
```

PART 1

SECOND PROGRAM

```
10 REM FILE NAME---------CAPTURE--------------------------
20 REM  PROGRAM  COMPUTES  PARTICLE TRAJECTORIES  IN  FRONT
   OF A CIRCULAR FLANGED HOOD.
30 REM THE FACE OF  THE  FLANGED  HOOD  IS  VERTICAL   AND
   THE  PARTICLES  ARE  RELEASED  IN  FRONT  OF  THE  HOOD.
50 REM   LINES  90-220  ARE  INPUT  STATEMENTS  FOR  VALUES
   PROVIDED BY THE USER.
60 REM VARIABLES: RA IS THE AIR DENSITY IN (KG/M3).
                  MU IS THE AIR VISCOSITY IN (KG/M S).
```

```
                RE IS THE REYNOLDS NUMBER.
70 REM VARIABLES: UF,VF ARE PARTICLE VELOCITY AT END OF
                TIME STEP IN (M/S).
                X,Y ARE PARTICLE LOCATION AT END OF TIME
                STEP IN (M).
                TI,DT ARE ELAPSED TIME AND TIME STEPS
                IN (S).
80 REM VARIABLES: RP IS THE PARTICLE DENSITY IN (KG/M3).
                DP IS THE PARTICLE DIAMETER IN (MICRON).
                P IS THE AIR PRESSURE IN (ATM).
                D IS THE HOOD DIAMETER IN (M).
                T IS THE AIR TEMPERATURE IN (K).
                Q IS THE HOOD FLOW IN (M3/S).
                VC IS THE CROSSDRAFT VELOCITY IN (M/S).
                V IS THE PARTICLE VELOCITY IN VERTICAL
                DIRECTION IN (M/S).
                U IS THE PARTICLE VELOCITY IN HORIZONTAL
                DIRECTION IN (M/S).
90 INPUT "AIR PRESSURE IN (ATM)=";P
100 INPUT "AIR TEMPERATURE IN (K)=";T
110 INPUT "PARTICLE DENSITY IN (KG/M3)=";RP
120 INPUT "TIME STEP IN (SECONDS)=";DT
130 INPUT "PARTICLE DIAMETER IN (MICROMETERS)=";DP
140 INPUT "HOOD DIAMETER IN (M)=";D
150 INPUT "HOOD FLOW IN (M3/S)=";Q
170 INPUT "CROSSDRAFT VELOCITY IN VERTICAL DIRECTION IN
    (M/S)=";VC
180 REM INPUT INITIAL PARTICLE LOCATION AND VELOCITY.
190 INPUT "INITIAL PARTICLE DISTANCE FROM Y-AXIS IN (M)=";X
```

```
200 INPUT "INITIAL PARTICLE DISTANCE FROM X-AXIS IN (M)=";Y
210 INPUT "INITIAL PARTICLE VELOCITY IN VERTICAL DIRECTION
    IN (M/S)=";V
220 INPUT "INITIAL PARTICLE VELOCITY IN HORIZONTAL DIRECTION
    IN (M/S)=";U
230 PRINT "DP (MICROMETER)     X (M)            Y (M)      "
240 PRINT "-------------    ------------    --------------"
250 REM K IS A COUNTER.
260 K=0
270 RA=P*100/(.287*T)
280 MU=(13.554 + .6738*T - (3.808*T*T/10000) + (1.183*T*T*T/
10000000))/10000000
290 TI=0
300 REM  A  IS THE RADIUS OF THE HOOD.
310 A=D/2
320 PI=3.1415927
330 REM LINES 340-550 CALCULATES THE VELOCITY IN FRONT OF
    A CIRCULAR FLANGED HOOD A CCORDING TO THE FINAL MODEL
    DEVELOPED BY FLYNN AND ELLENBECKER.
340 GAMMA1=SQR(X^2+(A+Y)^2)
350 GAMMA2=SQR(X^2+(A-Y)^2)
360 REM  ECC  IS THE ECCENTRICITY.
370 ECC=(2*A)/(GAMMA1+GAMMA2)
380 ECC2=ECC^2
390 T1=A+Y
400 T2=Y-A
410 T3=GAMMA1+GAMMA2
420 T4=GAMMA1*GAMMA2
430 T5=4*A^2
```

```
440 T6=SQR(T3^2-T5)
450 T7=-Q/PI
460 T8=(T1*GAMMA2)+(T2*GAMMA1)
470 T9=T3*T4*T6
480 VR1=(T8/T9)*T7
490 VZ1=(T7*X)/(T4*T6)
500 V1=SQR(VR1^2+VZ1^2)
510 VTF=(Q*ECC2*SQR(3))/(2*PI*A^2*SQR(3-2*ECC2))
520 VR2=(VR1/V1)*VTF
530 VZ=.9*((VZ1/V1)*VTF)
540 UA=VZ
550 VRTOT=(2.6*ECC^18+.853)*VR2 + VC
560 VA=VRTOT
570 TI=TI+DT
580 REM CALCULATE: RELATIVE VELOCITY  (VR)
                   REYNOLDS NUMBER (RE)
                   DRAG COEFFICIENT (CD)
590 VR=SQR((U-UA)*(U-UA)+(V-VA)*(V-VA)
600 RE=RA*DP*VR/(MU*1000000)
610 CD=(24/RE ^0.646)
620 REM  LAM IS THE MEAN FREE PATH FOR AIR IN (MICRON).
630 LAM=.0667
640 REM  C  IS THE SLIP FACTOR ALSO CALLED THE CUNNINGHAM
        CORRECTION FACTOR.
650 C=1+(LAM/DP)*(2.514+.8*EXP(-.55*DP/LAM))
660 REM CALCULATE PARTICLE VELOCITY AND POSITION AT END OF
       TIME STEP.
       CALCULATE A1,B,AND D1 IN RUNGE-KUTTA METHOD.
670 F=RA/RP
```

```
690 A1=-.75*CD*VR*RA/(RP*DP*C/1000000)
700 B=-A1*UA
710 REM G IS THE EARTH GRAVITY ACCELERATION FIELD IN (M/S2)
720 G=9.8
730 N=1-F
740 D1=-(A1*VA)-G*N
750 UF=(U*(1+A1*DT/2)+B*DT)/(1-A1*DT/2)
780 VF=(V*(1+A1*DT/2)+D1*DT)/(1-A1*DT/2)
790 REM PRINT X AND Y EVERY 25 ITERATIONS
800 K=K+1
810 IF K=25 GOTO 880
820 REM CALCULATE NEW VALUES OF X AND Y AND RESET INITIAL
        VALUES OF U AND V.
830 X=X+DT*(UF+U)/2
840 Y=Y+DT*(VF+V)/2
850 U=UF
860 V=VF
870 GOTO 340
880 PRINT DP,X,Y
890 K=0
900 REM CALCULATE THE PARTICLE LOCATION WHEN THE PARTICLE
        IS VERY NEAR TO Y-AXIS IN ORDER TO FIND THE DISTANCE
        OF THE PARTICLE FROM X-AXIS.
910 IF X<= .003   GOTO 930
920 GOTO 340
930 PRINT
940 REM IF THE VALUE OF Y IS LESS THAN THE RADIUS OF THE
        HOOD THEN THE PARTICLE WILL BE CAPTURED.
950 END
```

PART 1

THIRD PROGRAM

```
10 REM FILE NAME---------CAPTURE---------------------------
20 REM  PROGRAM  COMPUTES  PARTICLE TRAJECTORIES  IN  FRONT
   OF A CIRCULAR FLANGED HOOD.
30 REM THE FACE OF THE  FLANGED HOOD IS HORIZONTAL  AND  THE
   PARTICLES  ARE  RELEASED  IN  FRONT  OF  THE  HOOD
   (THE HOOD FACE IS OVER THE RELEASED PARTICLES).
40 REM THE VALUE OF Y IS NEGATIVE IN THE INPUT DATA Y(-).
50 REM  LINES  90-220  ARE  INPUT  STATEMENTS  FOR  VALUES
   PROVIDED BY THE USER.
60 REM VARIABLES: RA IS THE AIR DENSITY IN (KG/M3).
                  MU IS THE AIR VISCOSITY IN (KG/M S).
                  RE IS THR REYNOLDS NUMBER.
70 REM VARIABLES: UF,VF, WF ARE PARTICLE VELOCITY AT END OF
                  TIME STEP IN (M/S).
                  X,Y  ARE PARTICLE LOCATION AT END OF TIME
                  STEP IN (M).
                  TI,DT ARE ELAPSED  TIME  AND  TIME  STEPS
                  IN (S).
80 REM VARIABLES: RP IS THE PARTICLE DENSITY IN (KG/M3).
                  DP IS THE PARTICLE DIAMETER IN (MICRON).
                  P IS THE AIR PRESSURE IN (ATM).
                  T IS THE AIR TEMPERATURE IN (K).
                  D IS THE HOOD DIAMETER IN (M).
                  Q IS THE HOOD FLOW IN (M3/S).
                  VC IS THE CROSSDRAFT VELOCITY IN (M/S).
                  V  IS THE PARTICLE VELOCITY IN VERTICAL
                     DIRECTION IN (M/S).
```

```
                    U  IS THE PARTICLE VELOCITY IN HORIZONTAL
                       DIRECTION IN (M/S).
90 INPUT "AIR PRESSURE IN (ATM)=";P
100 INPUT "AIR TEMPERATURE IN (K)=";T
110 INPUT "PARTICLE DENSITY IN (KG/M3)=";RP
120 INPUT "TIME STEP IN (SECONDS)=";DT
130 INPUT "PARTICLE DIAMETER IN (MICROMETERS)=";DP
140 INPUT "HOOD DIAMETER IN (M)=";D
150 INPUT "HOOD FLOW IN (M3/S)=";Q
160 REM THE CROSSDRAFT IS IN HORIZONTAL DIRECTION.
170 INPUT "CROSSDRAFT VELOCITY IN (M/S)=";VC
180 REM INPUT INITIAL PARTICLE LOCATION AND VELOCITY.
190 INPUT "INITIAL PARTICLE DISTANCE FROM Y-AXIS IN (M)=";X
200 INPUT "INITIAL PARTICLE DISTANCE FROM X-AXIS IN (M)=";
210 INPUT "INITIAL PARTICLE VELOCITY IN VERTICAL DIRECTION
    IN (M/S)=";V
220 INPUT "INITIAL PARTICLE VELOCITY IN HORIZONTAL DIRECTION
    IN (M/S)=";U
225 Z=0
230 PRINT "DP (MICROMETER)      X (M)          Y (M)         "
240 PRINT "----------------    -----------    -------------"
250 REM K IS A COUNTER.
260 K=0
270 RA=P*100/(.287*T)
280 MU=(13.554 + .6738*T - (3.808*T*T/10000) +
(1.183*T*T*T/10000000))/10000000
290 TI=0
300 REM  A  IS THE AREA OF THE HOOD IN (M2).
310 PI=3.1415927
```

```
320 A=PI*(D^2)/4
330 REM  UO  IS THE HOOD FACE VELOCITY IN (M/S).
340 UO=Q/A
350 REM X1,Y1,AND Z1 ARE NON-DIMENSIONAL DISTANCE.
360 X1=X/D
370 Y1=Y/D
380 Z1=Z/D
390 R=SQR(X1^2+Z1^2)
400 T1=SQR(Y1^2+(.5+R)^2)
420 T2=SQR(Y1^2+(.5-R)^2)
430 REM  ECC  IS THE ECCENTRICITY
440 ECC=1/(T1+T2)
450 T3=ECC^2
460 T4=1-T3
470 T5=T4/2*ECC
480 T6=1+T5
490 T7=1+ECC
500 T8=1-ECC
510 T9=T7/T8
515 REM UU IS THE NON-DIMENSIONAL VELOCITY MAGNITUDE.
520 UU=T3/(T6*LOG(T9))
530 BETA=ATN(T4*R/Y1)
540 GAMMA=ATN(Z1/X1)
550 UUY=-UU*COS(BETA)
560 UUR=-UU*SIN(BETA)
570 UUX=UUR*COS(GAMMA)
580 UUZ=UUR*SIN(GAMMA)
585 REM UY IS THE VELOCITY IN VERTICAL DIRECTION.
590 UY=-UUY*UO
```

```
595 REM UX IS THE VELOCITY IN HORIZONTAL DIRECTION.
600 UX=UUX*UO+VC
620 VA=UY
630 UA=UX
650 TI=TI+DT
660 REM CALCULATE: RELATIVE VELOCITY  (VR)
                   REYNOLDS NUMBER  (RE)
                   DRAG COEFFICIENT  (CD)
670 VR=SQR((U-UA)*(U-UA)+(V-VA)*(V-VA))
680 RE=RA*DP*VR/(MU*1000000)
690 CD=(24/RE^0.646)
700 REM LAM IS THE MEAN FREE PATH FOR AIR IN (MICRON).
710 LAM=.0667
720 REM C IS THE SLIP FACTOR ALSO CALLED THE CUNNINGHAM
          CORRECTION FACTOR.
730 C=1+(LAM/DP)*(2.514+.8*EXP(-.55*DP/LAM))
740 REM CALCULATE PARTICLE VELOCITY AND POSITION AT END OF
        TIME STEP.
        CALCULATE A1,B,AND D1 IN RUNGE-KUTTA METHOD.
750 F=RA/RP
770 A1=-.75*CD*VR*RA/(RP*DP*C/1000000)
780 B=-A1*UA
790 REM G IS THE EARTH GRAVITY ACCELERATION FIELD IN (M/S2).
800 G=9.8
810 N=1-F
820 D1=-(A1*VA)-G*N
830 UF=(U*(1+A1*DT/2) + B*DT)/(1-A1*DT/2)
840 VF=(V*(1+A1*DT/2) + D1*DT)/(1-A1*DT/2)
860 REM PRINT X AND Y EVERY 25 ITERATIONS.
```

```
870 K=K+1
880 IF K=25 GO TO 970
890 REM CALCULATE NEW VALUES OF X AND Y AND RESET INITIAL
        VALUES OF U AND V.
900 X=X+DT*(UF+U)/2
910 Y=Y+DT*(VF+V)/2
930 U=UF
940 V=VF
960 GOTO 360
970 PRINT DP,X,Y
980 K=0
990 REM CALCULATE THE PARTICLE LOCATION WHEN THE PARTICLE
        IS VERY NEAR TO X-AXIS IN ORDER TO FIND THE DISTANCE
        OF THE PARTICLE FROM Y-AXIS.
1000 IF Y>=-.003 OR X<=-5*D THEN GOTO 1200
1100 GOTO 360
1200 PRINT
1300 REM IF THE VALUE OF X IS LESS THAN THE RADIUS OF THE
         HOOD THEN THE PARTICLE WILL BE CAPTURED.
1400 END
```

PART 2

FIRST PROGRAM

```
10 REM FILE NAME---------CAPTURE---------------------------
20 REM  PROGRAM  PLOTS  PARTICLE TRAJECTORIES IN  FRONT  OF
   A CIRCULAR FLANGED HOOD.
30 REM THE FACE OF THE FLANGED HOOD IS HORIZONTAL  AND  THE
       PARTICLES  ARE  RELEASED  IN  FRONT  OF  THE   HOOD
       (THE HOOD FACE IS OVER THE RELEASED PARTICLES).
40 REM THE VALUE OF Y IS NEGATIVE IN THE INPUT DATA Y (-) .
50 REM   LINES  90-220  ARE  INPUT  STATEMENTS  FOR  VALUES
   PROVIDED BY THE USER.
60 REM VARIABLES: RA IS THE AIR DENSITY IN (KG/M3).
                  MU IS THE AIR VISCOSITY IN (KG/M S).
                  RE IS THE REYNOLDS NUMBER.
70 REM VARIABLES: UF,VF ARE PARTICLE  VELOCITY  AT  END  OF
                  TIME STEP IN (M/S).
                  X,Y ARE PARTICLE LOCATION AT END OF  TIME
                  STEP IN (M).
                  TI,DT ARE ELAPSED  TIME  AND  TIME  STEPS
                  IN (S).
80 REM VARIABLES: RP IS THE PARTICLE DENSITY IN (KG/M3).
                  DP IS THE PARTICLE DIAMETER IN (MICRON).
                  P IS THE AIR PRESSURE IN (ATM).
                  T IS THE AIR TEMPERATURE IN (K).
                  D IS THE HOOD DIAMETER IN (M).
                  Q IS THE HOOD FLOW IN (M3/S).
                  VC IS THE CROSS-DRAFT VELOCITY IN (M/S).
                  V IS THE PARTICLE VELOCITY IN VERTICAL
                  DIRECTION IN (M/S).
```

```
                    U IS THE PARTICLE VELOCITY IN HORIZONTAL
                    DIRECTION IN (M/S).
90 INPUT "AIR PRESSURE IN (ATM)=";P
100 INPUT "AIR TEMPERATURE IN (K)=";T
110 INPUT "PARTICLE DENSITY IN (KG/M3)=";RP
120 INPUT "TIME STEP IN (SECONDS)=";DT
130 INPUT "PARTICLE DIAMETER IN (MICRON)=";DP
140 INPUT "HOOD DIAMETER IN (M)=";D
150 INPUT "HOOD FLOW IN (M3/S)=";Q
160 REM THE CROSS-DRAFT IS IN HORIZONTAL DIRECTION.
170 INPUT "CROSS-DRAFT VELOCITY IN (M/S)=";VC
180 REM INPUT INITIAL PARTICLE LOCATION AND VELOCITY.
190 INPUT "INITIAL PARTICLE DISTANCE FROM Y-AXIS IN (M)=";X
200 INPUT "INITIAL PARTICLE DISTANCE FROM X-AXIS IN (M)=";Y
210 INPUT "INITIAL PARTICLE VELOCITY IN VERTICAL DIRECTION
    IN (M/S)=";V
220 INPUT "INITIAL PARTICLE VELOCITY IN HORIZONTAL DIRECTION
    IN (M/S)=";U
230 DIM P(3000,2)
240 COUNT=0
250 REM THE I LOOP PERFORMS THE VELOCITY CALCULATIONS
    ACCORDING TO THE FINAL MODEL DEVELOPED BY FLYNN AND
    ELLENBECKER,AND GENERATES THE POINTS TO BE PLOTTED.
260 FOR I=1 TO 3000
270 RA=P*100/(.287*T)
280 MU=(13.554 + .6738*T - (3.808*T*T/10000) + (1.183*T*T*T/
10000000))/10000000
290 TI=0
300 REM  A  IS THE RADIUS OF THE HOOD.
```

```
310 A=D/2
320 PI=3.1415927
330 REM LINES 340-550 CALCULATES THE VELOCITY IN FRONT OF
    A CIRCULAR FLANGED HOOD A CCORDING TO THE FINAL MODEL
    DEVELOPED BY FLYNN AND ELLENBECKER.
340 GAMMA1=SQR(Y^2+(A+X)^2)
350 GAMMA2=SQR(Y^2+(A-X)^2)
360 REM  ECC  IS THE ECCENTRICITY.
370 ECC=(2*A)/(GAMMA1+GAMMA2)
380 ECC2=ECC^2
390 T1=A+X
400 T2=X-A
410 T3=GAMMA1+GAMMA2
420 T4=GAMMA1*GAMMA2
430 T5=4*A^2
440 T6=SQR(T3^2-T5)
450 T7=-Q/PI
460 T8=(T1*GAMMA2)+(T2*GAMMA1)
470 T9=T3*T4*T6
480 VR1=(T8/T9)*T7
490 VZ1=(T7*Y)/(T4*T6)
500 V1=SQR(VR1^2+VZ1^2)
510 VTF=(Q*ECC2*SQR(3))/(2*PI*A^2*SQR(3-2*ECC2))
520 VR2=(VR1/V1)*VTF
530 VZ=.9*((VZ1/V1)*VTF)
540 VA=VZ
550 VRTOT=(2.6*ECC^18+.853)*VR2+VC
560 UA=VRTOT
570 TI=TI+DT
```

```
580 REM CALCULATE: RELATIVE VELOCITY  (VR)
                   REYNOLDS NUMBER (RE)
                   DRAG COEFFICIENT (CD)
590 VR=SQR((U-UA)*(U-UA)+(V-VA)*(V-VA)
600 RE=RA*DP*VR/(MU*1000000)
610 CD=(24/RE^0.646)
620 REM  LAM IS THE MEAN FREE PATH FOR AIR IN (MICRON).
630 LAM=.0667
640 REM  C  IS THE SLIP FACTOR ALSO CALLED THE CUNNINGHAM
        CORRECTION FACTOR.
650 C=1+(LAM/DP)*(2.514+.8*EXP(-.55*DP/LAM))
660 REM CALCULATE PARTICLE VELOCITY AND POSITION AT END OF
       TIME STEP.
       CALCULATE A1,B,AND D1 IN RUNGE-KUTTA METHOD.
670 F=RA/RP
690 A1=-.75*CD*VR*RA/(RP*DP*C/1000000)
700 B=-A1*UA
710 REM G IS THE EARTH GRAVITY ACCELERATION FIELD IN (M/S2)
720 G=9.8
730 N=1-F
740 D1=-(A1*VA)-G*N
750 UF=(U*(1+A1*DT/2)+B*DT)/(1-A1*DT/2)
780 VF=(V*(1+A1*DT/2)+D1*DT)/(1-A1*DT/2)
790 REM CALCULATE NEW VALUES OF X AND Y AND RESET INITIAL
       VALUES OF U AND V.
800 X=X+DT*(UF+U)/2
810 Y=Y+DT*(VF+V)/2
820 U=UF
830 V=VF
```

```
840 P(I,1)=X
850 P(I,2)=Y
860 REM CALCULATE THE PARTICLE LOCATION WHEN THE PARTICLE
        IS VERY NEAR TO X-AXIS IN ORDER TO FIND THE DISTANCE
        OF THE PARTICLE FROM Y-AXIS.
870 IF Y>=-.003 OR X<=-5*D THEN I=3000 ELSE COUNT=I+1
880 NEXT I
890 REM LINES 900-960 GENERATE THE HOOD,FLANGE AND
CENTERLINE.
900 SCREEN 1
910 WINDOW (-.53,-.36)-(.53,.36)
920 LINE (A,0)-(.33,0)
930 LINE (A,0)-(A,.02)
940 LINE (0,.02)-(0,-.33)
950 LINE (-A,0)-(-.33,0)
960 LINE (-A,0)-(-A,.02)
970 REM THE J LOOP PLOTS THE POINTS GENERATED IN THE I LOOP.
980 FOR J=1 TO COUNT
990 S=P(J,1)
1000 H=P(J,2)
1010 PSET(S,H)
1020 NEXT J
1030 KEY OFF
1040 LOCATE 8,1 :PRINT"D=";D;"(M)";
1050 LOCATE 9,1 :PRINT"Q=";Q;"(M3/S)";
1060 LOCATE 10,1 :PRINT"VC=";VC;"(M/S)";
1070 LOCATE 11,1 :PRINT"DP=";DP;"(MICRO.M)";
1080 A$=INKEY$:IF A$="C" THEN 1100 ELSE 1090
1090 IF A$="X" THEN 1110
```

```
1100 LPRINT CHR$(12)
1110 END
```

PART 2

SECOND PROGRAM

```
10 REM FILE NAME---------CAPTURE--------------------------
20 REM  PROGRAM  PLOTS  PARTICLE TRAJECTORIES IN FRONT  OF
   A CIRCULAR FLANGED HOOD.
30 REM THE FACE OF THE FLANGED HOOD IS VERTICAL   AND  THE
       PARTICLES  ARE  RELEASED  IN  FRONT  OF  THE  HOOD.
50 REM   LINES  90-220  ARE  INPUT  STATEMENTS  FOR  VALUES
   PROVIDED BY THE USER.
60 REM VARIABLES: RA IS THE AIR DENSITY IN (KG/M3).
                  MU IS THE AIR VISCOSITY IN (KG/M S).
                  RE IS THE REYNOLDS NUMBER.
70 REM VARIABLES: UF,VF ARE PARTICLE  VELOCITY  AT  END  OF
                  TIME STEP IN (M/S).
                  X,Y ARE PARTICLE LOCATION AT END OF  TIME
                  STEP IN (M).
                  TI,DT ARE ELAPSED  TIME  AND  TIME  STEPS
                  IN (S).
80 REM VARIABLES: RP IS THE PARTICLE DENSITY IN (KG/M3).
                  DP IS THE PARTICLE DIAMETER IN (MICRON).
                  P IS THE AIR PRESSURE IN (ATM).
                  T IS THE AIR TEMPERATURE IN (K).
                  D IS THE HOOD DIAMETER IN (M).
                  Q IS THE HOOD FLOW IN (M3/S).
                  VC IS THE CROSS-DRAFT VELOCITY IN (M/S).
```

```
                    V IS THE PARTICLE VELOCITY IN VERTICAL
                    DIRECTION IN (M/S).
                    U IS THE PARTICLE VELOCITY IN HORIZONTAL
                    DIRECTION IN (M/S).
90 INPUT "AIR PRESSURE IN (ATM)=";P
100 INPUT "AIR TEMPERATURE IN (K)=";T
110 INPUT "PARTICLE DENSITY IN (KG/M3)=";RP
120 INPUT "TIME STEP IN (SECONDS)=";DT
130 INPUT "PARTICLE DIAMETER IN (MICRON)=";DP
140 INPUT "HOOD DIAMETER IN (M)=";D
150 INPUT "HOOD FLOW IN (M3/S)=";Q
160 REM THE CROSS-DRAFT IS IN VERTICAL DIRECTION.
170 INPUT "CROSS-DRAFT VELOCITY IN (M/S)=";VC
180 REM INPUT INITIAL PARTICLE LOCATION AND VELOCITY.
190 INPUT "INITIAL PARTICLE DISTANCE FROM Y-AXIS IN (M)=";X
200 INPUT "INITIAL PARTICLE DISTANCE FROM X-AXIS IN (M)=";Y
210 INPUT "INITIAL PARTICLE VELOCITY IN VERTICAL DIRECTION
    IN (M/S)=";V
220 INPUT "INITIAL PARTICLE VELOCITY IN HORIZONTAL DIRECTION
    IN (M/S)=";U
230 DIM P(3000,2)
240 COUNT=0
250 REM THE I LOOP PERFORMS THE VELOCITY CALCULATIONS
    ACCORDING TO THE FINAL MODEL DEVELOPED BY FLYNN AND
    ELLENBECKER,AND GENERATES THE POINTS TO BE PLOTTED.
260 FOR I=1 TO 3000
270 RA=P*100/(.287*T)
280 MU=(13.554 + .6738*T - (3.808*T*T/10000) + (1.183*T*T*T/
10000000))/10000000
```

```
290 TI=0
300 REM  A  IS THE RADIUS OF THE HOOD.
310 A=D/2
320 PI=3.1415927
330 REM LINES 340-550 CALCULATES THE VELOCITY IN FRONT OF
    A CIRCULAR FLANGED HOOD A CCORDING TO THE FINAL MODEL
    DEVELOPED BY FLYNN AND ELLENBECKER.
340 GAMMA1=SQR(X^2+(A+Y)^2)
350 GAMMA2=SQR(X^2+(A-Y)^2)
360 REM  ECC  IS THE ECCENTRICITY.
370 ECC=(2*A)/(GAMMA1+GAMMA2)
380 ECC2=ECC^2
390 T1=A+Y
400 T2=Y-A
410 T3=GAMMA1+GAMMA2
420 T4=GAMMA1*GAMMA2
430 T5=4*A^2
440 T6=SQR(T3^2-T5)
450 T7=-Q/PI
460 T8=(T1*GAMMA2)+(T2*GAMMA1)
470 T9=T3*T4*T6
480 VR1=(T8/T9)*T7
490 VZ1=(T7*X)/(T4*T6)
500 V1=SQR(VR1^2+VZ1^2)
510 VTF=(Q*ECC2*SQR(3))/(2*PI*A^2*SQR(3-2*ECC2))
520 VR2=(VR1/V1)*VTF
530 VZ=.9*((VZ1/V1)*VTF)
540 UA=VZ
550 VRTOT=(2.6*ECC^18+.853)*VR2 + VC
```

```
560 VA=VRTOT
570 TI=TI+DT
580 REM CALCULATE: RELATIVE VELOCITY  (VR)
                   REYNOLDS NUMBER (RE)
                   DRAG COEFFICIENT (CD)
590 VR=SQR((U-UA)*(U-UA)+(V-VA)*(V-VA)
600 RE=RA*DP*VR/(MU*1000000)
610 CD=(24/RE^0.646)
620 REM  LAM IS THE MEAN FREE PATH FOR AIR IN (MICRON).
630 LAM=.0667
640 REM  C  IS THE SLIP FACTOR ALSO CALLED THE CUNNINGHAM
        CORRECTION FACTOR.
650 C=1+(LAM/DP)*(2.514+.8*EXP(-.55*DP/LAM))
660 REM CALCULATE PARTICLE VELOCITY AND POSITION AT END OF
       TIME STEP.
       CALCULATE A1,B,AND D1 IN RUNGE-KUTTA METHOD.
670 F=RA/RP
690 A1=-.75*CD*VR*RA/(RP*DP*C/1000000)
700 B=-A1*UA
710 REM G IS THE EARTH GRAVITY ACCELERATION FIELD IN (M/S2)
720 G=9.8
730 N=1-F
740 D1=-(A1*VA)-G*N
750 UF=(U*(1+A1*DT/2)+B*DT)/(1-A1*DT/2)
780 VF=(V*(1+A1*DT/2)+D1*DT)/(1-A1*DT/2)
790 REM CALCULATE NEW VALUES OF X AND Y AND RESET INITIAL
       VALUES OF U AND V.
800 X=X+DT*(UF+U)/2
810 Y=Y+DT*(VF+V)/2
```

```
820 U=UF
830 V=VF
840 P(I,1)=X
850 P(I,2)=Y
860 REM CALCULATE THE PARTICLE LOCATION WHEN THE PARTICLE
        IS VERY NEAR TO Y-AXIS IN ORDER TO FIND THE DISTANCE
        OF THE PARTICLE FROM X-AXIS.
870 IF X<= .003 OR Y<=-5*D THEN I=3000 ELSE COUNT=I+1
880 NEXT I
890 REM LINES 900-960 GENERATE THE HOOD,FLANGE AND
CENTERLINE.
900 SCREEN 1
910 WINDOW (-.53,-.36)-(.53,.36)
920 LINE (A,0)-(.33,0)
930 LINE (A,0)-(A,.02)
940 LINE (0,.02)-(0,-.33)
950 LINE (-A,0)-(-.33,0)
960 LINE (-A,0)-(-A,.02)
970 REM THE J LOOP PLOTS THE POINTS GENERATED IN THE I LOOP.
980 FOR J=1 TO COUNT
990 S=P(J,1)
1000 H=P(J,2)
1010 PSET(S,H)
1020 NEXT J
1030 KEY OFF
1040 LOCATE 8,1 :PRINT"D=";D;"(M)";
1050 LOCATE 9,1 :PRINT"Q=";Q;"(M3/S)";
1060 LOCATE 10,1 :PRINT"VCH=";VCH;"(M/S)";
1070 LOCATE 11,1 :PRINT"VCV=";VCV;"(M/S)"
```

```
1080 LOCATE 12,1 :PRINT"DP=";DP;"(MICRO.M)";
1090 A$=INKEY$:IF A$="C" THEN 1110 ELSE 1100
1100 IF A$="X" THEN 1120
1110 LPRINT CHR$(12)
1120 END
```

PART 2

THIRD PROGRAM

```
10 REM FILE NAME---------CAPTURE---------------------------
20 REM  PROGRAM  PLOTS  PARTICLE TRAJECTORIES IN FRONT  OF
   A CIRCULAR FLANGED HOOD.
30 REM THE FACE OF THE FLANGED HOOD IS HORIZONTAL  AND  THE
       PARTICLES  ARE  RELEASED  IN  FRONT  OF  THE  HOOD
       (THE HOOD FACE IS OVER THE RELEASED PARTICLES).
40 REM THE VALUE OF Y IS NEGATIVE IN THE INPUT DATA Y (-) .
50 REM  LINES  90-220  ARE  INPUT  STATEMENTS  FOR  VALUES
   PROVIDED BY THE USER.
60 REM VARIABLES: RA IS THE AIR DENSITY IN (KG/M3).
                  MU IS THE AIR VISCOSITY IN (KG/M S).
                  RE IS THE REYNOLDS NUMBER.
70 REM VARIABLES: UF,VF ARE PARTICLE  VELOCITY  AT  END  OF
                  TIME STEP IN (M/S).
                  X AND Y ARE PARTICLE LOCATION AT  END  OF
                  TIME STEP IN (M).
                  TI,DT ARE ELAPSED  TIME  AND  TIME  STEPS
                  IN (S).
80 REM VARIABLES: RP IS THE PARTICLE DENSITY IN (KG/M3).
                  DP IS THE PARTICLE DIAMETER IN (MICRON).
                  P IS THE AIR PRESSURE IN (ATM).
```

```
                    T IS THE AIR TEMPERATURE IN (K).
                    D IS THE HOOD DIAMETER IN (M).
                    Q IS THE HOOD FLOW IN (M3/S).
                    VC IS THE CROSSDRAFT VELOCITY IN (M/S).
                    V IS THE PARTICLE VELOCITY IN  VERTICAL
                    DIRECTION IN (M/S).
                    U IS THE PARTICLE VELOCITY IN HORIZONTAL
                    DIRECTION IN (M/S).
90 INPUT "AIR PRESSURE IN (ATM)=";P
100 INPUT "AIR TEMPERATURE IN (K)=";T
110 INPUT "PARTICLE DENSITY IN (KG/M3)=";RP
120 INPUT "TIME STEP IN (SECONDS)=";DT
130 INPUT "PARTICLE DIAMETER IN (MICRON)=";DP
140 INPUT "HOOD DIAMETER IN (M)=";D
150 INPUT "HOOD FLOW IN (M3/S)=";Q
160 REM THE CROSSDRAFT IS IN HORIZONTAL DIRECTION.
170 INPUT "CROSSDRAFT VELOCITY IN (M/S)=";VC
180 REM INPUT INITIAL PARTICLE LOCATION AND VELOCITY.
190 INPUT "INITIAL PARTICLE DISTANCE FROM Y-AXIS IN (M)=";X
200 INPUT "INITIAL PARTICLE DISTANCE FROM X-AXIS IN (M)=";Y
210 INPUT "INITIAL PARTICLE VELOCITY IN VERTICAL DIRECTION
    IN (M/S)=";V
220 INPUT "INITIAL PARTICLE VELOCITY IN HORIZONTAL DIRECTION
    IN (M/S)=";U
225 Z=0
230 DIM P(3000,2)
240 COUNT=0
```

```
250 REM THE I LOOP PERFORMS THE VELOCITY CALCULATIONS
    ACCORDING TO THE NON-DIMENSIONAL MODEL DEVELOPED BY
    JANSSON, AND GENERATES THE POINTS TO BE PLOTTED.
260 FOR I=1 TO 3000
270 RA=P*100/(.287*T)
280 MU=(13.554 + .6738*T - (3.808*T*T/10000) + (1.183*T*T*T/
10000000))/10000000
290 TI=0
300 REM  A  IS THE AREA  OF THE HOOD IN (M2).
310 A=PI*(D^2)/4
320 PI=3.1415927
315 REM  UO IS THE HOOD FACE VELOCITY IN (M/S).
330 REM LINES 340-600 CALCULATES THE VELOCITY IN FRONT OF
    A CIRCULAR FLANGED HOOD A CCORDING TO JANSSON  MODEL.
340 UO=Q/A
350 REM X1, Y1, AND Z1 ARE NON-DIMENSIONAL DISTANCE.
360 X1=X/D
370 Y1=Y/D
380 Z1=Z/D
390 R=SQR(X1^2+Z1^2)
400 T1=SQR(Y1^2+(.5+R)^2)
410 T2=SQR(Y1^2+(.5-R)^2)
420 REM  ECC  IS THE ECCENTRICITY.
430 ECC=1/(T1+T2)
440 T3=ECC^2
450 T4=1-T3
460 T5=T4/2*ECC
470 T6=1+T5
480 T7=1+ECC
```

```
490 T8=1-ECC
500 T9=T7/T8
505 REM UU IS THE NON-DIMENSIONAL VELOCITY MAGNITUDE.
510 UU=T3/(T6*LOG(T9))
520 BETA=ATN(T4*R/Y1)
530 GAMMA=ATN(Z1/X1)
540 UUY=-UU*COS(BETA)
550 UUR=-UU*SIN(BETA)
560 UUX=UUR*COS(GAMMA)
570 UUZ=UUR*SIN(GAMMA)
575 REM UY IS THE VELOCITY IN VERTICAL DIRECTION.
580 UY=-UUY*UO
585 REM UX IS THE VELOCITY IN HORIZONTAL DIRECTION.
590 UX=UUX*UO+VC
610 VA=UY
620 UA=UX
640 REM CALCULATE: RELATIVE VELOCITY  (VR)
                   REYNOLDS NUMBER (RE)
                   DRAG COEFFICIENT (CD)
650 VR=SQR((U-UA)*(U-UA)+(V-VA)*(V-VA))
660 RE=RA*DP*VR/(MU*1000000)
670 CD=(24/RE^0.646)
680 REM  LAM IS THE MEAN FREE PATH FOR AIR IN (MICRON).
690 LAM=.0667
700 REM  C  IS THE SLIP FACTOR ALSO CALLED THE CUNNINGHAM
        CORRECTION FACTOR.
710 C=1+(LAM/DP)*(2.514+.8*EXP(-.55*DP/LAM))
```

```
720 REM CALCULATE PARTICLE VELOCITY AND POSITION AT END OF
        TIME STEP.
        CALCULATE A1,B,AND D1 IN RUNGE-KUTTA METHOD.
730 F=RA/RP
750 A1=-.75*CD*VR*RA/(RP*DP*C/1000000)
760 B=-A1*UA
770 REM G IS THE EARTH GRAVITY ACCELERATION FIELD IN (M/S2)
780 G=9.8
790 N=1-F
800 D1=-(A1*VA)-G*N
810 UF=(U*(1+A1*DT/2)+B*DT)/(1-A1*DT/2)
820 VF=(V*(1+A1*DT/2)+D1*DT)/(1-A1*DT/2)
830 REM CALCULATE NEW VALUES OF X AND Y AND RESET INITIAL
        VALUES OF U AND V.
840 X=X+DT*(UF+U)/2
850 Y=Y+DT*(VF+V)/2
860 U=UF
870 V=V
880 P(I,1)=X
890 P(I,2)=Y
900 REM CALCULATE THE PARTICLE LOCATION WHEN THE PARTICLE
        IS VERY NEAR TO X-AXIS IN ORDER TO FIND THE DISTANCE
        OF THE PARTICLE FROM Y-AXIS.
910 IF Y>=-.003 OR X<=-5*D THEN I=3000 ELSE COUNT=I+1
920 NEXT I
930 REM LINES 940-1000 GENERATE THE HOOD,FLANGE AND
    CENTERLINE.
940 SCREEN 1
950 WINDOW (-.53,-.36)-(.53,.36)
```

```
960 LINE (A,0)-(.33,0)
970 LINE (A,0)-(A,.02)
980 LINE (0,.02)-(0,-.33)
990 LINE (-A,0)-(-.33,0)
1000 LINE (-A,0)-(-A,.02)
1010 REM THE J LOOP PLOTS THE POINTS GENERATED IN THE I
     LOOPE.
1020 FOR J=1 TO COUNT
1030 S=P(J,1)
1040 H=P(J,2)
1050 PSET(S,H)
1060 NEXT J
1070 KEY OFF
1080 LOCATE 8,1 :PRINT"D=";D;"(M)";
1090 LOCATE 9,1 :PRINT"Q=";Q;"(M3/S)";
1100 LOCATE 10,1 :PRINT"VC=";VC;"(M/S)";
1110 LOCATE 11,1 :PRINT"DP=";DP;"(MICRO.M)";
1120 A$=INKEY$:IF A$="C" THEN 1140 ELSE 1130
1130 IF A$="X" THEN 1140
1140 LPRINT CHR$(12)
1150 END
```